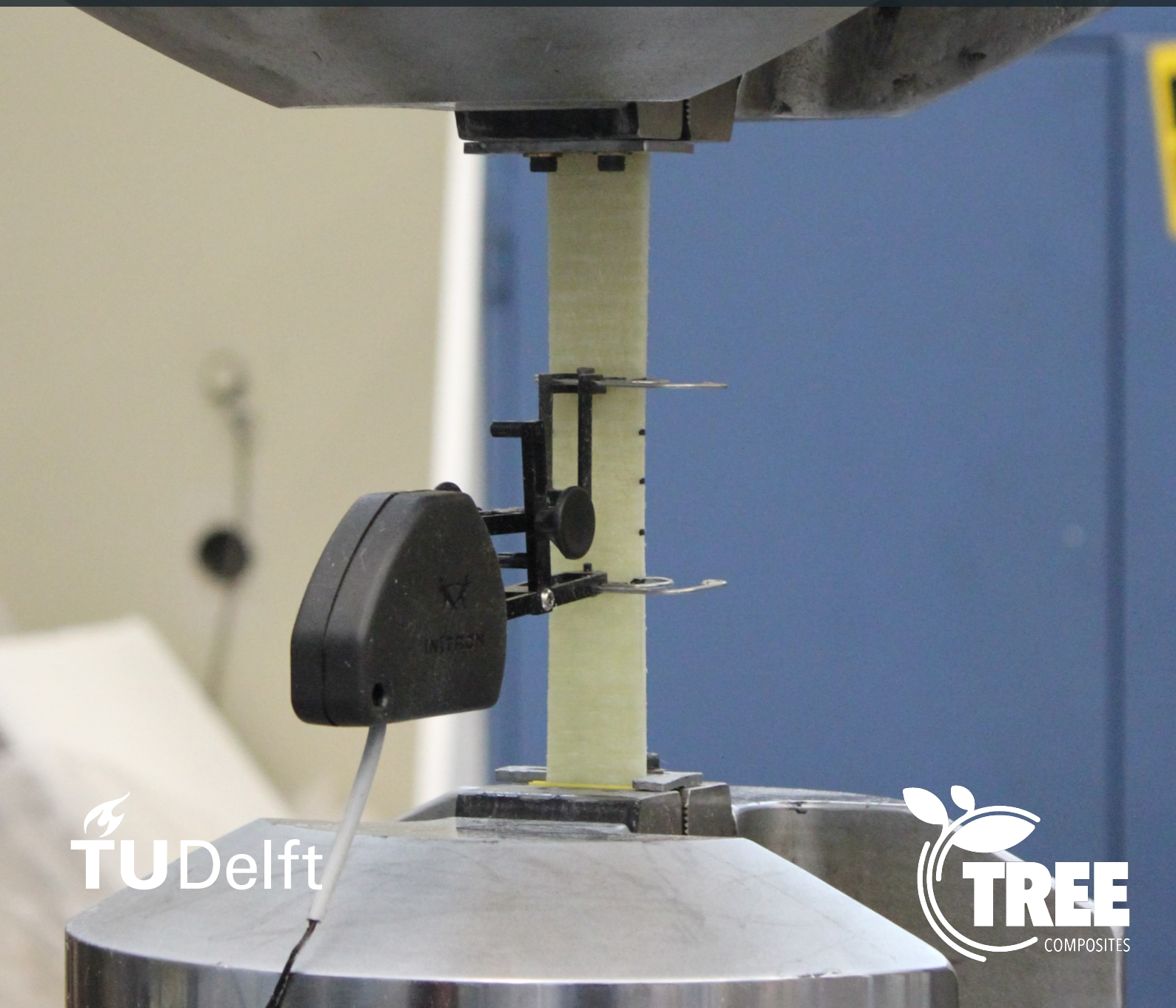
Impact of freeze-thaw cycles on wrapped composite joint durability

An experimental and numerical study

Janneke Kortsmit



Impact of freeze-thaw cycles on wrapped composite joint durability

An experimental and numerical study

Thesis report

by

Janneke Kortsmit

to obtain the degree of Master of Science
at the Delft University of Technology
to be defended publicly on September 26, 2024 at 14:00

Thesis committee:

Chair:	Dr. M. Pavlovic
Supervisors:	Dr. M. Moreira Arouche
	ir. M. Wolters
Committee Members:	Dr. O. Copuroglu
	Dr. S. Cabral-Fonseca
Place:	Faculty of Civil Engineering, Delft
Project Duration:	August, 2023 - September, 2024
Student number:	4447751

An electronic version of this thesis is available from 26-09-2026 at http://repository.tudelft.nl/.

Faculty of Civil Engineering · Delft University of Technology



Copyright © Janneke Kortsmit, 2024
All rights reserved.

Preface

This master thesis report forms the conclusion of my academic journey at the TU Delft, after which I can officially call myself a Civil Engineer. It has been a great honour to end this educational journey with such a challenging, exciting and rewarding master thesis research. I want to thank Marko Pavlovic, for introducing me to the possibility of finalising my academic journey as a part of the Wrapped Composite Joints research group. Your guidance, not only during my progress meeting, but also during the research group meetings, has been of great value to this research, and my development as an engineer.

The research posed many challenges, and my feelings towards the project went through quite some freeze-and-thaw cycles themselves, as moments of great frustration were alternated by moments of immense joy. I would very much like to thank my daily supervisors Marcio Moreira Arouche and Mees Wolters for their patience and motivating words throughout the project, guiding me on how to catch the hypothetical glimpses of sun to move from my freezing stages to thawing.

I would like to extend these words of gratitude to my other committee members, Susana Cabral-Fonseca and Oguzhan Copuroglu.

Susana, thank you for all your guidance and support. I enjoyed the interactions we had, your immense knowledge and how you share this with such passion and positivity are a real example to look up to and I feel honoured you took the time to handle me and my work with such patience and devotion.

Oguzhan, thank you for your guidance, out-of-the-box ideas and critical thinking. You helped me not to lose sight of what was the final goal and how I should develop myself during this master thesis research.

Next to my committee, I would like to give a special thanks to Fred Schilperoort, without whom the automated ageing system would not have taken flight in such a short time frame. I learned so many things which previously felt so intimidating and unknown. You opened up a new world, where I feel the possibility and courage to discover what a bit of coding and an Arduino can bring. I appreciate the patience with which you explained everything to me and helped me with the process.

Additionally, I would like to thank my family and friends. Your endless support and love have helped me pursue my education next to all the different orchestras I had the pleasure of playing in.

Last but not least, I would like to thank my partner, Mees. Your endless support, positivity and motivational words kept me going. Both graduating within the same year has not been an easy ride, but I can say that I am proud of what we have both accomplished during this year and I look forward to this next step in life together with you.

Janneke Kortsmit
September 2024

Abstract

Climate change and the growing need for energy independence have resulted in a quickly expanding offshore wind energy industry. Foundations of these structures made from welded steel hollow sections are prone to fatigue. The wrapped composite joints omit welds, greatly increasing fatigue life. But is this technology equipped to handle the harsh offshore environment?

This research aims to gain first insight into a subject not studied in the context of the wrapped composite joint before, the effect of freeze-thaw cycles. A broad overview is created by including a vast range of experimental and numerical subjects discussing the external degradation and internal degradation, through (microscopic) surface investigation, gravimetric measurements, quasi-static tensile tests and a numerical evaluation of heat transfer and developing strains on joint geometries.

Glass fibre-reinforced modified vinyl ester composites are aged for a maximum of 199 freeze-thaw cycles. This is done for composites two different types of composites, where one has a 15 percentage point higher fibre volume fraction. One freeze-thaw cycle consists of 3 hours of freezing at -20 °C and 3 hours of thawing submerged in +23 °C water with 3.5 weight% salt to mimic seawater. This methodology is applied by an automated system developed for this research.

The degradation of the surface is evaluated by determining the wetting angle and surface profile changes, such as visual changes, height profile and surface roughness. Especially material with a higher fibre volume fraction, with a thinner resin-rich outer layer, shows significant surface degradation, with a 16% reduction of wetting angle and 200% increase of surface roughness. This raised the expectation that external damages would increase the susceptibility of the material to uptake moisture.

However, the gravimetric measurements conducted to track weight change do not indicate an increase in weight change and show no definitive sign of weight loss, which would indicate there is no increase in saltwater uptake for material exposed to freeze-thaw cycles, compared to continuous submersion.

This internal degradation is however visible in the retention of tensile properties. The tensile modulus reduces 6% after 199 freeze-thaw cycles independent of fibre-volume fraction, but it becomes apparent that a higher fibre-volume fraction results in less reduction of tensile strength and strain. Material with a low fibre-volume fraction presents with an 11% reduction of tensile strength and a 6% reduction of rupture strain, whereas high fibre-volume fractions show only a reduction of 6% in strength and a 4% increase in strain. How significant these degradations are, can however be questioned, as all tests performed show a high standard deviation, expected to be caused by the non-symmetric layup of the composite resulting in non-uniform internal stress build up as ageing continues. On top of that, the retention of through-thickness shear properties can be questioned, as a multitude of tensile coupons showed significant delamination after testing.

To further investigate these effects of temperature, and set the context to the end product, a numerical heat transfer analysis is performed on a medium-scale and full-scale joint with chord and brace under 90°angle. The temperature development and accompanying strains along the steel-composite interface are determined after exposure to a 4-hour warm morning and a fictitious cold night with a minimum of -30°C. It shows full-scale joints present with minimal temperature changes and strain development in the root of the joint, but show a similar magnitude of through-thickness strains along the edges of the composite wrap in the order of magnitude of 10^{-3}. Further research will be necessary to conclude if the cyclic development of strains of this magnitude, and higher with bigger temperature ranges, can negatively impact not only the edges of the composite wrap but expand towards the root.

Contents

1 Introduction **1**
1.1 Background information . . . 1
1.1.1 Wrapped composite joint . . . 2
1.1.2 Offshore environmental conditions . . . 3
1.1.3 Impact of environmental factors . . . 3
1.2 Problem statement . . . 4
1.3 Scope . . . 5
1.4 Research questions . . . 6
1.5 Research methodology . . . 6
1.6 Structure of research report . . . 6

2 State of the art **8**
2.1 Background theory . . . 8
2.1.1 Diffusion . . . 8
2.1.2 Wetting angle . . . 11
2.1.3 Heat transfer . . . 12
2.2 Literature review . . . 16
2.2.1 Tensile property retention . . . 18
2.2.2 In-plane shear property retention . . . 19
2.2.3 Inter-laminar shear property retention . . . 20
2.2.4 Compression strength . . . 20
2.2.5 Degradation bonded interface . . . 22
2.2.6 Moisture uptake . . . 23
2.2.7 Influence sustained loading during ageing . . . 23
2.2.8 Conclusion . . . 24
2.3 Review freeze-thaw ageing methods . . . 24
2.3.1 NEN-EN 12371 - Natural frost resistance natural stones . . . 24
2.3.2 ASTM C666 - Concrete Resistance to Rapid Freezing and Thawing . . . 25
2.3.3 ASTM D6944 - Resistance Cured coatings to thermal cycling . . . 25
2.3.4 ASTM D7792 - Freeze-thaw cycles on pultruded composites . . . 25
2.3.5 Ageing methods from literature . . . 26
2.3.6 Conclusion freeze-thaw ageing methods . . . 26

3 Effects of freeze-thaw cycles **27**
3.1 Development ageing methodology . . . 27
3.1.1 Development methodology . . . 27
3.1.2 Applied methodology . . . 31
3.1.3 Irregularities during ageing . . . 32
3.2 Microscopic investigation of surface degradation . . . 32
3.2.1 Introduction . . . 32
3.2.2 Methodology and materials . . . 33
3.2.3 Results . . . 34
3.2.4 Discussion . . . 37
3.2.5 Conclusion . . . 37
3.3 Saltwater uptake . . . 37
3.3.1 Introduction . . . 38
3.3.2 Methodology . . . 38
3.3.3 Materials . . . 39
3.3.4 Results . . . 40
3.3.5 Discussion . . . 43

3.3.6 Conclusion . . . 43
3.4 Retention of tensile properties . . . 43
3.4.1 Introduction . . . 44
3.4.2 Methodology . . . 44
3.4.3 Material . . . 45
3.4.4 Results . . . 45
3.4.5 Discussion . . . 51
3.4.6 Conclusion . . . 52

4 Thermal response **53**
4.1 Introduction . . . 53
4.2 Methodology . . . 54
4.2.1 Experimental . . . 54
4.2.2 Numerical . . . 55
4.3 Materials . . . 58
4.3.1 Geometries . . . 58
4.3.2 Material properties . . . 58
4.4 Results . . . 59
4.4.1 Validation experiment . . . 59
4.4.2 Heat transfer and strain development during warm morning . . . 62
4.4.3 Heat transfer and strain development during cold night . . . 64
4.5 Discussion . . . 66
4.6 Conclusion . . . 68

5 Wrapping up **69**
5.1 Conclusion . . . 69
5.2 Recommendations . . . 72

References **78**

A Climate Modelling **79**
A.1 Introduction CMIP6 and CAS FGOALS-g3 . . . 79
A.2 Extracted data and results . . . 80
A.3 Jupyter Notebook climate data manipulation . . . 83

B Freeze-thaw ageing setup **88**
B.1 Experimental equipment used . . . 88
B.2 Arduino script . . . 90
B.3 Full setup script . . . 91

C KNMI data **104**

D Script calculating heat transfer coefficient **105**

Nomenclature

List of Abbreviations

CHS	Circular hollow section
CMIP	Climate Model Intercomparison Project
CSM	Chopped Strand Mat
CTE	Coefficient of thermal expansion
FEA	Finite Element Analysis
Fs	Full scale
FT	Freeze-thaw
HV_f	High fibre volume fraction
ILS	Inter-laminar shear
LBADSA	Lower Bound Asymmetric Drop Shape Analysis
LV_f	Low fibre volume fraction
Ms	Medium scale
TC	Thermocouple
UD	Unidirectional
X90	Joint where chord and brace make a 90°angle

List of Symbols

α	Absorptivity
β	Thermal volume expansion coefficient
κ_p	Pressure stress factor
κ_s	Temperature gradient factor
μ	Dynamic viscosity
ν	Kinematic viscosity
ϕ	Normalized concentration
ρ	Density
σ	Stefan-Boltzmann constant ($5.6697 \cdot 10^{-8} \frac{W}{m^2 K^4}$)
θ	Temperature
θ^0	Ambient temperature, sink temperature
θ^Z	Absolute zero temperature
ε	Emissivity
A	Surface area of a 1D surface
C	Concentration of particles
c_p	Specific heat capacity
D	Diffusion coefficient
dm	Change of amount of particles
dT	Temperature difference
dt	Small increment of time
E	Irradiance
g	Gravitational acceleration
h	Heat transfer coefficient, film coefficient
J	Flux of any particles
k	Thermal conductivity
L_c	Characteristic length
M_m	Maximum moisture content of material, saturation
Nu	Nusselt number
P	Perimeter
p	Equivalent pressure stress
Pr	Prandtl number
q	Heat transfer
Ra	Rayleigh number
Re	Reynolds number
Re_{crit}	Critical Reynolds number (10^5)
s	Solubility
T_a	Ambient temperature
T_s	Surface temperature
U	Mean velocity of flow

List of Figures

1.1 Offshore wind foundations [3] . . . 1
1.2 Components of a ply [7] . . . 2
1.3 Visual representation of a KK wrapped composite joint [8] . . . 2
1.4 Jacket position in sea (adapted from [10]) . . . 3

2.1 Fickian moisture content change [27] . . . 9
2.2 Hydrolysis of a vinyl ester polymer [30] . . . 10
2.3 Schematic representation of long-term diffusion contribution [31] . . . 10
2.4 Visualisation of internal forces in droplet [33] . . . 11
2.5 Variety in wetting angle (adapted from [33]) . . . 11
2.6 Visualisation laminar and turbulent flow [37] . . . 14
2.7 Ratio CTE of matrix and fibre in longitudinal direction [41] . . . 17

3.1 Modelled minimum near-surface air temperature over the North Sea [53] . . . 28
3.2 Modelled maximum near-surface air temperature over the North Sea [53] . . . 28
3.3 Modelled mean number of yearly FT cycles over the North Sea [53]. . . . 29
3.4 Modelled maximum number of FT cycles over the North Sea[53]. . . . 29
3.5 Internal setup of developed FT ageing system in the climate chamber . . . 30
3.6 Temperature of material and climate chamber during an extra long FT cycle . . . 30
3.7 Graph representing one FT cycle and temperature changes experienced by climate chamber and samples . . . 31
3.8 Graph representing one cycle and temperature changes experienced by climate chamber and samples without circulation step . . . 32
3.9 Representation of wetting angle θ[33] . . . 33
3.10 Example of a surface profile and roughness with a Keyence VR-6000 Profilometer . . . 33
3.11 Positions measurement . . . 34
3.12 Wetting angle setup . . . 34
3.13 Images of the back surface of plates after exposure to FT cycles . . . 35
3.14 Height profile at one location of bottom HV_f plate, yellow line = reference, blue line = after 77 freeze-thaw cycles of exposure . . . 35
3.15 Normalized increase/decrease in surface roughness after FT cycle exposure . . . 36
3.16 Example of droplet shape with LBADSA . . . 36
3.17 Change of wetting angle with exposure to FT cycles . . . 36
3.18 Coated plate [mm] . . . 39
3.19 Modelled plate part [mm] . . . 40
3.20 Weight change during FT cycles . . . 40
3.21 Geometry of previous experiment coupons [16]. Dimensions in mm . . . 41
3.22 Weight change of different geometries under different conditions . . . 42
3.23 Experimental and numerical moisture uptake of LV_f plate . . . 42
3.24 Experimental setup for tensile testing . . . 44
3.25 Tensile coupon with dimensions in mm . . . 45
3.26 Pictures showing failed LV_f coupons. Selected coupons are indicated by a green ribbon. . . . 47
3.27 Picture of delamination between plies for coupon 8 of LV_f material, aged for 69 FT cycles . . . 47
3.28 Pictures showing failed HV_f coupons.Selected coupons are indicated by a green ribbon. . . . 49
3.29 Pictures showing HV_f coupons showing delamination . . . 49
3.30 Results conducted tensile tests . . . 50

4.1 Setup of thermal validation experiment . . . 54

4.2 Locations of extracted temperatures of thermal images (blue dots on steel, red dots on composite wrap) and TC (numbered 1-2 and 4-9) 54
4.3 Used simplifications for weather data 55
4.4 Ambient temperature with used polynomial fit for cold night 56
4.5 Comparison steel temperature with FEA 60
4.6 Comparison composite wrap temperature with FEA 62
4.7 Thermal profile and temperature over chord and brace of Ms and Fs joint after 4 hours of exposure to sun and ambient temperatures 63
4.8 Developed numerically determined strains in in-plane (11) and through-thickness (33) direction for a Ms and Fs X90 joint at the end of the 4-hour warm morning along brace and chord steel-composite interface 64
4.9 Thermal profile and temperature over chord and brace of Ms and Fs joint at minimum reached temperature for the edges of the wrap, respectively 6.3 and 7.3 hours, of exposure to a cold night 65
4.10 Developed numerically determined strain in in-plane (11) and through-thickness (33) direction when the joints reached their coldest point at the edges of the wrap along the brace and chord steel-composite interface 66

A.1 Bias sea surface temperature FGOALS-g3 [71] 80
A.2 Minimum daily near-surface temperature [53] 81
A.3 Maximum daily near-surface temperature [53] 81
A.4 Mean yearly amount of FT cycles [53] 82
A.5 Maximum yearly amount of FT cycles [53] 83

B.1 Images of ageing setup 88
B.2 Picture of Arduino, relay and connections 89
B.3 Flow block diagram of setup 89

List of Tables

2.1 Continued on next page . . . 18
2.2 Summary in-plane shear property retention after FT cycles from literature . . . 19
2.3 Summary inter-laminar shear property retention after FT cycles from literature . . . 20
2.4 Summary compression property retention after FT cycles from literature. [1] Transverse direction 21
2.5 CTE of steel [50] and epoxy composite reinforced with either basalt, carbon or glass fibre [42] 23
2.6 Summary of moisture uptake under influence of FT cycles . . . 23
2.7 Summary results sustained loading during 300 FT cycles [46] . . . 24
2.8 Ageing procedure for submersion, freezing and thawing ageing method according to ASTM D6944 [21] . . . 25

3.1 Gripping pressure and length during testing of coupons aged 20 FT cycles. Underlined: failure close to grips. **Bold**: failure at grips. [1] After slipping, pressure increased to 10 MPa . . . 46
3.2 Waiting days in between stop of ageing and tensile test . . . 50
3.3 Percentage retention ± standard deviation of tensile properties after 199 FT cycles . . . 51

4.1 Properties of air at 25°C. [1] [67], [2] [68] . . . 59

C.1 KNMI weather data for 18/07/2024 [61] . . . 104

1

Introduction

The offshore wind energy industry is a quickly expanding field, contributing an additional 3.3 GW to the European electricity grid in 2021 alone [1]. Climate change and a growing need for energy independence raise the demand for renewable power sources, aiming for ambitious targets of 65 GW of European offshore wind energy by 2030, and 150 GW by 2050 [2]. This high demand for fast growth and development comes with numerous challenges. Structures need to be lightweight, cost-efficient, have an efficient construction time, and be highly durable in the harsh offshore environment. In this sense, the wrapped composite joint emerges as an innovative technology aiming to accelerate the growth of the offshore wind industry.

This chapter introduces the wrapped composite joint technology and describes its benefits compared to regular welded joints in Section 1.1. However, the harsh offshore environment still challenges the structure's durability, which is discussed in Section 1.1.2. This will be translated into the problem statement in Section 1.2. The boundaries of the research are then defined in Section 1.3, followed by the research questions Section 1.4 and methodology Section 1.5. To close off, a reading guide is added in Section 1.6

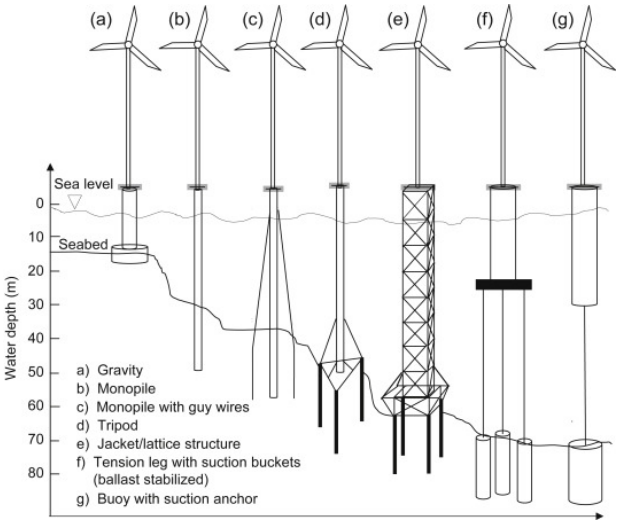


Figure 1.1: Offshore wind foundations [3]

1.1. Background information

Offshore wind foundations can be classified into roughly two groups; bottom-mounted and floating structures, as visualised in Figure 1.1. The monopile is a popular, cost-efficient bottom-mounted solution up to 30 m depth. The traditional structure becomes too flexible at greater depths, making jacket structures the structural stiffer and a better solution [3]. New XXL monopiles are developed to tackle these issues, for example, at Arcadis Ost 1, reaching water depths of 45 m [4]. However, these XXL monopiles weigh more than 2,000 tonnes each, doubling steel use compared to a regular jacket foundation [5, 6]. Combined with its suitability in only specific soil types and offshore wind development moving to deeper, rougher waters with rockier subsoil, the jacket becomes the more efficient solution.

Traditionally jackets are made of steel circular hollow sections (CHS) connected by welding, resulting in limited fatigue life due to local stress concentrations and hardening in the welded region. To reduce the impact of this, sections are locally thickened around the weld, increasing steel use in the structure. The design of the jackets is driven by this fatigue-prone region and optimisations are, with the current methodology of connecting by welding, difficult. The wrapped composite joint prevents the use of these complex welded joints opening up new possibilities for optimisation of jacket structures. The next section introduces the material, composites, and technology, together with the challenges it faces.

1.1.1. Wrapped composite joint

The wrapped composite joint is a technology under development, combining the high stiffness and strength of glass fibre with a modified vinyl ester matrix. This offers the possibility of producing a lightweight, low-cost and environmentally durable structure.

Composite

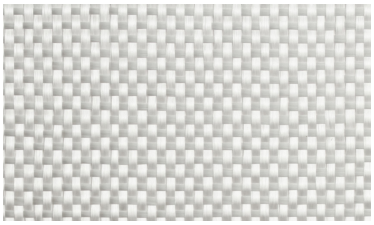
In the context of this research, composite refers to a material consisting of fibres which are embedded in a polymer matrix, hence the commonly used name fibre reinforced polymers (FRPs). The fibres generally have high stiffness and strength in the direction of the fibre, but low stiffness and strength in the transverse direction. The orientation of the fibres thus gives the flexibility to alter the strongest direction of the material based on its application.

The matrix protects the fibres against environmental degradation and distributes loads to all the fibres. This results in a more uniform stress over the material, which benefits its maximum capacity. For this load transfer, the interface between the fibre and matrix is vital.

The wrapped composite joints are produced using glass fibre and a modified vinyl ester matrix. One layer of glass fibre called a ply, consists of a Chopped Strand Mat (CSM) stitched to a bi-directional woven fabric. These components are shown in Figure 1.2. This results in a similar amount of fibres in all in-plane directions. These plies are stacked and embedded in a thermosetting polymer, vinyl ester, forming a laminate.



(a) Chopped Strand Mat (CSM)



(b) Bi-directional woven fabric

Figure 1.2: Components of a ply [7]

Before completion of production, the vinyl ester resin still consists of monomers and is liquid. An additive starts the curing of the resin, by starting a reaction forming chains of monomers, called polymers, and cross-linking the longer polymer chains together. This results in an interconnected network in three dimensions which gives the matrix its rigidity, but also increases its environmental durability.

Curing is a heat-releasing reaction, which helps in providing enough energy throughout the laminate to completely cure and form all cross-links. With thin laminates, the heat may dissipate too quickly, leaving the material cured incompletely, whereas with thick laminates, the temperature can increase too high, burning the matrix. For thick laminates, this means carefully considering the temperatures reached during production. For thin laminates, this can be solved by after production heating the specimens, so-called post-curing. This addition of heat gives an additional energy input, which will restart the curing reaction. A completely cured composite is more homogeneous and uniform with a matrix that is at its top mechanical performance and environmental durability.

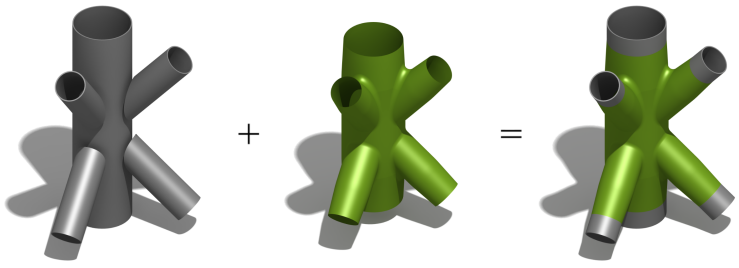


Figure 1.3: Visual representation of a KK wrapped composite joint [8]

The development of the wrapped composite joint

In the wrapped composite joint, the composite is applied directly on the steel without the use of an adhesive as shown in Figure 1.3. The composite wrap replaces the weld as the load-distributing component between the chord (leg) and brace (diagonal). The forces are distributed over the full contact surface of the wrap,

which is significantly larger than the surface area of a welded joint. On top of that the freedom of shape in composites, allows for optimising the shape, decreasing stress concentrations in the wrap [9].

This results in a longer fatigue life compared to a traditional welded joint alongside the opportunity to use thinner and smaller steel members without local thickening around welded sections whilst opening up the use of high-strength steel. This results in steel jackets even lighter and with better fatigue performance than a regular jacket. This makes the wrapped composite jacket an even more economical solution when compared to monopiles in deep waters. However, these wrapped composite joints as developing technology still have unknowns that should be tackled before widespread commercial use, such as the durability of the joint, the behaviour of joints in a jacket structure and the further development of a scalable and possibly automated production method. As this research is centred around the durability of the joint, the environmental conditions it has to endure in the offshore environment are now discussed.

1.1.2. Offshore environmental conditions

Despite all the advantages of the use of the wrapped composite joints compared to traditionally welded joints as just mentioned, the offshore environment still subjects the structure to harsh environmental factors, such as:

- Moisture
- Temperatures variations
- UV-radiation
- A combination of the above factors

These factors may result in (micro)cracking, corrosion, mismatched expansion and contraction between steel and composite and other effects potentially leading to degradation of the structure. Figure 1.4 shows a jacket positioned in the sea. The exposure zones can be divided into the atmospheric zone, the splash & tidal zone and the submerged zone [11]. These zones will now be discussed separately.

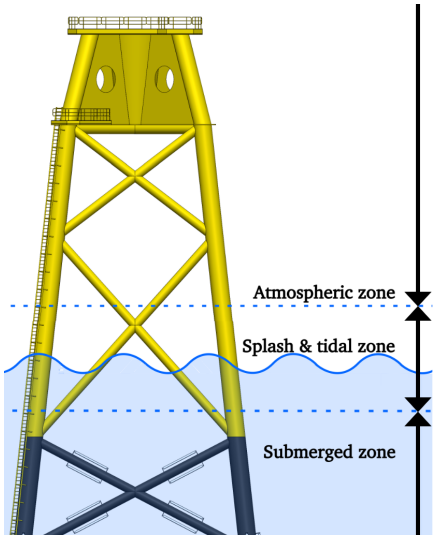


Figure 1.4: Jacket position in sea (adapted from [10])

Atmospheric zone

In the atmospheric zone, joints are never submerged. The main environmental influences are exposure to wind, spray of water, high humidity saline air, UV-radiation, temperature changes and combinations of these factors. As the joints are not continuously submerged, temperatures can reach both below and above the freezing point.

Splash and tidal zone

Joints in the splash and tidal zone are during service life intermittently submerged in seawater, caused by wind or tidal action. In addition, they can be exposed to temperature changes, UV radiation and combinations of these factors. As they are not constantly submerged, they can still be exposed to sub-zero temperatures. Compared to the atmospheric zone, in the splash and tidal zone, the exposure is more diverse, as there is a more extreme exposure to moisture.

Submerged zone

In the submerged zone, joints are completely submerged during their full lifetime, making the primary environmental influence the continuous exposure to saltwater.

1.1.3. Impact of environmental factors

All these aforementioned environmental factors have a different impact on the wrapped composite joint. As a part of the development of the technology, extensive research into different factors has already been conducted.

Continuous submersion of a wrapped composite joint may result in various short- and long-term degradation mechanisms of the composite, such as plasticisation, swelling, hydrolysis, micro-cracking and polymer relaxation. The impact of saltwater ageing is evaluated on the composite (interface) coupon

level, steel-composite interface coupon level and joint level and is extensively being researched as part of the development in the Wrapnode-I and Wrapnode-II projects [12].

Literature shows that UV radiation is an exposure that primarily affects the top layer of the composite. This means that adding sacrificial non-structural layers of material or using a carefully selected protective coating could form a suitable solution [13, 14, 15].

The effects of constant sub-zero or high temperature are shown to influence the composite material properties, but to have little effect on fatigue delamination of the composite material [16, 17].

In all this research the effect of cyclic changes in temperatures is not yet considered. In the offshore context as just discussed in Section 1.1.2 it is visible that the splash and tidal zone is the most detrimental as the material can be exposed to intermittent submersion, sub-zero temperatures and above zero temperatures. Freeze-thaw (FT) cycles in the splash and tidal zone can thus be seen as the most detrimental uninvestigated exposure for two reasons:

- The difference in coefficient of thermal expansion (CTE) between the materials will result in uneven expansion and contraction. As this discrepancy is present both between the bulk composite and the steel material and within the composite between the fibre and matrix, this can lead to internal stresses resulting in micro-cracks in the matrix, along the fibre-matrix interface and the composite-steel interface. This could ultimately lead to damage in the wrap resulting in debonding. As heating and cooling are cyclically repeated, it may result in environmental fatigue, increasing internal stresses and possible detrimental effects.
- Due to the intermittent submersion, the outer perimeter of the wrap will become saturated with saltwater during service life. Apart from this entrapped moisture causing degradations, when the joint is exposed to sub-zero temperatures, the entrapped water will expand and salt particles will crystallize. This will result in additional internal stresses in the composite, which can lead to micro-cracking of the surface. This could impact material properties as well as the rate at which water can penetrate the composite.

The effects of FT cycles in this context can thus be divided into two parts, the effect of temperature, and the effect of the presence of moisture under sub-zero temperatures. Experimentally these effects can be evaluated combined, by testing material property retention of aged material exposed to freezing and thawing, with thawing stages submerged in water. Literature can help estimate material property retention, but should also be considered with care, as different materials, layup, production methods and ageing methodologies are combined. These factors all have an unknown effect, resulting in a lack of definitive answers on retention in this application. On top of that, effects on the steel-composite interface and the joint as a whole are impossible to assess via literature, as the bonding techniques and geometries are incomparable.

Numerically, there are no methodologies in place to predict the effects of either the presence of moisture during freeze-thaw cycles or the temperature changes occurring during freeze-thaw cycles. When considering these effects on the joint scale, the main region of interest is the interface between the steel and composite, especially near the root of the joint. As moisture will not reach the interface during service life [18], the possibility of determining the effect of temperature changes numerically, would aid in determining the effects of FT cycles on wrapped composite joints.

1.2. Problem statement

The current research gap regarding the durability of the wrapped composite joint thus identifies the effect of FT cycles. The effects of these temperature changes under exposure to moisture are a relevant research topic with direct applicability to the wrapped composite joint. This can be explained by the following

- Different combinations of fibre and resin, manufacturing conditions and different composite layups respond differently to environmental exposure, reducing comparability and direct application of available research.
- The first standard for FT testing of composite was developed in 2015 for pultruded composites [19]. Other methods have been developed for different types of material, such as for concrete [20], or cured coatings [21]. This means that no specific ageing methodology has been proposed in the literature to cover the analysis of FT cycles on the wrapped composite bi-material joints. On top of that, all existing

standards for FT ageing do not indicate the applicability of the number of cycles or the temperature range used for a specific service life environment.

- Literature on the bonded interface between composite and a secondary material uses different, incomparable bonding techniques. The effect on the wrapped composite joint bi-material interface on coupon scale, or joint geometry is thus unpredictable.
- The magnitude of the effect of thermal cycles and temperature change in general on the interface between composite and steel remains unknown. On both coupon scale and joint geometry, there is no methodology in place to estimate these effects.

The problem statement is thus as follows:

Current research on the effects of freeze-thaw cycles on composite materials shows great variability related to the type of materials, manufacturing and testing methodology. Consequently, the results cannot be used to predict the impact of freeze-thaw cycles on the durability of the wrapped composite joint

1.3. Scope

The research is conducted on glass fibre-reinforced modified vinyl ester matrix composites. The fibre plies are made of bi-directional woven fabric stitched to a chopped strand mat (CSM). Two types of materials are produced and tested, a low fibre volume fraction composite (LV_f) and a high fibre volume fraction composite (HV_f), which has a 15 percentage point higher fibre volume fraction. All experimental material tests are conducted on both materials.

To tackle such a broad topic, assessing the impact of FT cycles is limited to composite material. This is done by:

- Microscopically investigating the composite surface and determining if damage is inflicted by FT cycles. This is done by measuring surface roughness, profile height, wetting angle and registering visual changes.
- Investigating the influence of FT cycles on saltwater uptake of the composite material.
  Experimentally this is assessed for LV_f and HV_f material and numerically by Finite Element Analysis (FEA) only for LV_f material.
- Determining the composite tensile property retention.
  [22, 23, 24, 25] give the impression tensile and compressive properties are affected heavily by FT cycles. Tensile properties are tested as this forms a relatively easy test to assess the impact.

To set the first steps in numerically predicting the effects of FT cycles, thermal analysis will be conducted to determine the development of internal strains caused by the differences in CTE of the composite and steel. The thermal response of LV_f joints where the chord and brace are at a 90°angle, X90, is evaluated on two scales:

- Medium-scale (Ms) joint with CHS diameter of 168.3 mm. This scale is used for FEA validation with an experiment.
- Full-scale (Fs) joint with CHS diameter of 610 mm which is a scale joint representative for a jacket supporting a 14 MW turbine in an environment of 40 m water depth.

The longitudinal and through-thickness strains developed due to the temperature change, the different CTE of composite and steel and the connection between the two materials are evaluated on the interface between composite and steel. The difference between the CTE of the glass fibres and the vinyl ester matrix is not taken into account. Two temperature exposures are considered:

- A warm morning will be assessed experimentally and numerically to act as a validation of the model.
- A hypothetical cold night with an assumed temperature change.

The cyclic change between temperatures is not assessed as a part of the development of the thermal models.

1.4. Research questions

The main goal of this research is to investigate the impact of FT cycles on the wrapped composite joint and gain a first insight into the effects. To focus this research fitting within the time frame the main research question is supported by a selection of sub-questions as follows:

What is the impact of freeze-thaw cycles on the durability of the wrapped composite joint?

1. *What method can be used for freeze-thaw ageing of composite material used in the wrapped composite joint?*
2. *What physical effects can be observed on the surface of the composite material as a consequence of the freeze-thaw cycles?*
3. *What changes in saltwater uptake can be seen as a result of exposure to freeze-thaw cycles compared to constant immersion?*
4. *What is the effect of freeze-thaw cycles on the tensile properties of the composite material?*
5. *What is the impact of temperature changes on the steel-composite interface of a Fs X90 joint?*

1.5. Research methodology

The research can be divided into four parts:

- State of the art
  Firstly, background theory on water uptake, surface degradation and thermal behaviour is explained. With this knowledge, a literature review into FT ageing and its effects on material properties is presented. To conclude, a summary of a selection of FT ageing methods is presented and the main takeaways from these different methods are discussed.
- Effect of FT cycles
  Based on the analysis of different FT ageing methods and the service life conditions of an offshore supporting structure, the ageing methodology is determined. This methodology is applied to LV_f and HV_f material. After a selection of FT cycles, these materials are microscopically investigated, weighed to determine saltwater uptake and cut into coupons to test tensile property retention. To help determine the meaning of the experimental weighing of the material during ageing, a numerical analysis is performed on LV_f material.
- Thermal response
  Firstly, the methodology applied to model the thermal response of a joint is discussed. Secondly, the numerically determined heat transfer within the joint on a warm morning is validated with an experiment on a Ms X90 joint. This validated model is then extrapolated to a Fs X90 joint. The strains developed on the interface between steel and composite are determined. Thirdly, a hypothetical cold night is numerically evaluated for both Ms and Fs.
- Wrapping up
  This part combines all knowledge gained in this research, experimentally and numerically, into the conclusion with discussion and recommendations for further research.

1.6. Structure of research report

The structure of the upcoming chapters in this research can be summarised as follows

2 State of the art
  - Background theory
  - Literature review
  - Review of ageing methods in standards and literature

3 Effects of freeze-thaw cycles
  - Development FT ageing methodology
  - Impact of FT ageing on the surface of the composite material
  - Impact of freeze-thaw ageing on saltwater uptake

- Impact of freeze-thaw ageing on tensile resistance

4 Thermal response
- Methodology for modelling
- Impact of a warm morning on developed strains
- Impact of a cold night on developed strains

5 Wrapping up: conclusion and recommendations

Appendices

2

State of the art

This chapter will discuss three types of literature reviews that have been performed in preparation for this research. Firstly, the theory forming the conceptual backgrounds for the diffusion of water in composite materials, wetting angle and heat transfer are discussed in Section 2.1. Secondly, existing literature on the effects of FT cycles on different composite material properties and interface properties between steel-composite bonded joints is summarised in Section 2.2. Thirdly, and lastly, a selection of FT cycles ageing methodologies are summarised and discussed in Section 2.3.

2.1. Background theory

This section forms a summary of the theoretical knowledge used in this research. It can be divided into three parts:

1. Diffusion of water.
   This part will shortly describe the processes influencing the diffusion of water into composites and the possible detrimental effects it can have.
2. Wetting angle.
   From the proposed surface investigation methods in this research, visual changes, surface roughness, profile height and wetting angle, the latter does not directly intuitively show its meaning. To help understand the wetting angle, and what a change in wetting angle could mean, the theory behind it is introduced.
3. Heat transfer.
   To be able to adequately develop a methodology for modelling and validating heat transfer in a wrapped composite joint, knowledge about the processes involved is essential. To guide the reader in understanding these different principles, they are introduced one by one together with their governing equations.

The goal is that this theoretical knowledge will help the reader understand the concepts that will be discussed in this research.

2.1.1. Diffusion

As described in Section 1.1 the zone where FT cycles can take place, can also submerge due to tidal action. This will cause mass diffusion of water into the composite. This section describes the processes at play, and the degradation of the material this can have as a result. The flux of particles can be described by, amongst many, Fick's law, which is as follows [26]:

$$J = \frac{dm}{dtA} = -D \cdot \frac{\partial C}{\partial x} \tag{2.1}$$

Where

J = flux of any particles (for example ions) [mol/m^{2}s]
dm = the change of the amount of particles [mol]
dt = small increment of time [seconds]
A = surface area of the 1D surface [m^2]
D = diffusion coefficient [m^2/s]
C = concentration of particles in the volume [mol/m^3]
x = position [m]

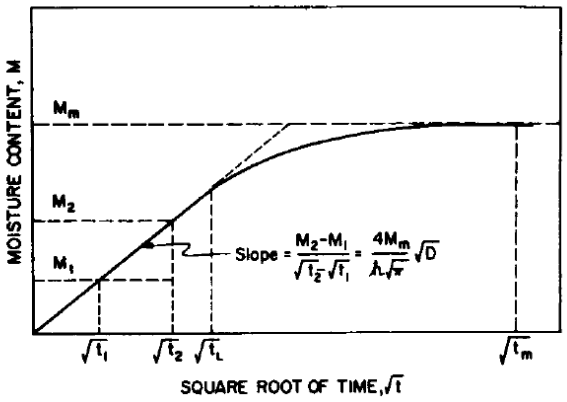


Figure 2.1: Fickian moisture content change [27]

Diffusion is gradient driven, but can be accelerated by the presence of porous material, micro-cracks in the matrix, and micro-cracks along the fibre-matrix interface resulting in a capillary effect as a result of the present (manufacturing) defects [28].

The equation shows the movement of particles from high to low concentration. The driving influence in this equation is the concentration gradient [26]. It is assumed that pressure and temperature are constant.

The movement of particles will continue until saturation is reached, M_m, as shown in Figure 2.1. The figure shows a constant diffusion rate at the beginning, which can be calculated as follows [27]:

$$D = \pi \left(\frac{h}{4 \cdot M_m} \right)^2 \left(\frac{M_2 - M_1}{\sqrt{t_2} - \sqrt{t_1}} \right)^2 = \pi \left(\frac{h}{4 \cdot M_m} \right)^2 \cdot slope^2 \tag{2.2}$$

Where

h = thickness of material [mm]
M_m = maximum moisture content of material [%]

It is assumed diffusion takes place in one direction, which is only true when edges are sealed, for example by coating, or when the diffusion is dominant in one direction due to, for example, a minimised thickness.

Diffusion of water will initially follow the graph presented in Figure 2.1 but will be disrupted by degradation. This degradation can be reversible and irreversible and can change the diffusion rate and the saturation moisture content. For fibre-reinforced composites these effects will be most severe when cross-linking has not fully formed, connecting the polymer chains. To develop sufficient cross-linking, the matrix should reach a sufficient temperature during production to fully cure, or the material should be post-cured.

Plasticisation and swelling are both forms of short-term damage, which are reversible when the material is dried after short exposure to moisture. During plasticisation, water acts as a plasticiser, increasing the flexibility of the matrix and softening it. Swelling of the matrix pushes polymer chains apart, increasing volume and weakening the bond between fibre and matrix [29].

Hydrolysis, micro-cracking and polymer relaxations are examples of long-term non-reversible damages. During hydrolysis water molecules react with the polymer chain, cutting it into smaller parts, shown in Figure 2.2. This causes the formation of voids, micro-cracks and loss of mass, reducing the strength [30].

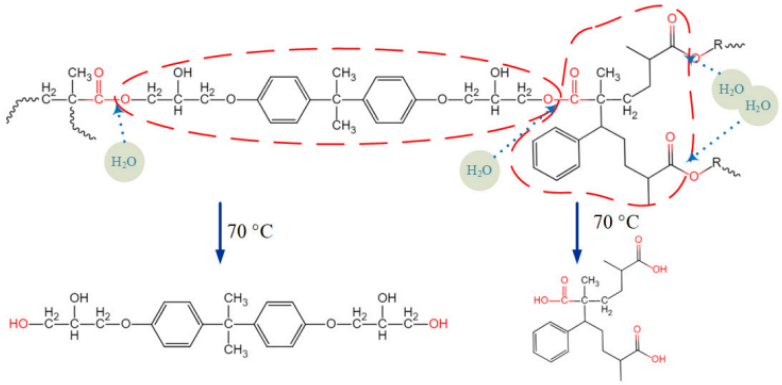


Figure 2.2: Hydrolysis of a vinyl ester polymer [30]

Polymer relaxation occurs when polymer chains move to a new equilibrium state, reducing internal stresses caused by the diffused water. This new equilibrium state causes voids to redistribute, making room for more water to diffuse into the material. This will increase the maximum moisture content above the Fickian saturation, M_m as shown in Figure 2.1 [32].

These degradation mechanisms can result in moisture uptake curves of composites being non-Fickian curves, either due to weight loss by the leaching of components, or additional weight gain by for example polymer relaxation [32]. Figure 2.3 shows an example of a moisture uptake graph with long-term degradation effects increasing the maximum moisture content [31].

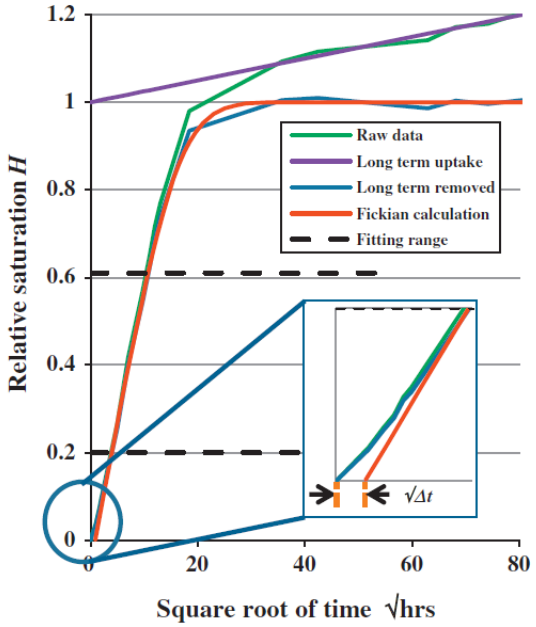


Figure 2.3: Schematic representation of long-term diffusion contribution [31]

When a material is subjected to FT cycles and water is embedded, more non-reversible degradation due to the presence of water may take place. When saltwater freezes it expands and salt particles crystallize, resulting in internal pressure, just as with swelling, which eventually could lead to micro-cracking. This means that there is a possibility that the addition of FT cycles could increase the rate of diffusion and the saturation moisture content. Section 3.3 will shed further light on this uncertainty by experimentally and numerically determining the effect of FT cycles on saltwater uptake.

2.1.2. Wetting angle

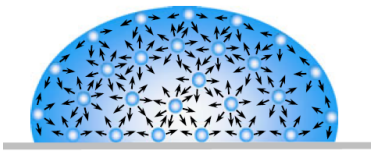


Figure 2.4: Visualisation of internal forces in droplet [33]

One way to determine if a surface tends to absorb a liquid, is by measuring the contact angle, or wetting angle. This angle represents the balance of forces between the three phases: liquid, solid and vapour (air) [33].

Inside a droplet, cohesive forces between neighbouring molecules pull at each other to create a force balance. However, at the contact line with air and the solid, the molecules are only pulled inward, giving the droplet its shape, shown in Figure 2.4[33].

The shape of this droplet will adjust to minimise the overall surface free energy, balancing these internal forces and the forces related to the interaction with the air and solid [33]. When diving deeper into these balancing interactions the following can be seen [34]

- Energy is released at the interface between the solid and the liquid as the liquid further spreads over the surface and the area of the solid-liquid interface grows.
- Energy is consumed by the increase of the size of the interface between liquid and air.

When these processes reach an equilibrium, the droplet stops spreading and the contact angle can be measured.

In case of increased surface roughness, the contact area between the droplet and the solid increases compared to a smooth solid. This means that more energy is released over the same apparent area, resulting in further spread of the droplet to facilitate the equilibrium between the solid-liquid and liquid-vapor interface. In the case of a solid with high surface energy, meaning a wetting angle below 90°, a rougher surface will result in an even smaller contact angle [34].

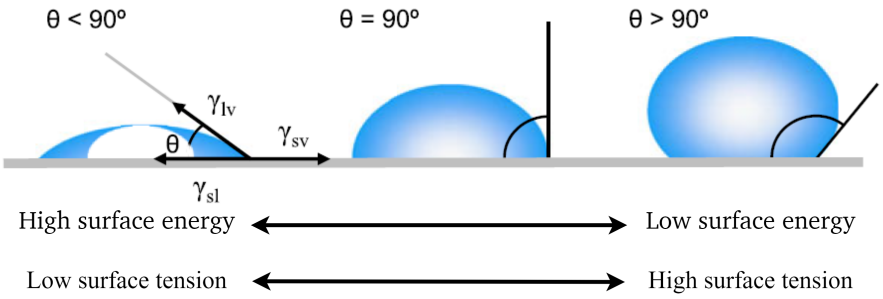


Figure 2.5: Variety in wetting angle (adapted from [33])

When considering the relationship between the wetting angle and the water absorption rate, research into medicine and wood polymers has shown a negative relationship. This means that as the wetting angle decreases, the rate of water absorption increases [35, 36]. This can be explained by the surface energy increasing and the surface tension reducing. This will result in increased capillary action on the surface and increased interaction between the solid and the water droplet, resulting in the absorption of the liquid.

In the context of this research, a decrease in the wetting angle could form an indicating parameter for an increase in saltwater diffusion rate. To determine if this relationship is present, the surface roughness, wetting angle and saltwater uptake of material exposed to FT cycles is measured.

2.1.3. Heat transfer

The transfer of heat can be described by different processes:

- Conduction - the transfer of thermal energy through a solid, liquid or gas by direct contact. This transfer will occur from a region of high temperature to a region of low temperature.
- Convection - the transfer of heat in fluid due to the physical movement of particles. This movement is generated by either temperature difference or mechanically, for example by the wind.
- Radiation - radiation emitted by a warm body is partially absorbed by another body and transformed into heat

These processes are crucial in understanding how to adequately model the impact of temperature on the joint in Chapter 4. These processes will now separately be addressed.

Conduction

Conduction is the process of heat transfer through a solid, liquid or gas by microscopic particles in the substance transferring energy from particles with high energy to particles with lower energy [37]. This can be represented by Fourier's one-dimensional law of conduction [38]:

$$q_{conduction} = -k \cdot \frac{dT}{dx} \tag{2.3}$$

Where

q = heat transfer [$\frac{\mathrm{W}}{\mathrm{m}^2}$]
k = thermal conductivity [$\frac{\mathrm{W}}{\mathrm{m} \cdot ^\circ\mathrm{C}}$]
dT = temperature difference between cold and warm side [°C]
dx = thickness of material [m]

The equations show that heat transfer takes place in the direction of the gradient, from high to low temperature. Thermal conductivity represents the ability of a material to conduct heat. A low thermal conductivity represents a low heating rate of a material based on a temperature gradient within that material. Equation 2.3 is based on a few assumptions:

- The heat transfer rate is constant over time
- The material considered has uniform properties in all directions
- The thermal conductivity is independent of temperature change
- The material itself does not generate heat

Convection

Convection is a macroscopic process where a fluid flows over an object and, when there is a temperature difference, transfers heat in the direction of the lower temperature. This transfer of heat takes place by the physical movement of particles in the fluid in the direction of the temperature gradient [37]. This can take place through free convection, forced convection or mixed convection. In all types of convection, the heat transfer rate is determined by the heat transfer coefficient h. Convection is described by Newton's law of cooling [37]:

$$q_{convection} = \pm h(T_s - T_a) \tag{2.4}$$

Where

h = heat transfer coefficient [W/m^2°C]
T_s = temperature of the surface of the object [°C]
T_a = temperature of air [°C]

The heat transfer coefficient is however dependent on multiple factors:

- Properties of the air: density, viscosity, thermal conductivity and specific heat
- Type of flow, either laminar or turbulent
- Shape of the area the flow passes through: through a circle, through a rectangle or over a flat surface
- Roughness of the surface
- Orientation of the surface to gravity

This complicates determining this factor. The following section will explain how this factor can be estimated. This will be done by first introducing all dimensionless numbers defined in heat transfer. Afterwards, it is explained how the different types of convection can be characterized. Here the assumptions are made that all convection discussed in this research can be described as flow over a flat surface, and if applicable, characteristics are averaged over the surface, instead of considered locally.

Nusselt Number
Considering flow over a flat surface, the fluid layer adjacent to the solid has no velocity due to the no-slip condition. This stationary layer is called the thermal boundary layer and only transfers heat by conduction. The heat transfer between the flat surface and the thermal boundary layer is thus purely by conduction.

Fluid layers farther away from the solid are however not stationary, resulting in heat transfer by convection between the thermal boundary layer and the moving fluid. The Nusselt number, *Nu*, is a non-dimensional number describing the ratio between convective and conductive heat transfer and is defined as follows [37]:

$$Nu = \frac{h \cdot L_c}{k} \tag{2.5}$$

Where

L_c = characteristic length [m]
k = thermal conductivity of the fluid [J/(kg°C)]

In case $Nu = 1$, it shows convection and conduction are equal over the characteristic length. However, in most scenarios, convection is more effective, resulting in $Nu > 1$.

For flow over a flat plate with constant temperature, the following equation can be used for the characteristic length [37]:

$$L_c = A/P \tag{2.6}$$

Where

A = surface area of flat plate [m^2]
P = perimeter of flat plate[m]

By determining Nu it is possible to determine the heat transfer coefficient by Equation 2.5. The following equations can be used to determine Nu [37]:

$$Nu = \begin{cases} C \cdot Ra^m & \text{free convection} \\ C \cdot Re^m \cdot Pr^n & \text{forced convection} \end{cases} \tag{2.7}$$

Where

Ra = Rayleigh number [-]
Re = Reynolds number [-]
Pr = Prandtl number [-]
C, m, n = experimentally determined constants

Now the other non-dimensional numbers will be discussed.

Reynolds number
For determining the effectiveness of the convection from the thermal boundary layer to the moving fluid, it is important to know the type of flow over the object. Flow can either be described as laminar or turbulent, as visualised in Figure 2.6.

For convection, it is important to know the type of flow over the object. This can be described by calculating the ratio of internal forces to viscous forces in a fluid flow, known as the Reynolds number, *Re*, and is calculated as follows [37]:

$$Re = U \cdot \frac{L_c \cdot \rho}{\mu} \tag{2.8}$$

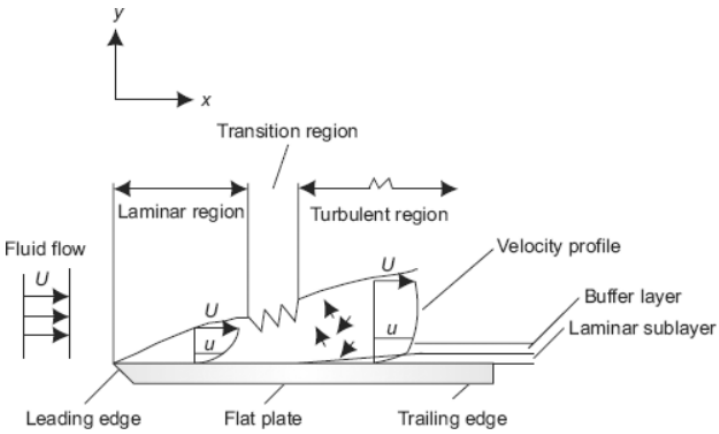


Figure 2.6: Visualisation laminar and turbulent flow [37]

Where

U = mean velocity of flow [m/s]
ρ = density of the fluid [kg/m^3]
μ = dynamic viscosity of the fluid [kg/(ms)]

When the Reynolds number is low, the viscous forces dampen out the inertia forces causing fluctuations in the velocity profile and the flow is laminar. When the Reynolds number is above the critical value of $5 \cdot 10^5$, the inertia forces become so large compared to viscous forces that the flow becomes more chaotic, and turbulent. This means that there is more heat transfer when the flow is turbulent.

Prandtl number
The Prandtl number, *Pr*, is the ratio between the rate at which momentum is transferred and the rate at which heat is conducted. $Pr << 1$ indicates that heat diffuses quickly compared to velocity changes, and vice versa for $Pr >> 1$. For most gasses $Pr \approx 1$. The Prandtl number can be calculated as follows [37]:

$$Pr = \frac{\mu \cdot c_p}{k} \tag{2.9}$$

Where

c_p = specific heat capacity [W/m°C]

Grashof number
The Grashof number, Gr, is used to indicate the ratio between buoyancy forces and viscous forces at play with free convection and can be calculated as follows [37]:

$$Gr = \frac{g \cdot \beta \cdot \Delta T \cdot L_c^3}{\nu^2} \tag{2.10}$$

Where

g = gravitational acceleration[m/s^2]
β = thermal volume expansion coefficient [°C^{-1}]
ΔT = temperature difference between surface and fluid [°C]
ν = Kinematic viscosity [m^2/s]

Rayleigh number
The Rayleigh number, Ra, is analogous to the Reynolds number, but then for free convection, and characterizes if the flow is laminar or turbulent [37]:

$$Ra = Gr \cdot Pr \tag{2.11}$$

If $Ra > 10^7$ the flow over a flat plate is turbulent.

Determining type of convection
To determine if convection is free, forced or mixed, the following equations can be considered[37]:

$$\begin{cases} Gr/Re^2 << 0.1 & \text{forced convection, free convection negligible} \\ Gr/Re^2 >> 10 & \text{free convection, negligible forced convection} \\ 0.1 < Gr/Re^2 \approx 10 & \text{mixed convection} \end{cases} \tag{2.12}$$

When the type of convection is known, the Nusselt number can be calculated by using empirical formulas as shown in Equation 2.7.

Forced convection
Equation 2.8 should be used to determine if the flow is turbulent or laminar. When the flow is turbulent, however, it should be determined if the size of the laminar region, as visible in Figure 2.6, can be neglected. This is done by determining the critical length, x, in $metres$, over which the flow is laminar [37]:

$$x = \frac{Re_{crit} \cdot \nu}{U} \tag{2.13}$$

Where $Re_{crit} = 5 \cdot 10^5$. In case $x/L_c << 1$, the laminar flow can be neglected. The average Nusselt number can now be calculated as follows [37]:

$$\begin{cases} Nu = 0.664\sqrt{Re} \cdot Pr^{1/3} & \text{for } Pr \geq 0.6 \text{ and } Re < 5 \cdot 10^5 \\ Nu = 0.036 \cdot Re^{4/5} \cdot Pr^{1/3} & \text{for } 0.6 < Pr < 60 \text{ and } 5 \cdot 10^5 < Re \\ Nu = \left(0.036 \cdot Re^{4/5} - 836\right) \cdot Pr^{1/3} & \text{for } 0.6 < Pr < 60 \text{ and } 5 \cdot 10^5 < Re \text{ with laminar region} \end{cases} \tag{2.14}$$

All formulas presented above should be used with caution when $Re > 10^7$, as this is formally outside of the experimental range used.

Free convection
Equation 2.11 should be used to determine if the flow is turbulent or laminar. Then it should be considered if the flat plate considered is the upper or lower surface of a hot plate[37]:

- Upper surface of a hot plate

$$\begin{cases} Nu = 0.54 \cdot Ra^{1/4} & \text{for } 10^4 < Ra < 10^7 \\ Nu = 0.15 \cdot Ra^{1/3} & \text{for } 10^7 < Ra < 10^{11} \end{cases} \tag{2.15}$$

- Lower surface of a hot plate

$$\{Nu = 0.27 \cdot Ra^{1/4} \quad \text{for } 10^5 < Ra < 10^{11} \tag{2.16}$$

Mixed convection
When the convection is mixed between free and forced, both the forced and free Nusselt number should be calculated, to determine the mixed Nusselt number as follows [37]:

$$Nu^m = Nu^m_{forced} \pm Nu^m_{free} \tag{2.17}$$

Where $m = 3$ is recommended, and the sign of the formula is determined by the direction of the free and forced convection flow.

Radiation

Radiation is the process where electromagnetic waves cause heat transfer. The waves obey the laws of light, and can thus be considered light with a wavelength between 0.1μm and 100μm, as this is the wavelength known to be converted to heat when absorbed by a body [37]. The governing equation is the Stefan-Boltzmann law [37]:

$$q_{radiation} = \sigma \cdot T^4 \tag{2.18}$$

Where

σ = Stefan-Boltzmann constant $5.6697 \cdot 10^{-8} \frac{\text{W}}{\text{m}^2 \text{°C}^4}$
T = temperature [°C]

However, Equation 2.18 assumes that all energy is absorbed or emitted, as a black body would. By using reduction factors describing emissivity (ε) and absorptivity (α) based on the surface material and finish, we can more realistically describe the radiation [37].

In case the material is to any degree transparent, radiation can pass through the body. This effect is not considered here as all materials part of this master thesis are not translucent.

2.2. Literature review

As discussed in Impact of environmental factors (Section 1.1.3), FT ageing can cause multiple types of degradation. As discussed by [22, 23, 39, 40], they can be summed up as follows:

- Damage to the fibre matrix interface
  As the fibre is the main contributor to the strength and stiffness of composites, this interface is crucial to the load transfer between the two elements.
  - Due to the differences in CTE, inter-laminar shear can develop in the interface. This can lead to debonding. Especially cyclic temperature loading will enhance this effect due to the repeated unequal expansion and contraction around the interface.
  - When water particles are present, they will expand during freezing, which will cause additional wicking that can damage the interface between composite and steel.
- Damage to the matrix
  - The difference in CTE of the matrix and fibre will cause the matrix to contract more when exposed to subzero temperatures than the fibre. This contraction is however prevented by the fibres. This will result in internal stresses, which can cause micro-cracks in the matrix. This can increase, for example, water ingress, but also decrease the overall strength and dimensional stability of the matrix.
  - When water is present in the matrix, during freezing it will expand, resulting in micro-cracking of the matrix. In case salt deposits are present, the salt can crystallize and expand, even further damaging the matrix.
  - The subzero temperatures can lead to matrix hardening, making the matrix more brittle. This increased stiffness but reduced ductility makes it prone to plastic deformations. If the temperature is below the matrix freezing point, these effects will be enhanced to a catastrophic extent.
  - During curing of the matrix shrinkage occurs, resulting in internal stresses directly after production. If a composite is then placed in a cold environment, there is no possibility of relaxation of shrinkage stresses, only an increase, which will increase matrix micro-cracking.

The majority of degradation due to FT cycles can be explained by the difference in CTE of fibre and matrix. However, in literature a variety of fibres and matrices are combined, reducing direct comparability between research. Figure 2.7 shows the ratio between the CTE of the matrix and fibre for different combinations in longitudinal direction [41], as primarily in that direction there is a high variability. The dotted lines represent the range for a vinyl ester matrix and glass fibre comparable to the material applied in this research. All ratios above 125 are omitted for readability of the figure.

Next, it should be noted that carbon fibres have a negative CTE in the longitudinal direction, which is, for readability, shown in absolute value. This negative CTE compensates for the large CTE of the matrix, which can result in composites produced with these fibres showing lower overall CTE of the composite. However, due to these differences in the CTE of fibre and matrix, internal stresses in these composites will be higher. [42] has for example shown internal longitudinal strains of glass fibre-reinforced epoxy composites are on average 7 times larger than carbon fibre, and basalt fibre-reinforced epoxy composites are on average 8 times larger. But, when regarding the internal stresses in carbon fibre composites, they are 11% higher than in glass fibre and basalt fibre reinforced epoxy composites due to carbon fibre's high stiffness [42].

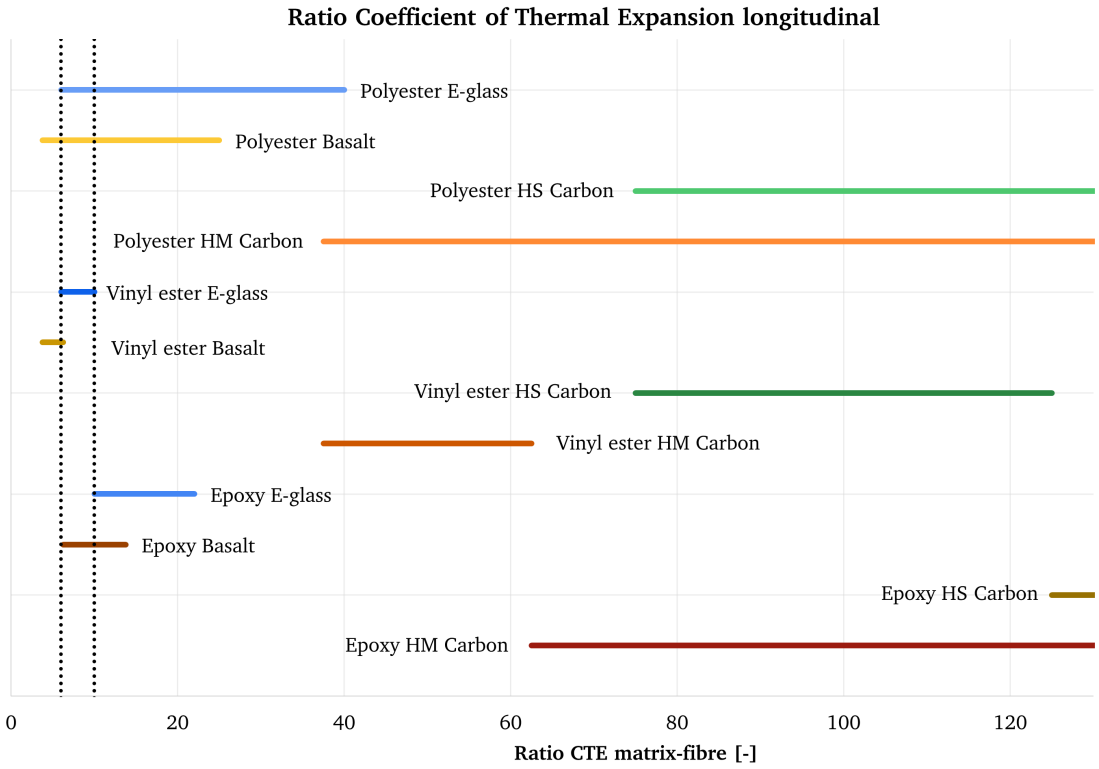


Figure 2.7: Ratio CTE of matrix and fibre in longitudinal direction [41]

Next to these differences of CTE, apart from basalt fibres, all fibres have a thermal conductivity which is at least 10 times higher than resin. Generally speaking, this will result in composites with a higher fibre volume fraction showing a faster transfer of heat. Figure 2.7 and the knowledge about the conductivity of composites, aids in comparing different studies with each other, to finally conclude what degradation is expected and which properties are most affected by FT cycles in the context of the wrapped composite joints. This literature review will discuss the following properties and types of tests: tensile strength, inter-laminar shear strength, in-plane shear strength, compression strength, sustained loading, bonded interface tests and moisture uptake tests.

These properties will be addressed for FT ageing performed without and with the presence of moisture, either during the ageing or during the conditioning of material before the start of ageing. The results of the literature review are presented per property and primarily in tables to aid in comparing literature. Next to this, the emphasis is on longitudinal properties, as the ply lay-up used in the wrapped composite joint, Section 1.3, has only a minor difference in fibre fraction in the longitudinal and transverse direction.

To conclude, it is summarised which ageing condition and which material property seems to have the most detrimental impact on the wrapped composite joint, to guide in an appropriate testing plan.

2.2.1. Tensile property retention

Table 2.1 shows a literature summary of tensile property retention after exposure to FT cycles. It is visible that ageing with water, either during a preconditioning stage or during the thawing stages, greatly reduces property retention. When only regarding material with a CTE ratio, Figure 2.7, close to fibre glass-vinyl ester; (results for basalt fibres and glass fibres) results considering FT cycles with moisture (either preconditioning or wet thawing cycle) on average indicate a reduction of 10% in tensile strength, minor reduction, or maybe increase in modulus and an unclear response for tensile strain after exposure to FT cycles [22, 25, 24, 43, 44]. Of this research, when mentioned, fibre volume fractions of the used materials are 45% or higher. Literature reporting degradation after preconditioning phases shows -2% to -5% strength reduction during preconditioning [24, 43].

Regarding the effect of FT cycles on tensile properties, it should be considered that reaching the full capacity of the fibres is only possible with adequate load transfer between fibres and matrix. FT cycles are expected to degrade the matrix and as an effect of that also the interface between the fibres and matrix, resulting in a lower tensile strength after ageing [22]. As the modulus is predominantly determined by the glass fibre, FT cycles are not expected to affect it.

Table 2.1: Summary tensile property retention after FT cycles from literature

Tensile properties										
Source	Fibre	Matrix	Wet/dry	Precondition [days, °C]	ΔT [°C]	Time per cycle [h]	FT	Strength	Modulus	Strain
[22]	Glass	Polyester	Dry	-	30	1.3	300	+11.8%	+10.1%	-
				224, 25				-13%	-4%	-
[23]	Carbon	Vinyl ester	Dry	-	32.5	24	100	-8.17%	-6.02%	-
			Wet distilled	-				-9.75%	-6.93%	-
			Wet salt	-				-16.1%	-6.93%	-
[25]	Glass	Vinyl ester	Dry	-	32.5	24	100	-9.13%	-3.9%	-
			Wet distilled	-				-9.57%	-4.93%	-
			Wet salt	-				-13.5%	-10.5%	-
[42]	Basalt	Epoxy	Dry	-	60	24	90	0%	0%	+10%
	Carbon			-				-18%	-16%	0%
	Glass			-				0%	0%	+15%
[24]	Basalt	Polyester	Wet	30, 20	43	14	300	-16%	-6%	-
[45]	Carbon	Epoxy	Wet	-	28	5 - 6	300	0%	-6.1%	

Table 2.1: Summary tensile property retention after FT cycles from literature (Continued)

[43]	Glass	Polyester	Wet	30, 20	43	13.4	200	-7% (dry) -11% (wet)	-	-
	Glass	Vinyl ester						+3% (dry) -3% (wet)	-	-
[44]	Basalt	Epoxy	Wet	Preconditioned, but unknown duration and temperature	45	3 - 5	200	-1%	+10%	-10%
	Carbon							-14%	-2.7%	-14%
	Glass							-15%	0%	-16%
[39]	Glass	Epoxy	unclear	unclear	40	24	90	-15.39%	-	-

2.2.2. In-plane shear property retention

Almost all results in Table 2.2 refer to fibre-matrix combinations that can be within range for glass-vinyl ester, except carbon-epoxy. Apart from the results of [22], where especially the preconditioning stage results in degradation, the suspicion is raised that in-plane shear properties will be affected minimally by FT cycles.

Table 2.2: Summary in-plane shear property retention after FT cycles from literature

In-plane shear properties										
Source	Fibre	Matrix	Wet/dry	Precondition [days, °C]	ΔT [°C]	Time per cycle [h]	FT	Strength	Modulus	Strain
[22]	Glass	Polyester	Dry	-	30	1.3	300	-2.7%	-2.2%	-
				224, 25				-29.7%	+2.5%	-
[24]	Basalt	Polyester	Wet	30, 20	43	14	300	-7%	-16%	-
[43]	Glass	Polyester	Wet	30, 20	43	13.4	200	+8% (dry) +3% (wet)	-	-
	Glass	Vinyl ester						+8% (dry) 0% (wet)	-	-
[46]	Basalt	Epoxy	Wet	-	25	3 - 4	200	0%	+11%	-6%
	Carbon							-13%	-2%	-13%
	Glass							-13%	0%	-13%

2.2.3. Inter-laminar shear property retention

Table 2.3 shows a contradicting view of the effect of FT cycles on inter-laminar shear properties at first glance, however, [24] shows a -19% strength reduction after the preconditioning phase. This raises the hypothesis that effects due to moisture penetration are more degrading for composites than exposure to FT cycles.

Table 2.3: Summary inter-laminar shear property retention after FT cycles from literature

Inter-laminar shear								
Source	Fibre	Matrix	Wet/dry	Precondition [days, °C]	ΔT [°C]	Time per cycle [h]	FT	Strength
[24]	Basalt	Polyester	Wet	30, 20	43	14	300	-8%
[43]	Glass	Polyester	Wet	30, 20	43	13.4	200	+3.5% (dry) +2.5% (wet)
	Glass	Vinyl ester						+2/% (dry) +7% (wet)
[39]	Glass	Epoxy	unclear	unclear	40	24	90	-5.11%

2.2.4. Compression strength

Table 2.4 shows that transverse compression strength is severely impacted by FT cycles. As the interface between the fibre and matrix degrades, the confinement of the fibre preventing buckling and kink reduces. This effect is that, alongside local imperfections, the compression strength is heavily impacted. Longitudinal compression in [24, 43] already shows significant strength degradation after preconditioning, respectively -21% and -4% (polyester) and -9% (vinyl ester). This raises the question of whether during the service lifetime of the wrapped joint moisture content would be high enough to show similar degradation when FT cycles occur.

Table 2.4: Summary compression property retention after FT cycles from literature. [1] Transverse direction

Compression properties								
Source	Fibre	Matrix	Wet/dry	Precondition [days, °C]	ΔT [°C]	Time per cycle [h]	FT	Strength
[23]	Carbon	Vinyl ester	Dry	-	32.5	24	100	-17.5%[1]
			Wet distilled	-				-25.9%[1]
			Wet salt	-				-29.8%[1]
[25]	Glass	Vinyl ester	Dry	-	32.5	24	100	-9.5%[1]
			Wet distilled	-				-25.8%[1]
			Wet salt	-				-29.5% [1]
[24]	Basalt	Polyester	Wet	30, 20	43	14	300	-15%
[43]	Glass	Polyester	Wet	30, 20	43	13.4	200	+6% (dry) -13% (wet)
	Glass	Vinyl ester						-8% (dry) -19% (wet)
[39]	Glass	Epoxy	unclear	unclear	40	24	90	-8.21%

2.2.5. Degradation bonded interface

Composites have been used throughout the years for varying strengthening systems with steel and concrete. In the majority of cases, an adhesive is used between the composite and secondary material. Even though it is not directly comparable with the wrapped composite joint, as it is not adhesively bonded, literature can gain an understanding of key aspects at play when subjecting these joints to FT cycles.

Without moisture

The majority of available research, shows results for FT cycles with water. However, [47] also tested unidirectional (UD) pultruded epoxy reinforced with carbon fibre composites adhesively bonded with steel, exposed to 'dry' FT cycles. Applying an FT cycle from -20°C to 20°C with a duration of 6 hours per step, double shear tests showed only a minor increase of +4.5% in strength after 250 FT cycles. The failure mode remained a cohesive failure throughout ageing, indicating the interface between the adherent and the composite and steel was not excessively damaged by FT cycles.

With moisture

When [47] includes an 18-month of a 36-month preconditioning stage in demineralised or saltwater of 45°C, the results change drastically. Preconditioning turned out to be the most detrimental environmental effect, with up to 65% reduction of bond strength after 36 months of saltwater preconditioning. However, after subjecting the material to FT cycles, properties are regained, resulting in a maximum of 5%. additional damage.

A contradictory image is shown in [48], where single lap shear bonded joints are tested. Depending on the used adhesive, up to 26% reduction of bond strength of UD carbon fibre reinforced epoxy composites adhered to steel is observed after only 30 FT cycles. The main difference between the ageing methods, is [48] showing a larger temperature range between +38°C and -18°C and a longer cycle duration of 24 hours. Apart from that, it is observed that the failure modes are vastly different. Before ageing complete delamination of the composite or cohesive failure took place. As FT cycles increased, the failure moved from delamination to adhesive failure and from cohesive failure to adhesive failure. This means the integrity of the bond between the adherent and the composite degraded, which may be an indication of the suitability of the type of adherent resulting in failure leaning more towards failure in the composite or at the composite bonded interface.

Using the same adherend [45] shows a degradation of 18% in single lap shear strength after 300FT cycles (6 hours per cycle, $\Delta T = 28$°C). On top of that, all carbon fibre-reinforced composite-steel specimens failed in the delamination of the composite.

When comparing [47, 48, 45], two conclusions can be drawn:

- The susceptibility of an adhering system between components to moisture is an important factor to take into account, as this is shown to cause the most degradation.
- Rapid FT cycles when using similar adherent systems, may result in less damage. This could be explained by internal thermal stresses not being fully developed in all materials, and between all materials, resulting in less internal stress build-up when shorter cycle times with less temperature range are used.

When putting these results in the context of the wrapped composite joint, it is imperative to notice two things.

Firstly, previous research has shown that water will not reach the interface between steel and composite during service lifetime [18]. This reduces the impact shown in [44, 49, 46] of water reaching the adherend.

Secondly, the CTE ratio of composites produced with carbon fibres and epoxy resin can be a minimum of 6 times larger than for glass fibre-reinforced vinyl ester composites, resulting in higher internal stresses. As the CTE of carbon is negative in the longitudinal direction, the CTE of the composite as a whole will be lower than for example a composite produced with glass fibres and epoxy resin. Nonetheless, the difference between the CTE of steel in the case of carbon fibres is significant, as summarised in Table 2.5, resulting in large stresses on the interface.

Table 2.5: CTE of steel [50] and epoxy composite reinforced with either basalt, carbon or glass fibre [42]

Material		CTE [$\cdot 10^{-6}$°C^{-1}]
Steel		11
Fibre	Matrix	
-	Epoxy	72.8
Basalt	Epoxy	12.4
Carbon	Epoxy	1.9
Glass	Epoxy	11

2.2.6. Moisture uptake

Table 2.6: Summary of moisture uptake under influence of FT cycles

Moisture uptake								
Source	Fibre	Matrix	Wet/dry	Post cured	ΔT [°C]	Time per cycle [h]	FT	Uptake [%]
[23]	Carbon	Vinyl ester	Wet distilled	Ambient	32.5	24	100	0.19
			Wet salt	Ambient				0.26
[25]	Glass	Vinyl ester	Wet distilled	Ambient	32.5	24	100	0.20
			Wet salt	Ambient				0.21
[42]	Basalt	Epoxy	Dry	Post cured	60	24	60	-0.09
	Carbon			Post cured				-0.12
	Glass			Post cured				-0.26
[22]	Glass	Polyester	Dry	Unclear	30	1.3	300	-0.42

Table 2.6 shows moisture loss and moisture gain in different scenarios during FT ageing. [22, 42] show the progression of moisture loss during ageing. In the first 10%-20% of the total amount of cycles, moisture decrease fluctuates heavily. Thereafter it progresses at a stable rate and shows a decline in weight loss rate at the last 20% of ageing in both cases.

[23, 25] show that moisture uptake with saltwater is slightly higher than for distilled water. This would raise the hypothesis that the saltwater during FT cycles degrades the surface more, resulting in more free paths for the water to ingress. However, the measuring interval is large and the material is not post-cured. The latter results in less polymer cross-linking which leaves the material more vulnerable to environmental degradation.

2.2.7. Influence sustained loading during ageing

Not much research is openly available discussing the combined effects of FT ageing and sustained loading for fibre-reinforced composites without encasement in concrete. [46] tested glass fibre, carbon fibre and basalt fibre reinforced epoxy composites under sustained loading and ageing. Rapid FT cycles were used for 3 to 4 hours per cycle, with a temperature range of +8°C to -17°C and submerged thawing. Composites reinforced by glass fibre and basalt fibre were loaded with a sustained tensile load of 30% of their ultimate resistance, and carbon fibre 40% during 300 FT cycles. Table 2.7 shows the retention of tensile strength, modulus and strain under sustained loading, and sustained loading and FT cycles for the different composites. This table shows that the addition of FT ageing to sustained loading only results in a minor decrease of properties compared to sustained loading without FT cycles and compared to tensile testing after FT cycles shown in Table 2.1.

Table 2.7: Summary results sustained loading during 300 FT cycles [46]

	Strength		Modulus		Strain	
FT aged or not		FT		FT		FT
Basalt	-2%	-3%	+1%	+7%	-7%	-12%
Carbon	-7%	-11%	-1%	0%	-9%	-15%
Glass	-13%	-19%	0%	-1%	-18%	-22%

2.2.8. Conclusion

This chapter has shown a review of the effects FT cycles could have on composite and composite-steel bonded material. It shows varying results, even for similar fibre and matrix combinations. Some clear conclusions can however be made:

- Introducing moisture to FT cycles causes the material to degrade more [23, 25].
- Tensile strength is expected to reduce by 10% due to FT cycles when considering the average of research on materials within the range of the CTE of glass fibre-reinforced vinyl ester composites. Tensile modulus and rupture strain are expected to be affected minimally.
- Compressive strength is expected to reduce at least 15% due to FT cycles.
- Due to the combination of glass fibre-reinforced vinyl ester composite and steel, it is expected that the interface between the materials is significantly affected by FT cycles. Due to the bond not being adhesive, it is however not possible to determine this extent of degradation without experimental testing.

When regarding the above comments, and the design methodology of the wrapped composite joint being centred around tensile strength, instead of compressive strength, a logical first step would be to test tensile property degradation due to FT cycles.

2.3. Review freeze-thaw ageing methods

This chapter summarizes FT ageing methods available from standards and deviating methods applied in the literature. The methods are shortly described to determine the most suitable testing method for this application and available equipment. The following methods are discussed:

1. NEN-EN 12371 - Natural frost resistance natural stones [51]
2. ASTM C666 - Concrete Resistance to Rapid Freezing and Thawing [20]
3. ASTM D6944 - Resistance Cured coatings to thermal cycling [21]
4. ASTM D7792 - Freeze-thaw cycles on pultruded composites [19]
5. Alternative methods described in the literature

To conclude this chapter it is discussed which ageing procedure is used as a basis for this research.

2.3.1. NEN-EN 12371 - Natural frost resistance natural stones

This standard is developed to determine the frost resistance of natural stones by FT ageing them and afterwards performing either mechanical or identification tests. Specimen size and number are determined based on the tests performed after the ageing [51]. Next to test specimens, one specimen with a thermocouple (TC) embedded mid-plane is positioned in the middle of the ageing environment. The number of cycles is continued to a maximum of 168. No further explanation on the determination of this amount of cycles is given. Ageing can be interrupted earlier based on the progression of visual damage. During ageing at prescribed intervals, specimens are rotated 180°around their horizontal axis.

Before ageing starts, specimens are submerged in tap water to saturate them. One ageing cycle consists of 6 hours of freezing in air of -12°C, and 6 hours submerged in water of 20°C. Per time-step, it is prescribed what the internal temperature of specimens should be. The environment should be altered to fit these margins.

If ageing is interrupted, specimens should be immersed in water. If the interruption is longer than 96 hours, specimens are taken out and wrapped to avoid evaporation.

The described procedure is not referred to in the literature. However, this standardized method comes accompanied by ageing equipment specially made to follow the ageing regime. The potential availability of such an integrated climate chamber eases the ageing process significantly.

When used for composites, an adapted regime should be followed, as time-temperature responses are now validated and based on natural stones, which is a material with a vastly different conductivity.

2.3.2. ASTM C666 - Concrete Resistance to Rapid Freezing and Thawing

This standard is developed for the ageing of concrete exposed to freezing and thawing. In literature [45, 44, 46] adopted a method similar to this method for testing, namely Chinese Standard GB/T 50082-2009. Numerous types of equipment have been produced to follow this standard FT ageing regime automatically following the strict margins for heating and cooling times.

The procedure is divided into two types of FT ageing: in combination with moisture during the full cycle (procedure A), and with moisture only during thawing (procedure B).

Procedure A describes each specimen should be surrounded by 1 mm - 3 mm of water at all times, whilst for procedure B this is only during the thawing phase. Temperature ranges are between -18°C and +4°C. Duration of each cycle is determined by the internal temperature of specimens, but should range from 2 hours to 5 hours total. When operations are interrupted, specimens should be stored frozen.

Compared to other standards, it is mentioned that tested specimens are advised to be replaced by dummies during the whole ageing procedure to create as uniform as possible conditions for all tested specimens. Where NEN-EN 12371 [51] suggests rotating specimens in the same place, ASTM C666 suggests rotating specimens over the full climate chamber [20].

Every 36 cycles specimens should be taken out to be tested. Testing is continued until 300 FT cycles in total, or when the relative dynamic modulus of elasticity has reached 60% of the initial value.

2.3.3. ASTM D6944 - Resistance Cured coatings to thermal cycling

This standard is developed to determine the effect of thermal cycles on coating (systems) [21]. They are intended to test properties determining the integrity of the system, such as adhesion and cracking. The method is one of two used for determining the ageing procedure in [39].

Two types of procedures are described: one involving submersion, freezing and thawing and one only involving freezing and thawing. The first procedure involves the cycle as presented in Table 2.8 and will be repeated for at least 30 cycles. The second procedure elongates the duration of exposure to 50°C to 8 hours, and immediately after cools down to -29°C.

Table 2.8: Ageing procedure for submersion, freezing and thawing ageing method according to ASTM D6944 [21]

Condition	Temperature [°C]	Time [h]
Air	50	4
Tap water	25	4
Air	-29	16

When ageing is interrupted, panels are kept in freezing conditions. Apart from that, the specimens are evaluated on defects every 5 cycles, or at the end of 30 cycles.

2.3.4. ASTM D7792 - Freeze-thaw cycles on pultruded composites

This standard is developed to set a method to determine the percentage retention of mechanical properties after exposure to FT cycles for pultruded composites. This retention is compared to samples exposed to an equivalent time of submersion in water without freezing. The main goal is not to mimic service life conditions

or obtain equilibrium conditions but to present a testing regime which is reproducible. An adapted version of this method is used in a variety of research [39, 24, 43].

The method describes FT cycles after 30 days of precondition in 23°C distilled water. The FT cycle consists of at least 3 hours of freezing in -20°C air, and 3 hours ± 10 minutes of thawing in 23°C distilled water. 100 FT cycles are executed. No reasoning for the amount of cycles is provided.

When ageing is interrupted specimens are left in freezing condition. After removing specimens from ageing, they should be tested as soon as possible.

[23, 25] use a similar temperature regime, but elongates freezing and thawing to 8 hours each. To compare the influence of moisture, specimens are thawed by air, in distilled water or saltwater. Specimens are exposed to 90 cycles, which correspond to a 25-year to 50-year life span in an offshore environment according to the author.

[47] uses a similar temperature regime as well, but swells 6 hours at the maxima. These are repeated for 250 cycles, based on local weather and previous research according to the author.

2.3.5. Ageing methods from literature

FT ageing methods used in literature that cannot be easily subdivided in the aforementioned standards, are discussed in this section. They can be divided into two types:

- Rapid freezing and thawing
  [22] defines an ageing regime between -10°C and 20°C, where there is a 20 minutes hold on each maximum. This is repeated for 300 cycles, which, according to the author, represents 25 years of offshore service life, and 125 years of service life for bridges.
- Long duration freezing and thawing
  [48] applies an ageing regime ranging between -30°C and +30°C with a 12 hours dwell at each maximum. TC is used to check that the material reaches the maximum temperatures during ageing. Thawing is done under 100% relative humidity to mimic a moist environment.

2.3.6. Conclusion freeze-thaw ageing methods

This chapter has shortly described a variety of ageing methods applied in literature and available in standards. The main points taken along for the development of an FT ageing methodology are as follows:

- The use of TC in specimens can be a useful tool to determine what temperature changes the specimens experience throughout a cycle.
- When ageing has to be interrupted specimens are stored in freezing conditions to not vastly increase potential moisture uptake or loss.
- Based on Section 2.2 a method should be used with a thawing phase including moisture.

Section 3.1 and Section 3.3.2 will describe how these points are then translated to the adapted methodology in this research.

3

Effects of freeze-thaw cycles

This chapter will discuss the effects of FT cycles on different aspects of the composite material. This will be done by experimentally ageing and testing material and comparing the results to material that is not aged by FT cycles.

Section 3.1 will discuss the developed ageing methodology used in this experimental research. To determine the appropriate ageing regime, climate models simulating air temperatures over the North Sea are used, which is the goal application area of the wrapped composite joint. This will guide in determining the temperature range and amount of FT cycles applied. This temperature range is then applied with the developed experimental setup.

This developed ageing methodology is then used to age LV_f and HV_f material. Both materials are taken into account to assess if in application one should have, from a durability standpoint, a preference over the other. Intermittently material is temporarily taken out of ageing to assess if and to what extent the surfaces of the material are damaged due to the FT cycles. This is determined by using different microscopic surface analyses registering changes in surface profile, surface roughness, wetting angle and visual changes in Section 3.2.

To assess if these damages directly influence the material, intermittently it is taken out and weighed. This will help determine if registered surface degradation increases saltwater uptake of the composite. On top of that, the results are compared to a FEA model for continuous submersion of a similar geometry as tested. This is discussed in Section 3.3.

To wrap up, the effect of these internal and external damages to the material when exposing it to FT cycles are assessed by determining the tensile property retention of the material after a maximum of 199 FT cycles in Section 3.4.

3.1. Development ageing methodology

This section describes the FT ageing methodology applied in this research and how this methodology was developed. By determining the temperature range applicable for a wrapped composite joint placed in the North Sea, the number of FT cycles and the duration of each FT cycle, it can be assessed whether an already existing standard or a specially defined ageing method is the most representative. This applied methodology is then described, and irregularities occurring during the experimental ageing are discussed.

3.1.1. Development methodology

The different steps performed to determine the temperature range, the number of cycles and the limitations of the experimental setup are hereafter described. To gain an understanding of the temperatures that can occur on the North Sea, historical model runs of the Climate Model Intercomparison Project (CMIP) from the sixth phase are used. These are climate models based on temperature measurements and observations of forcings, such as volcanic and solar, on the climate system as a whole. These complex models are validated against measured data and afterwards used as a basis to predict future climate. Appendix A describes the used climate model and the used script to extract and manipulate the data in more detail.

In the following subsections, this historical model data is used to determine the temperature range and number of cycles. Closing off, by experimenting with the setup, the duration of each cycle is determined.

Temperature range

As shown in Section 2.2 and Section 2.3, a variety of temperature cycles has been applied in literature and standards. DNV design standards for offshore wind turbines state that design temperatures should be between -20 °C and 50 °C [52]. However, this full range of temperature is a purely theoretical range when looking into the ambient temperatures at the North Sea, not accounting for the heating up of structures due to heat transfer.

To determine the ambient temperature range, daily minimum and maximum near-surface air temperatures at 2m height, respectively tasmin and tasmax, between 1850 and 2014 are extracted using CMIP CAS FGOALS-g3 historical experiment data [53]. Figure 3.1 shows that the minimum near-surface air temperatures registered over the North Sea are approximately -20 °C. Next to that, Figure 3.2 shows that the maximum temperature is between 20 °C and 25 °C.

These graphs represent the maximum and minimum temperatures for all seasons and all years. The maximum temperatures are registered in summer months, the minimum in winter months. This means, that on one day, the ambient temperatures will not be -20 °C and +20 °C. However, to enhance comparability with research and standards whilst making sure the temperature gradient is large enough to gain knowledge on this subject and degrade the material, a temperature range between -20 °C and +23 °C is used.

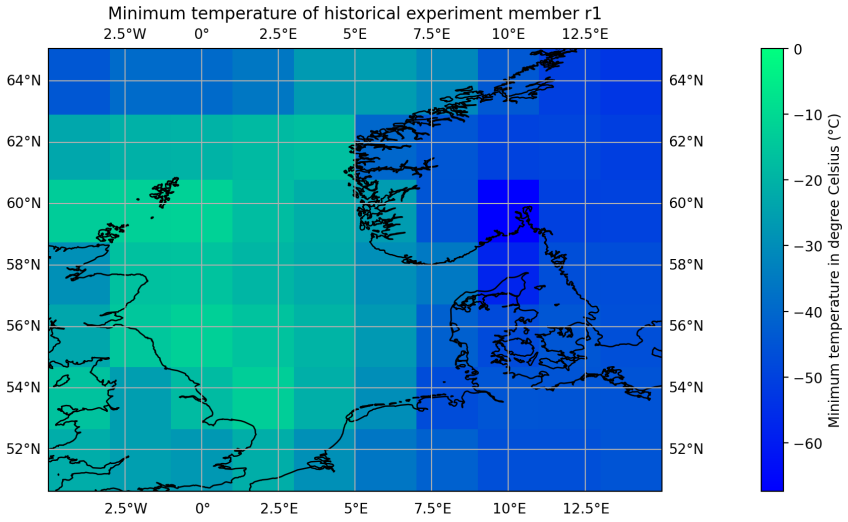


Figure 3.1: Modelled minimum near-surface air temperature over the North Sea [53]

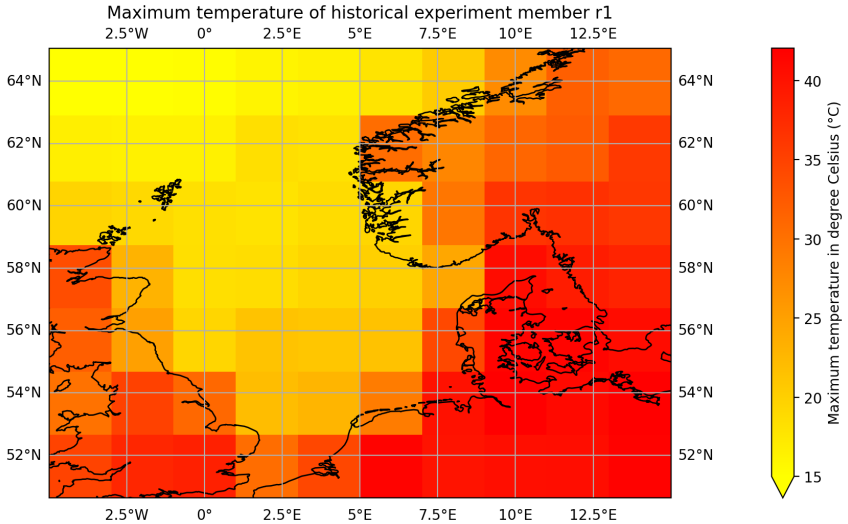


Figure 3.2: Modelled maximum near-surface air temperature over the North Sea [53]

Number of cycles

To know how many FT cycles a structure endures on the North Sea during a 35-year service life, the yearly amount of FT cycles is calculated using CMIP6 CAS FGOALS-g3 historical experiment data [53]. As discussed in Section 3.1.1 the maximum and minimum temperature on one day on the North Sea will not be respectively 23 °C and -20 °C. To get a first estimation of the number of FT cycles, the minimum temperature is set at -10 °C, and the maximum at thawing at 0 °C. The amount of FT cycles is calculated using xclim atmospheric indicator calculating the FT cycles that take place during one day [54].

Figure 3.3 shows the mean yearly amount of FT cycles between 1850 and 2014. It is shown that the majority of the North Sea has a yearly average of one FT cycle. Figure 3.4 shows the maximum yearly amount of FT cycles. This shows a maximum of 2 to 3 FT cycles in southern parts, but 6 FT cycles in northern parts. Combining the knowledge of both figures, whilst taking into account that FT cycles taking place over more than 1 day are not accounted for, a maximum amount of 200 FT cycles is considered in this research. This is equivalent to 6 FT cycles in a 35-year service life. This ensures that the results of this research are also applicable when considering northern parts of the North Sea.

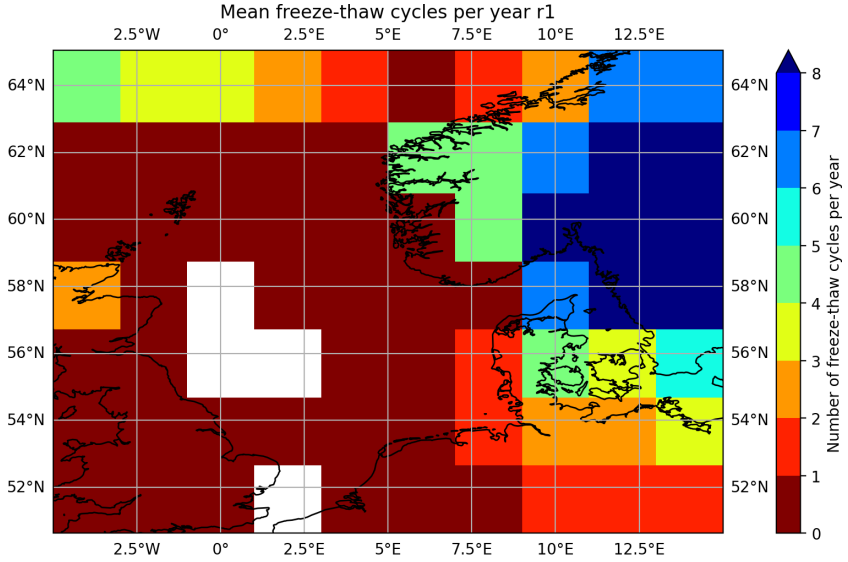


Figure 3.3: Modelled mean number of yearly FT cycles over the North Sea [53].

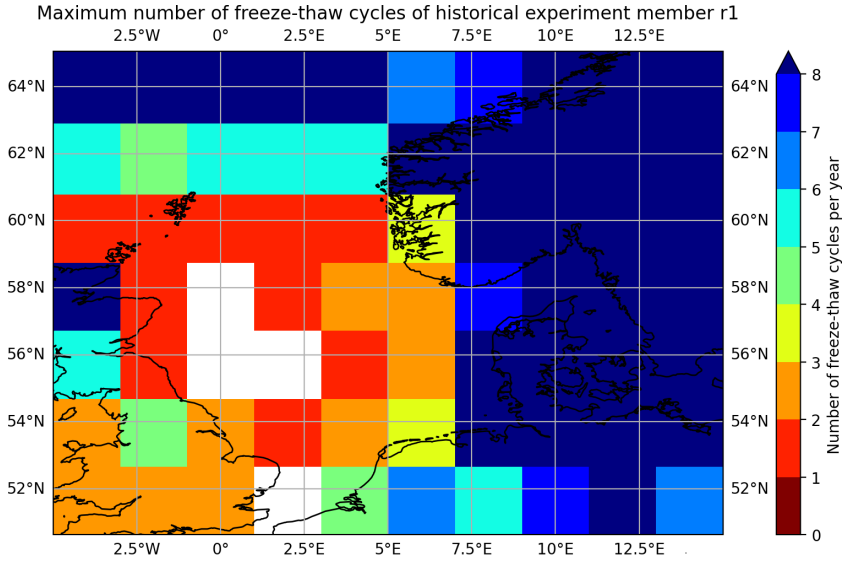
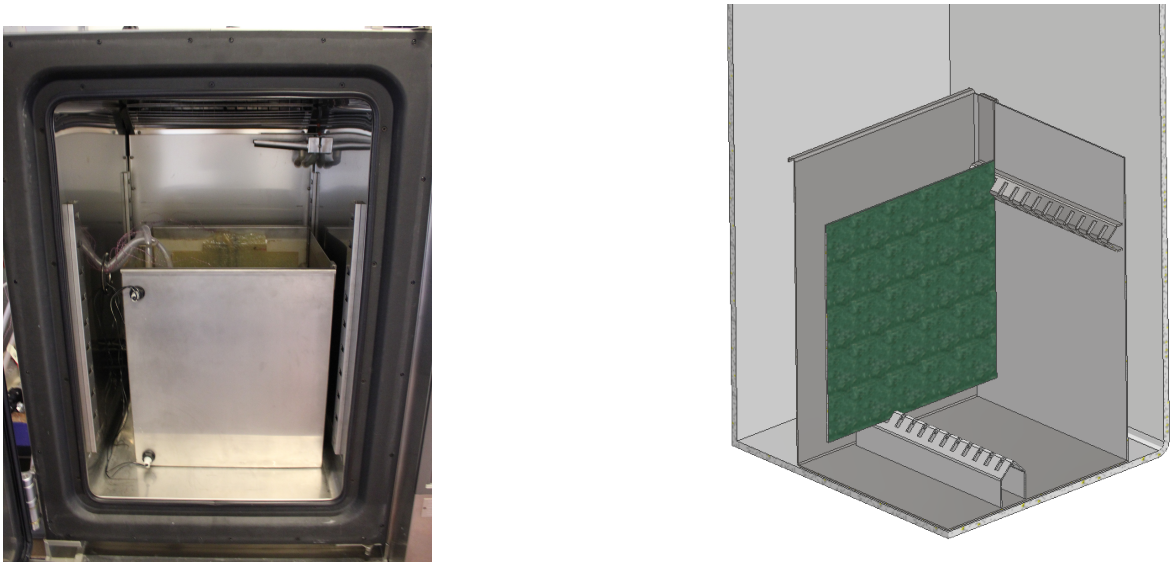


Figure 3.4: Modelled maximum number of FT cycles over the North Sea[53].

Duration per cycle

To ensure the thermal cycle is fully performed, it is important that the material has reached a uniform temperature distribution within. As seen in various standards ([51, 20]) and literature ([24, 43, 22]) embedded TC can be a suitable method to determine the internal temperature. To track the temperature in the setup, two plates with TC embedded in the middle of a plate with similar geometry as the aged plates, are put in the internal water tank in the climate chamber as shown in Figure 3.5. The internal distance between plates is a minimum of 2 cm to leave sufficient room for water to move.



(a) Positioning internal water tank in climate chamber

(b) Positioning plates within internal water tank

Figure 3.5: Internal setup of developed FT ageing system in the climate chamber

Figure 3.6 shows a trial FT cycle. After the climate chamber reaches -20 °C, it is kept for 3 hours. The figure shows that the internal temperature reaches -20 °C 30 minutes later.

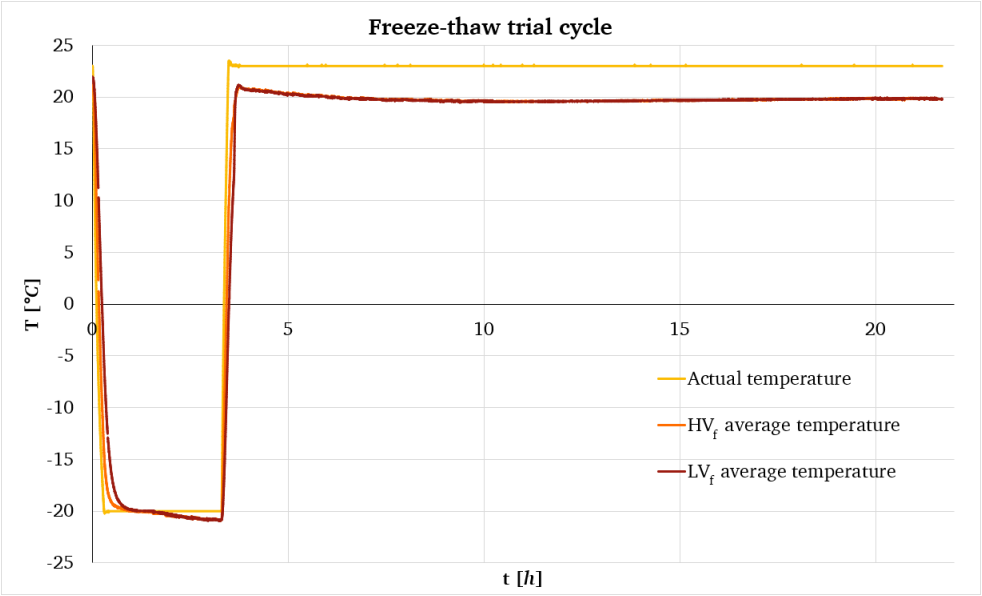


Figure 3.6: Temperature of material and climate chamber during an extra long FT cycle

After 3 hours, the temperature is set to +23 °C. After the climate chamber reaches +23 °C, +23±2 °C water is pumped into the internal water tank. After 15 minutes, the complete internal tank is filled. Figure 3.6 shows that in the following 18 hours of submerged thawing, the internal temperature drops below 20°C. The setup does not have the power to prevent the water from cooling down under the influence of the cold material: composite plates, internal water tank and internal components of the climate chamber. As a result, two steps are taken:

- As the available machines forming the setup cannot sufficiently warm the composite plates, a predetermined thawing stage of 3 hours is defined, analogue to ASTM D7792 [19]. This aligns with the temperature range that has been selected in Section 3.1.1, which is analogue to ASTM D7792 [19].
- To prevent the water from cooling down, during the thawing stage the water pumps are used 3 times for 15 minutes to extract cooled-down water and add water of 23 °C from the external water tank. A continuous circulation of saltwater is not possible, as the available water pumps are only suitable for intermittent use, and would overheat when used continuously.

3.1.2. Applied methodology

ASTM D7792 is used as a framework for the ageing procedure [19]. Plates were conditioned in the air before ageing, contradictory to the prescribed submerged conditioning for 30 days. This opens up the possibility of measuring saltwater uptake. Every FT cycle consists of 3 hours of exposure to -20 ±2 °C. This is followed by 3 hours of full submersion in demineralised water of 23 ±2 °C mixed with 3.5 weight% pure sodium chloride salt, to represent seawater to mimic service life conditions. The process of pumping out the water and the climate chamber reaching -20 °C takes a little under 30 minutes in total.

The FT ageing is applied by using an Espec 2PL-2KPH climate chamber in combination with water pumps and a stainless steel water tank. During the submersion stage, the pumps are used to circulate the water with an external water tank, with water of 23 ±2 °C, 3 times. This will help to ensure the water temperature remains within 23 ±2 °C. The setup is controlled with the software Mp3. A more detailed description, used scripts and a flow block diagram of the interconnection of the different components of the setup can be found in Appendix B.

In Figure 3.7 an applied FT cycle is shown. The temperature of the sample is measured with TC embedded in the mid-plane at the middle of the laminate. The LV_f TC plate is positioned in the back of the setup, and the HV_f TC plate is in the middle. The average of three TC measurements per plate is shown. This cycle is repeated 199 times.

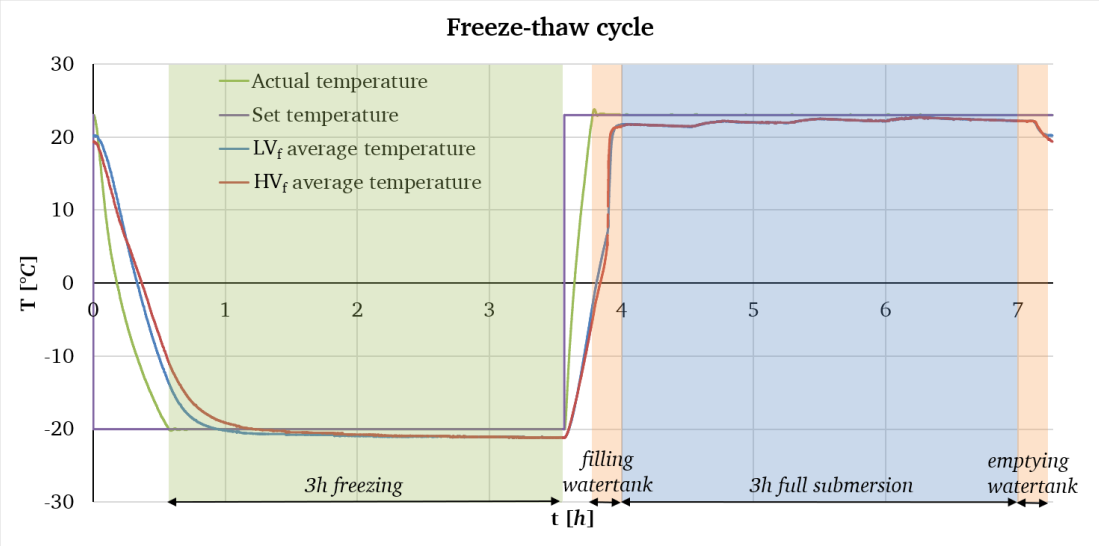


Figure 3.7: Graph representing one FT cycle and temperature changes experienced by climate chamber and samples

3.1.3. Irregularities during ageing

The following irregularities occurred during the ageing of the plates:

- At the beginning of cycles 3, 21, 31, 41, 48, 154 and 182 the cooler of the climate chamber experienced blockage due to frost build-up. All specimens were moved in a frozen state from the climate chamber to an external freezer and kept at -20 °C until cycles could resume.
- After 47 FT cycles, one water pump encountered capacity problems. To prevent flooding of the stainless steel tank, the circulation of water during submersion was discontinued. This results in water cooling down 2 °C during the thawing stage, as shown in Figure 3.8. This may reduce moisture uptake, as lower temperatures are known to negatively impact diffusivity.
- At cycle 181 the setup malfunctioned, resulting in full submersion of specimens for 11 hours.
- During the ageing, the water had a weight% of pure sodium chloride salt of 3.5 - 4.0 %. Variations were caused by excessive water evaporation. This may reduce moisture uptake.

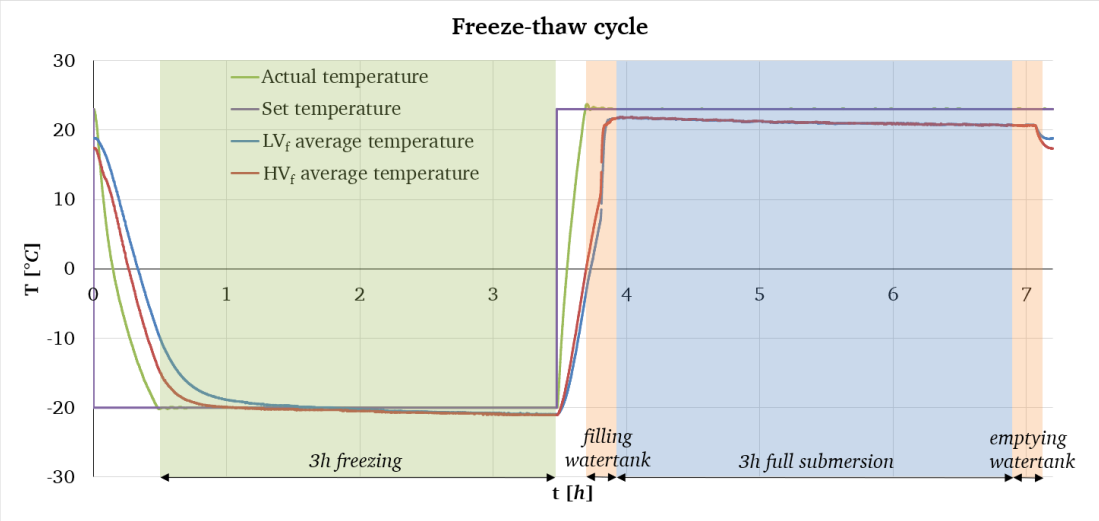


Figure 3.8: Graph representing one cycle and temperature changes experienced by climate chamber and samples without circulation step

3.2. Microscopic investigation of surface degradation

To investigate the possibilities of quantifying the degradation on the surface of the material after exposure to FT cycles, two types of microscopy techniques were used. Section 3.2.1 first introduces the different parameters measured and their significance. Section 3.2.2 discusses the methods used to determine the different parameters. Section 3.2.3 summarises all results, which will be discussed and concluded in respectively Section 3.2.4 and Section 3.2.5.

3.2.1. Introduction

Exposure to FT cycles may result in a variety of damages developing internally and on the surface of the material. The temperature differences and variation of the CTE of the fibres and matrix may result in micro-cracking on the surface, which can, combined with degradation due to moisture exposure, lead to material loss. These damages can roughen the surface, resulting in a more varied height profile. These changes can make the surface more susceptible to moisture uptake. When the material uptakes moisture at a faster rate, internal degradation can quicken and impact the strength of the material faster. This section aims to measure these external damages and assess if surface investigation can show the severity of FT ageing effects. This will be aimed at surface profile changes and the change of the wetting angle.

As described in Section 2.1.2, the wetting angle is the angle between a droplet and the surface as shown in Figure 3.9. A wetting angle smaller than 90 °is a sign of high wettability. As a droplet forms on the surface, energy is released at the solid-liquid interface as it grows. On the other hand, energy is consumed by the increase of the liquid-air interface. When these energies are in equilibrium, the droplet stops moving and

the contact angle can be determined. As the roughness of a surface increases, the solid-liquid interface area increases resulting in a further increase of the liquid-air interface to reach equilibrium and a lower wetting angle. The relationship between the wetting angle and water absorption rate of the solid is considered to be negative [35, 36].

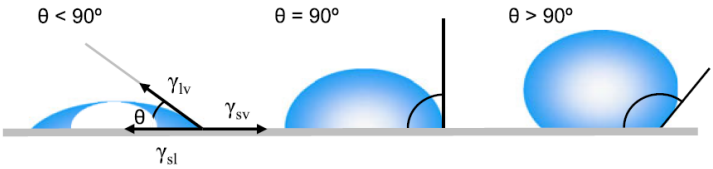


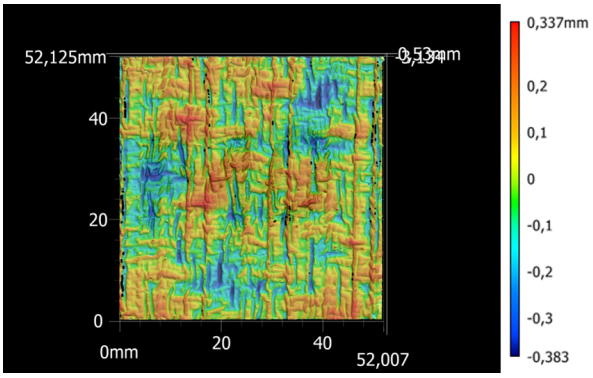
Figure 3.9: Representation of wetting angle θ[33]

The wetting angle could thus be an indicator of not only the wettability of the surface but also an indicator of an increase in the water absorption rate of the solid. Due to the induced damages during FT cycles, it is expected that the wetting angle will reduce under the impact of the surface damage increasing the solid-liquid interface, resulting in a better wettability of the surface, and a higher water absorption rate of the material. The first part of this hypothesis is tested in this chapter by the measurement of the surface roughness, surface profile and the wetting angle.

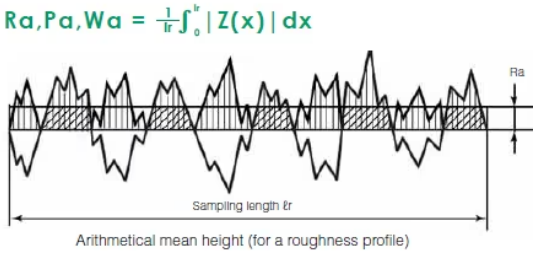
3.2.2. Methodology and materials

Surface profile

To measure the surface profile, a Keyence VR-6000 Profilometer was used. It is a non-contact measuring system that registers height differences of 0.1 μm. The machine maps the whole specimen and the differences in height. This data can then be post-processed with the software of the manufacturer, enabling the comparison between different measurements. This feature is used to measure the same specimen after exposure to a different number of FT cycles and compare these measurements. The Profilometer was used to measure two things of both the top and bottom surface of the material. Firstly the surface profile, Figure 3.10a, and secondly the surface roughness, which is an extension of the line roughness explained in Figure 3.10b. It is a measure of the mean surface profile differences compared to the reference plane. To prevent the sides of the specimens are taken into account, a maximum height difference below the reference plane of 0.5 mm is taken. The software shows afterwards which locations are taken into account, which is used to validate that no measurement points are falsely disregarded.



(a) 3D profile image of a profiled side of a tested plate surface with a Keyence VR-6000



(b) Line roughness parameter Ra [55]

Figure 3.10: Example of a surface profile and roughness with a Keyence VR-6000 Profilometer

Wetting angle

To determine if the surface of the composite becomes more prone to moisture absorption after exposure to FT cycles, the wetting angle is determined. Before ageing and after 29, 77 and 119 FT cycles the wetting angle is measured at the locations shown in Figure 3.11 by measuring two different droplets at every location for reference measurements and three droplets for all other measurements. These droplets are placed using a plastic pipette with demineralised water.

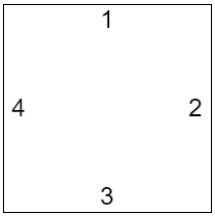


Figure 3.11: Positions measurement

A Keyence VHX-7000 Digital Microscope head is placed on a table in combination with a small-scale scissor lift as shown in Figure 3.12. The droplets are applied close to the edge of the plates, to allow for a small enough distance to manually focus the droplet with the microscope head.

The microscopic images are then post-processed using the software imageJ in combination with the Lower Bound Asymmetric Drop Shape Analysis (LBADSA) of the drop shape analysis plug-in [56]. Due to the high variability of the surface profile on the top, and the decreased visibility of the interface between the droplet, the surface and the air, measurements are only performed on the bottom of the plates.

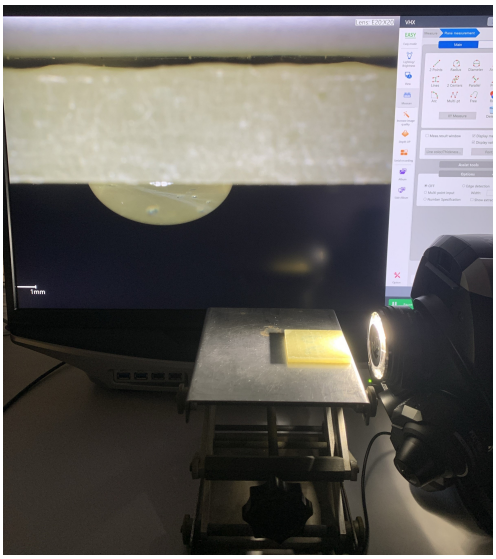


Figure 3.12: Wetting angle setup

Used materials

For both experiments one 50 x 50 mm plate is used per material. Surfaces were cleaned with demineralised water before testing. Cleaning with chemicals was prevented to prevent the onset of chemical degradation of the surface. On top of that, specimens were handled with gloves to prevent contamination.

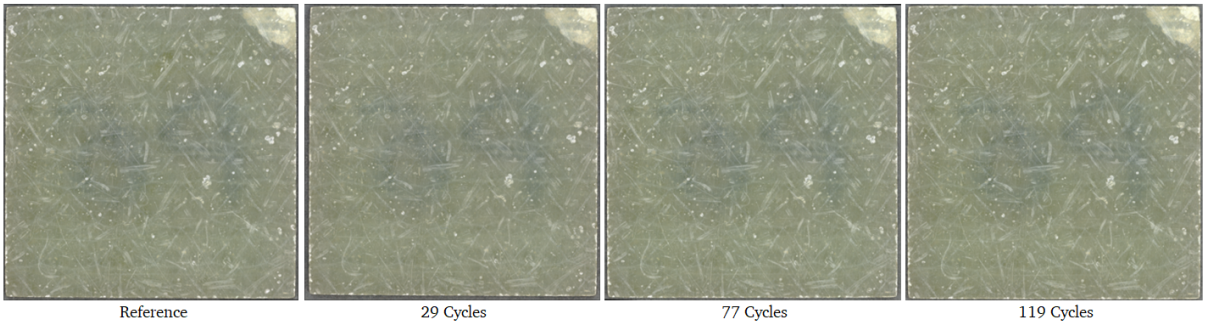
3.2.3. Results

Surface profile

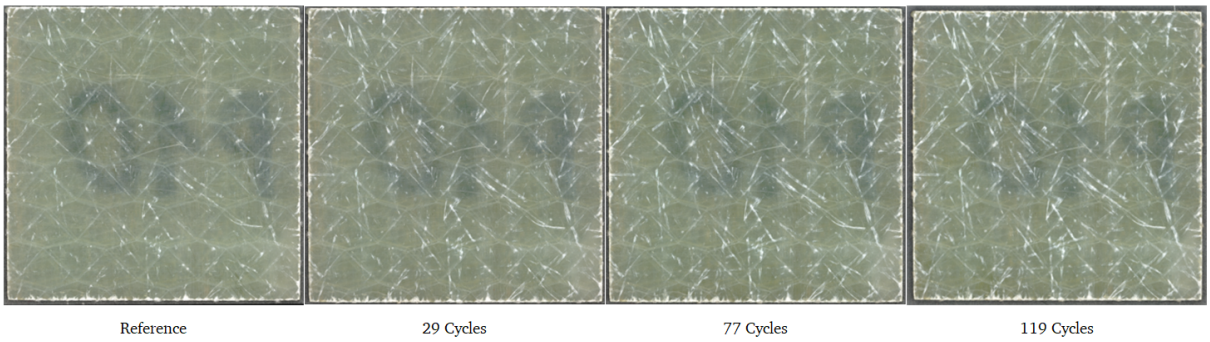
For clarity the results are divided into three parts, visual changes, height profile and surface roughness.

Visual changes

Figure 3.13 shows the change of the bottom surface of both LV_f and HV_f specimens. Figure 3.13a shows no clear degradation of the plate surface, except for delamination in the top right corner resulting from water jet cutting of the plates. Figure 3.13b however, shows exposure to the FT cycles causes fibre blooming. Next to that, both plates have a reflective bottom surface, causing measuring errors for the profilometer.



(a) LV_f plate



(b) HV_f plate

Figure 3.13: Images of the back surface of plates after exposure to FT cycles

Height profile

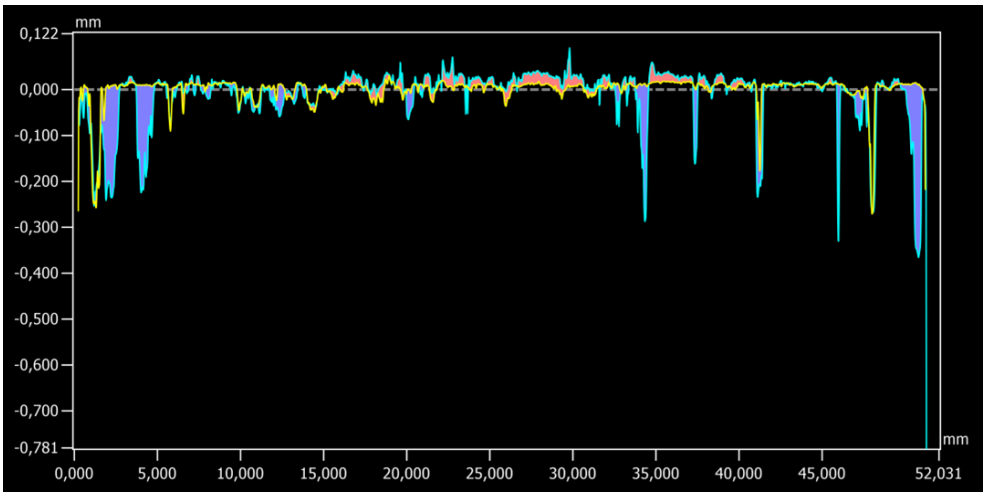


Figure 3.14: Height profile at one location of bottom HV_f plate, yellow line = reference, blue line = after 77 freeze-thaw cycles of exposure

Figure 3.14 shows an image of the height profile at one location at the bottom of an HV_f plate aged for 77 FT cycles. The yellow line represents the profile of the reference plate, blue represents the profile of the plate after 77 FT cycles of exposure. The image shows a clear loss of material (hashed in blue) and the development of cracks up to 0.3 mm deep. Hashed in red, 'added' material is shown. This is expected to be caused by faulty aligning of reference measurements with measurements of aged material.

When comparing measurements, the post-processing software cannot correctly automatically align samples. Manual alignment was impossible to do accurately, as no location on the plate can be used as a reference, due to degradation resulting in material loss at all surfaces. This proves this method is only suitable for investigating one set of measurements, and not for comparing different measurements with the absence of a constant reference plane.

Surface roughness

Measurement of the surface roughness has shown to be less challenging, as this method uses an average over the surface, which is less dependent on correct alignment due to the summation over the full surface, whilst taking into account locations above and below the average plane. Figure 3.15 shows the surface roughness of the HV_f and LV_f plates. The bottom of the HV_f plate shows a significant increase of surface roughness of more than 200% after 119 FT cycles. The bottom of the LV_f plate shows an increase of surface roughness of 30% after 119 FT cycles. This large increase can be directly correlated to the visual changes shown in Figure 3.13.

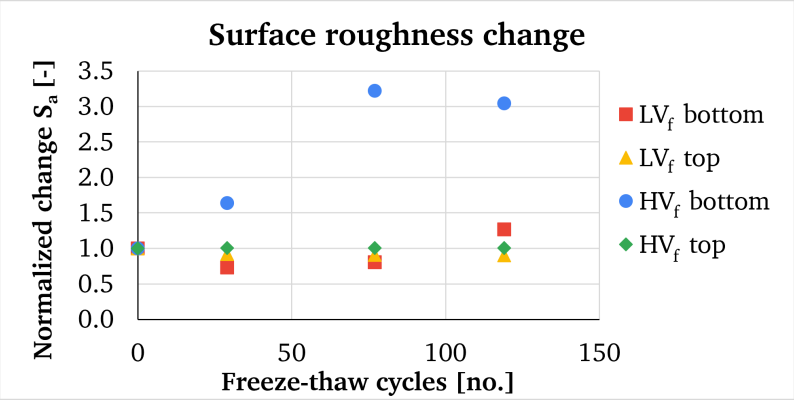


Figure 3.15: Normalized increase/decrease in surface roughness after FT cycle exposure

The initial surface roughness of both top surfaces is approximately 4 times higher than the bottom surfaces. On top of that, the surface roughness of the top surface of HV_f material is at least 25% higher than for LV_f material, and HV_f material primarily shows variability longitudinally in profile height and less in the out-of-plane direction. This results in a highly profiled surface which is difficult to clean properly.

Wetting angle

The wetting angle was measured from pictures taken by a Keyence digital microscope with LBADSA, as shown in Figure 3.16 [56]. Both HV_f and LV_f plates presented initially with a wetting angle below 90°. Figure 3.17 presents the normalised measured wetting angles for both a HV_f and LV_f plate after 29, 77 and 119 FT cycles. The error bars represent one standard deviation. It shows that after 29 FT cycles there is a significant change in the wetting angle for the HV_f plate, which is expected to be caused by hydrophilic agents used during production, which are not properly washed off.

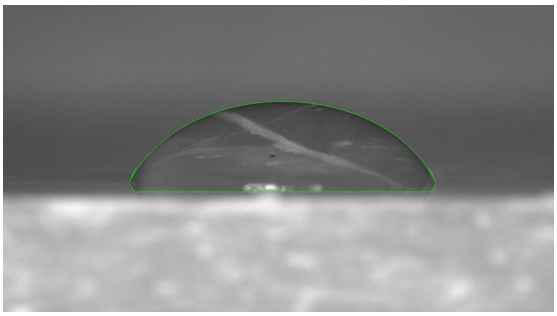


Figure 3.16: Example of droplet shape with LBADSA

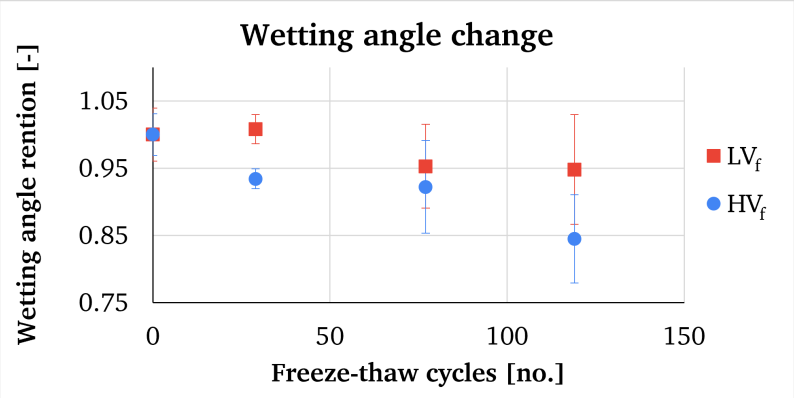


Figure 3.17: Change of wetting angle with exposure to FT cycles

The results show that as the number of FT cycles the material is exposed to increases, the standard deviation increases. This is expected to be a result of increased surface degradation, reducing the homogeneity of the surface, and increasing the difference between measurements that are not taken at the same location. A total reduction of the wetting angle of 5% is seen for LV_f material and 16% for HV_f material.

3.2.4. Discussion

Section 3.2.3 shows that after exposure to 119 FT cycles, both HV_f and LV_f material show measurable and visible degradation of the surface. On top of that, a correlation between different measuring techniques can be seen.

LV_f material has shown no significant visual degradation on the Surface profile. This may be the result of the presence of more resin on the surface, resulting in a thicker protective layer to underlying fibres when compared to HV_f material. This is expected to result in a later onset of visual damages and exposure of fibres and fibre blooming in LV_f material.

This is confirmed as well by the surface roughness change and the wetting angle, where HV_f material shows more significant degradation by an increase of more than 200% of the bottom surface roughness and a 16% decrease of the wetting angle, compared to an increase of 30% and decrease of 5% respectively for LV_f material.

However, in wetting angle measurements it is shown that as material is exposed to more FT cycles, the standard deviation of the measurements increases. This is expected to be caused by two factors:

- As material degrades it does so unevenly. This results in variations of surface roughness, which will result in variations of measurements when they are at approximately, but not exactly, the same location as a higher surface roughness results in a lower wetting angle.
- Repeatability of tests is reduced by not using standardised methods and devices for determining the wetting angle, not using an exact volume transfer pipette, the plates having uneven and not flat surfaces, manually focussing the droplet and post-processing methods being primarily manual. These factors will thus result in a higher deviation.

Next to that, all measurements performed with the Profilometer are susceptible to errors, as the surface of the material can be reflective and is partially translucent, causing measuring errors at highly reflective areas and delamination damages as shown in the LV_f sample.

Despite these factors, it should be noted that the results clearly show degradation of the surface of the material, which primarily seems to increase as the protective outer resin layer diminishes, which is a more pressing problem for HV_f material at the beginning of ageing than LV_f, as it has a thinner resin rich layer.

Apart from the significant results regarding the visual changes, surface roughness and wetting angle, it can be concluded that the height profile is not a suitable method of analysis when comparing unaged to aged material. As discussed in the section Surface profile, alignment of different measurements cannot be done automatically by the software and is impossible to do accurately manually due to uneven ageing over the material surface and no reference surface that remains equal throughout ageing. When the goal is not to compare different states of specimens, but to measure crack depths, this is a suitable method to do so.

3.2.5. Conclusion

The degradation of the surface of the material can be quantified by measuring the surface roughness, wetting angle and performing visual inspection. It has been shown that HV_f material shows a more significant surface degradation compared to LV_f, expected to be caused by the thinner protective resin-rich layer on the surface.

In line with these measurements, it can be expected that water uptake will increase for both materials. The hypothesis is primarily a more significant increase of water uptake rate for HV_f material as it shows a more significant increase of surface roughness and a decrease of wetting angle when subjected to FT cycles.

3.3. Saltwater uptake

This section describes the determination of the saltwater uptake of the composite material when subjected to FT cycles. This is done both experimentally and numerically. After an introduction to the topic and its relevancy in Section 3.3.1, Section 3.3.2 describes the gravimetric method applied to track the weight gain of specimens and the mass diffusion modelling methodology applied. Section 3.3.3 describes used materials. Results are presented in Section 3.3.4, followed by the discussion and conclusion in Section 3.3.5 and Section 3.3.6.

3.3.1. Introduction

Previous research has shown that after 121 days ($\approx 54\sqrt{\text{h}}$) of submersion 2-ply tensile LV_f coupons reach a weight uptake of approximately 0.43% and a tensile strength reduction of only 2.8%[16]. It is expected that exposure to FT cycles damages the composite material internally and on the surface, increasing not only the rate of saltwater uptake and increasing the maximum moisture content when compared to continuous submersion. This will result in the material that could introduce an earlier onset of degradation caused by moisture-induced mechanisms, such as hydrolysis and polymer relaxation as described in Section 2.1.1. The resulting formation of voids, micro-cracks and internal redistribution of moisture could even more adversely affect the composite when FT cycles are continued to be applied.

The previous section has shown that after exposure to 119 FT cycles, especially HV_f material shows significant surface degradation. On top of that, the hypothesis is raised that this will directly result in an increase in moisture diffusion. This section will test this hypothesis by experimentally and numerically determining the weight change of the materials.

Experimentally, the weight change of the material is the sum of diffused water and mass loss caused by degradation. This means that the measured weight change does not necessarily equal the total moisture uptake, as mass loss will result in a lower total weight change. Numerically mass loss and degradation are not taken into account, meaning that all weight change is modelled to be caused by the diffusion of moisture.

Previous research numerically analysing moisture diffusion into wrapped composite joint geometries has shown that under continuous submersion, saltwater will not reach the interface at the root of a Fs joint during service life [18]. If, as predicted, FT cycles result in additional degradation causing an increase in water uptake rate, this conclusion may no longer be valid. This would greatly impact the predicted durability of joints positioned in the splash and tidal zone.

3.3.2. Methodology

Experimental

The gravimetric method, as described in ASTM D5229 [57] is used to track the weight change of plates during exposure to FT cycles. At practically feasible intervals, three plates per material are weighed directly after the thawing stage. This is continued until the specific plate was taken out for further destructive testing. The automated ageing system is temporarily paused after the water has been extracted, but the temperature is still 23 °C. The specimens are handled with gloves and dried with paper towels to remove excess water on the surface. The balance used has an accuracy of 10 mg, measuring mass changes of less than 0.002% of the total weight. The balance is placed in a partially enclosed space, to prevent air flow destabilising measurements. The measurements are then used to create curves relating the weight change to the square root of submerged time, where only the time plates are fully submerged is taken into account. The relative weight change is then calculated as follows:

$$M\% = \frac{M_t - M_0}{M_0} \cdot 100 \tag{3.1}$$

$M\%$ = percentile weight change [%]
M_t = weight of specimen at time t [g]
M_0 = weight of specimen at t = 0 [g]

Numerical

Numerically the weight change is determined by the use of Abaqus mass diffusion analysis, assuming pure Fickian diffusion. This is a simplification of the general diffusion equation, shown in Equation 3.2 [58], and of degradation taking place, as it does not take into account potential mass loss. By not specifying temperature and pressure, thus assuming them to be constant, the governing equation is the 3D equivalent of Equation 2.1.

$$\mathbf{J} = -s\mathbf{D} \cdot \left[\frac{\partial \phi}{\partial \mathbf{x}} + \kappa_s \frac{\partial}{\partial \mathbf{x}} \left(ln \left(\theta - \theta^Z \right) \right) + \kappa_p \frac{\partial p}{\partial \mathbf{x}} \right] \tag{3.2}$$

Where

$\mathbf{J}$ = flux of concentration [$\frac{\text{kg}}{\text{m}^2 \cdot \text{s}}$]
s = solubility [kg/m^3]
$\mathbf{D}$ = diffusivity [m^2/s]
ϕ = normalized concentration [-]
$\mathbf{x}$ = position [m]
κ_s = temperature gradient factor [°C^{-1}]
θ = temperature [°C]
θ^Z = absolute zero temperature [°C]
κ_p = pressure stress factor [Pa^{-1}]
p = equivalent pressure stress [Pa]

The mass concentration boundary condition is set to 1, to represent full submersion of the plate. This however results in the outer surface of the material being directly saturated in the model, causing an initial jump in the results, which is mesh-size dependent. As the concentration inside is unknown at the beginning, it is set to zero. The total amount of solved material is computed by Abaqus over time. To calculate the moisture content over time, the solute is divided by the volume, as shown in Equation 3.3:

$$M_t = SOL/V_{tot} \tag{3.3}$$

Where

M_t = Moisture content in the volume [%]
SOL = Amount of solute summed over the total volume [ppm $\cdot$ m^3]
V_{tot} = Total volume [m^3]

The results can then be plotted against the square root of time to compare with the experimental results. In this way, intermittent submersion during FT ageing is compared with numerical continuous submersion.

3.3.3. Materials

Experimental

For this research 4-ply non-symmetric composites are produced with a high and low fibre volume fraction. To reduce edge effects and represent bulk-material behaviour as best as possible, plates of 320 mm x 340 mm are aged. In joint application, the edges of the composite material will not be cut, as it has a tapered shape, seen in Figure 1.3. To prevent diffusion along the fibre and other edge effects, the outer 1 cm and sides of every plate are coated with an Enguard isophthalic polyester resin-based topcoat reducing diffusion to a minimum as shown in Figure 3.18.

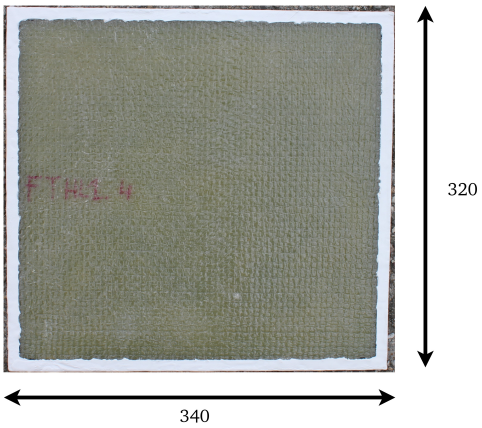


Figure 3.18: Coated plate [mm]

The plates are cut from bigger produced plates using a water jet. Each plate is labelled with a marker. Next to this, all plates are post-cured at 60 °C for 1 hour per mm thickness to increase cross-linking between polymer chains. This ensures more homogeneity between different test specimens. Experimental data from previous research on continuous submersion of other geometries and numerical continuous submersion of a similar geometry is presented to put the results in context.

Numerical

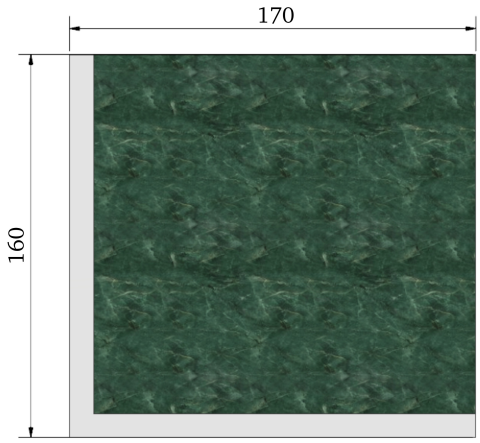


Figure 3.19: Modelled plate part [mm]

To reduce computation time, only 1/8 of the plate is modelled, half of the thickness and a quarter of the surface, as shown in Figure 3.19. A standard linear heat transfer hex (DC3D8) mesh of 1 mm in-plane and 0.3 mm through-thickness was used. Further reduction of mesh size did not significantly impact the initial jump and was thus deemed unnecessary.

Only LV_f material is considered, as for this material previous research on continuous submersion has been performed, and diffusion coefficients of the material are determined. The material has a solubility, or saturation moisture content, of 0.47%, and diffusion coefficient in-plane $D_{x,y} = 0.08\text{mm}^2/\text{day}$ and through-thickness $D_z = 0.03\text{mm}^2/\text{day}$ [59]. These parameters are determined based on post-cured and non-post-cured materials of different geometries than tested in this research.

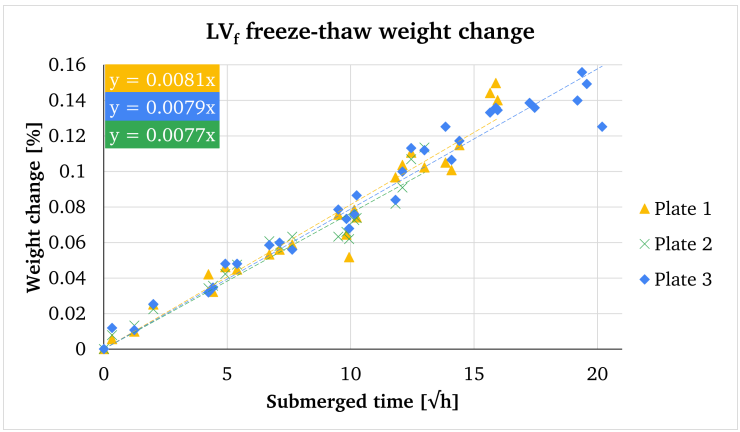
Due to the geometry of the plate, the main diffusion direction is through the thickness, as the thickness is less than 2% of the other dimensions. This means that the primary coefficients influencing the numerical approach are the saturation moisture content, as the main material property driving the gradient, and through-thickness diffusion coefficient D_z.

3.3.4. Results

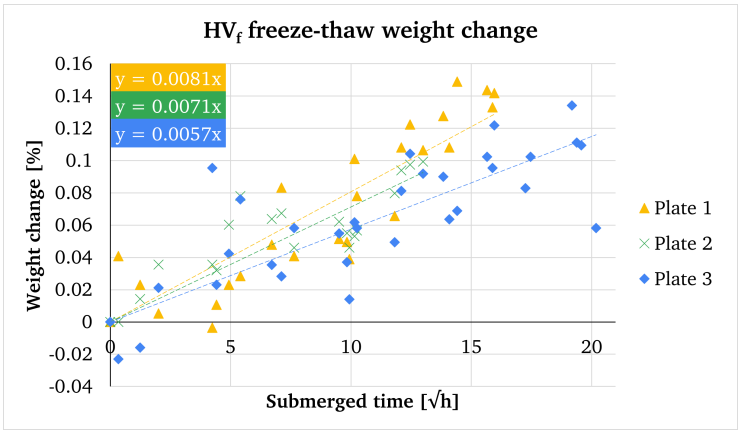
Experimental

This section describes the result of the experimental weight change measurements during FT cycles. To aid in the discussion and conclusion of the results, weight change under continuous submersion of LV_f material from previous research is presented alongside.

During the first cycles, the weight change shows significant variability as the plates have not yet acclimated to the ageing conditions. To make sure this does not cloud the results, the weight after 6 FT cycles, 18 hours of total submersion, is taken as a starting point. Figure 3.20 shows the percentile mass change of 3 LV_f and 3 HV_f plates against the square root of submerged time in hours. A linear trend line starting at (0,0) is inserted to aid in comparing results. One cycle is represented as 3 hours of submersion, so $t = 1.73\sqrt{\text{h}}$, as visualised in Figure 3.8.



(a) Weight change of three LV_f specimens



(b) Weight change of three HV_f specimens

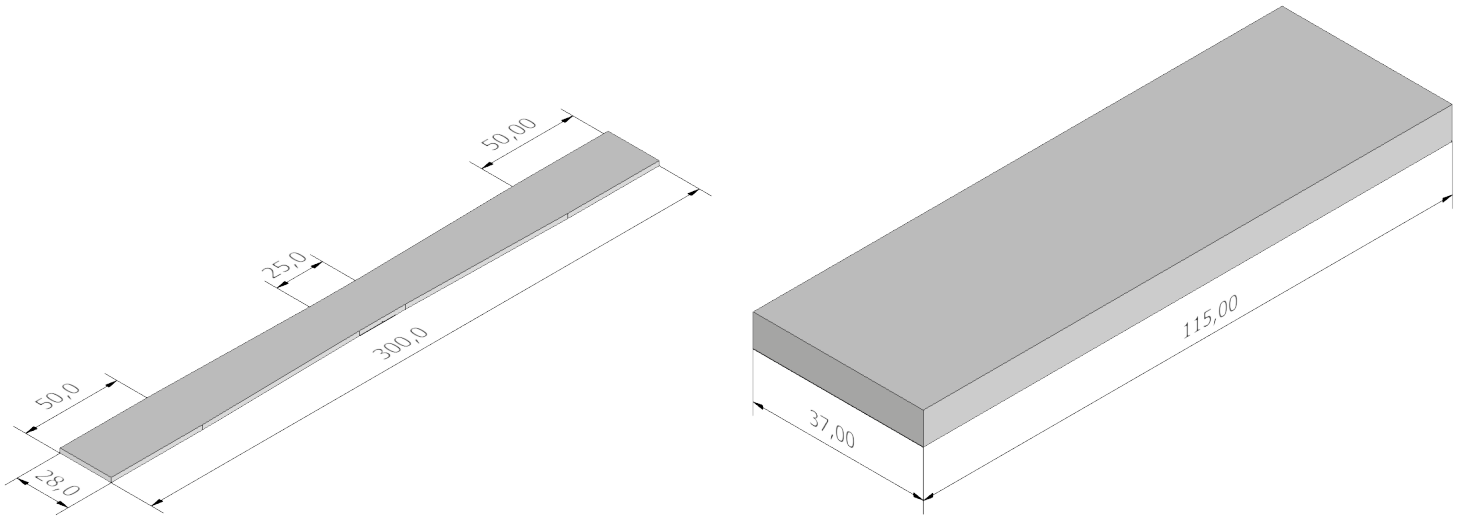
Figure 3.20: Weight change during FT cycles

When comparing the two graphs, it is clear that for both materials, there is a deviation in measurements of the different plates and between measuring moments. Especially for HV_f material, the scatter between

measurements is significant. For both materials, this is expected to be caused by the unsuitability of the tools available to dry the surface of the material. Due to the high variability in the top surface profile of the material, water could not be sufficiently removed. Especially for HV_f material, water was still visible on the surface, but not possible to remove with the available tools. This results in an inconsistent dryness of the material before weighing moments, resulting in a spread in the results. Next to that, it is visible that neither material has reached its saturation moisture content, as there is no clear flattening of the curve.

When considering the linear trendlines included in Figure 3.20, two HV_f plates show a slower weight change than all LV_f plates. Because the shape of the graphs is so inconsistent, it is however difficult to determine if this is caused by potential mass loss due to degradation, or simply a slower weight change due to the 15 percentage point lower volume percentage of resin in HV_f material.

To put the results in context to determine if saltwater uptake increases due to damages caused by the FT cycles, the results are compared to tensile and inter-laminar shear (ILS) coupons continuously submerged in 3.5 weight% salt water in previous research [16]. A similar ply build-up was used, where one ply consists of CSM stitched to a woven fabric. The tensile coupons have a 2-ply 0°/90° configuration, with the woven fabric facing outward. The ILS coupons have a stacked 6-ply 0° configuration. The coupons are post-cured but are not coated and have open, exposed, edges. The thickness of FT LV_f material is in between the thickness of the tensile and ILS coupon. Drawings with dimensions of the geometries are shown in Figure 3.21. Figure 3.22 shows the average weight change of LV_f and HV_f FT aged plates, and average tensile and inter-laminar shear (ILS) moisture uptake from previous research [16].



(a) Composite tensile coupon **(b)** ILS coupon

Figure 3.21: Geometry of previous experiment coupons [16]. Dimensions in mm

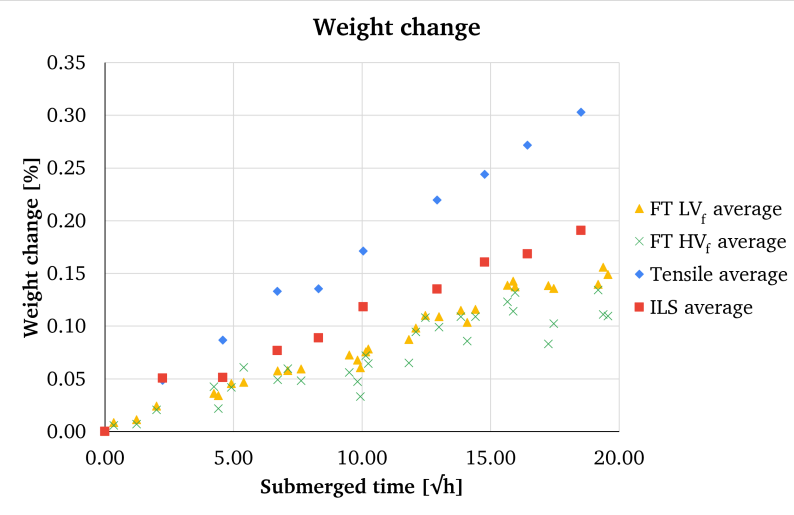


Figure 3.22: Weight change of different geometries under different conditions

The graph shows that both materials in this research show a slower weight change when compared to thicker and thinner materials under continuous submersion. This is different from the expected results, namely increased weight change for material exposed to FT cycles. However, as mentioned, the tensile and ILS coupons have open edges, and the diffusion coefficients of the material in-plane are almost thrice the diffusion coefficient through-thickness. The numerical analysis in the next section where a similar geometry to the FT aged material is modelled, will thus give a more complete view on this.

Numerical

Figure 3.23 shows the average experimental moisture uptake during FT ageing starting from the beginning of the ageing, and the results of a FEA of continuous submersion.

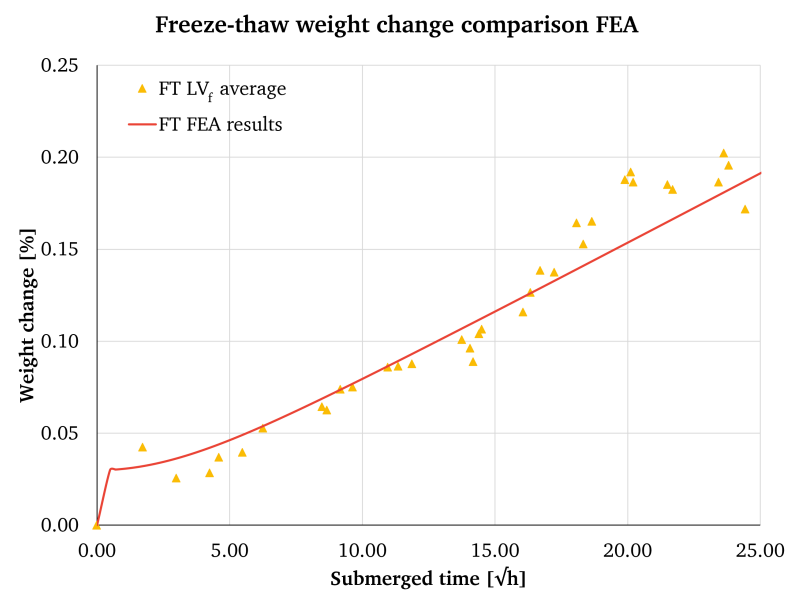


Figure 3.23: Experimental and numerical moisture uptake of LV$_f$ plate

It shows the difference between the experimental weight change under FT ageing and numerical continuous submersion is minimal. From $t = 17\sqrt{h}$ onwards, the experimental data shows higher weight change than numerical. It should be noted that at this point, only one out of the original three plates remains, reducing the significance of this comparison.

3.3.5. Discussion

Section 2.2.6 showed that moisture uptake during FT cycles is not a well-studied subject. Knowledge about this subject is essential to identify whether previous research into continuous submersion of the material applies to the splash and tidal zone, whilst taking into account that the material is only intermittently exposed to moisture. Therefore, this section describes the study performed, exposing composite material with a high and low fibre volume fraction to submersion in the thawing stage of FT cycles and exposed to continuous submersion. Intermittently, the material is weighed. The expectation was raised that degradation caused by FT cycles, which is visually and experimentally determined in Section 3.2, would result in a faster uptake of moisture and faster weight change when compared to continuous submerged material. The results indicate no clear evidence that moisture uptake will increase due to the developed damages in the material. However, a few things should be taken into consideration.

- Firstly, the material is not dried back after the experimental determination of weight change. This means there is no complete certainty that weight loss due to degradation did not play a significant role. If the material loses weight due to degradation, it would result in the total weight change determined in these experiments being lower, but the moisture uptake could be greater. The material is not dried back after ageing to determine weight loss, which leaves its magnitude unknown as well as the total uptake of moisture. However, from LV_f results, no clear kinks or jumps in the graph are visible, raising the hypothesis that no significant mass loss has occured curing ageing.
- Secondly, as visible in Figure 3.20 and discussed in Section 3.3.4, the results show a large scatter. This is expected to be caused by uneven dryness of samples throughout measurements due to the high surface roughness of the top surface especially in HV_f material, and by the accuracy of measurements possibly being impeded by the plates being larger than the surface area of the scale. This results in an inability to determine whether the change of weight and possible moisture uptake, is faster in the material with high or low fibre volume fraction.
- Thirdly, the numerical analysis is performed with diffusion coefficients and saturation values determined from different geometries and different levels of cure. The suitability of these numbers for the material in this research is thus questionable. It does however indicate that no great differences between continuous submersion and thawing stage submersion can be expected.

However, the results of this research are still significant. In this research, only the weight change at the end of the thawing stage is determined. Where it could be reasoned that weight could be lost due to desorption after this stage, this is highly unlikely, as the time from weighing to freezing is only 30 minutes. On top of that, Figure 3.20 shows no significant change in diffusion rate after $t = \sqrt{(47-6)\cdot 3} = 11.09\sqrt{\text{h}}$, at which time, as discussed in Section 3.1.3, circulation during the thawing stage stopped. This caused the water temperature to decrease by 2 °C. This indicates that the small inconsistencies occurring during ageing had no impact.

3.3.6. Conclusion

This section has shown that, whilst surface degradation is visible, there is no clear increase of weight change of, or clear difference between LV_f and HV_f material when exposed to FT cycles compared to continuous submersion. LV_f experimental measurements raise the hypothesis no significant weight loss occurs, as there are no clear sudden changes visible in the weight change. This would mean that all weight gain is attributed to the uptake of saltwater. The expected impact of lower temperature thawing water after 47 FT cycles, is not visible in the results, which indicated small temperature differences do not impact moisture uptake significantly.

To know with full certainty no significant mass loss occurs due to damages when exposed to FT cycles, the material should be dried back after ageing and weighed. On top of that, a suitable methodology to dry the surfaces of both materials consistently at each measurement should be investigated further to increase the accuracy of measurements.

3.4. Retention of tensile properties

This section describes the performed quasi-static tensile tests. After an introduction in Section 3.4.1, the methodology is described in Section 3.4.2, followed by the used materials in Section 3.4.3. Closing off with the results (Section 3.4.4) and accompanying discussions (Section 3.4.5) and conclusions (Section 3.4.6).

3.4.1. Introduction

In the sections before, the external and internal degradation of the material was evaluated by microscopically investigating the surface and determining the weight change over the submerged time during FT cycles, compared to continuous submersion. These sections have shown that the material degrades during the FT cycles, but when regarding the weight change, the impact seems to be limited. However, where these parameters can help indicate the severity of degradation after exposure to FT cycles, they cannot directly predict the impact on material properties and thus indirectly on joint performance under these conditions. To gain a part of this knowledge, quasi-static tensile tests are performed on composite coupons.

This section describes the results of tested LV_f and HV_f material after up to 199 FT cycles. Literature summarised in Section 2.2 shows that primarily tensile and compressive strength is expected to be impacted the most by FT cycles. In this research, the tensile properties are tested, as the test is easily executable and more pressing to investigate regarding the design methodology of the joint when compared to compressive strength.

As the material is exposed to FT cycles, the fibre and matrix repeatedly expand and contract at a different rate resulting in a build-up of internal stresses. This may degrade the interface between the fibre and matrix and thereby impact the transfer of loads between the two. However, as the tensile strength is primarily dependent on the fibre, and the fibre type is woven fabric stitched to CSM, the interface expected to be affected by the degradation most with a direct effect on the tensile performance is between the plies and not within the plies themselves. It is thus expected that FT cycles will reduce tensile strength, as with the damage of the fibre-matrix interface the fibres cannot reach their full capacity. This is expected to result in tensile strength reduction as seen in literature, namely around 10%, but is not expected to rise above this estimation. The stiffness is expected to reduce by 6% based on the literature presented in Section 2.2.1. This experimental research will determine whether suggested conversion factors of 0.85 for material exposed to, amongst other conditions, frequent freeze-thaw cycles, can be considered sufficient [41].



Figure 3.24: Experimental setup for tensile testing

3.4.2. Methodology

Testing methodology

For the tensile testing ISO 527-4 is followed [60]. The coupons are clamped in the crossheads of a Dowty Rotel with a capacity of 250 kN, as shown in Figure 3.24. Tests commenced with a gripping pressure of 4 MPa and a gripping length of 50mm, in combination with thick paper to prevent failure at the clamps. Gripping pressure and length will be altered if proven necessary during testing, and described in the results. To minimise stress concentrations, local excessive height differences are sanded off at the location of the grips and the gripping points of the extensometer. Displacement and applied force by the cross-heads are registered alongside extensions using a 50 mm extensometer in the middle of the coupon.

The tests are displacement-driven with a 2 mm/min speed until failure. Tests are performed after 20, 43, 69, 99, 153 and 199 FT cycles. Eight coupons per production type and amount of cycles are tested.

Post-processing methodology

When coupons fail outside of the nominal section, the middle 25 mm, a reduction factor is used to account for the bigger surface area at the location of the failure, as described in ISO 527-4 [60]. When clear jumps or shifts were seen in the last extensometer measurements, they were seen as an onset of failure and disregarded. The tensile modulus is determined by the slope of the stress-strain curve between a strain of 0.05% and 0.25%.

For the selection of valid test results, some results are disregarded, namely:

- Coupons failing in the grips
- Coupons failing outside of the middle 50 mm, where the extensometer is placed
- Coupons showing excessive inter-laminar failure, such as delamination of the ply 50 mm long or more

The results of the tests are then normalised based on their fibre volume fraction, to be able to compare if there is any effect visible caused by the differences in the amount of resin present in the material.

3.4.3. Material

Coupons are cut from aged 320 mm x 340 mm composite plates using water jet cutting. The longitudinal direction of the coupons is aligned with the most fibre-rich orientation of the material, which has about 10% more fibres than in the transverse direction. Type 4 ISO 527-4 geometry was followed [60], shown in Figure 3.25. This geometry has been proven in previous research with similar materials to prevent failure in the grips of the testing machine.

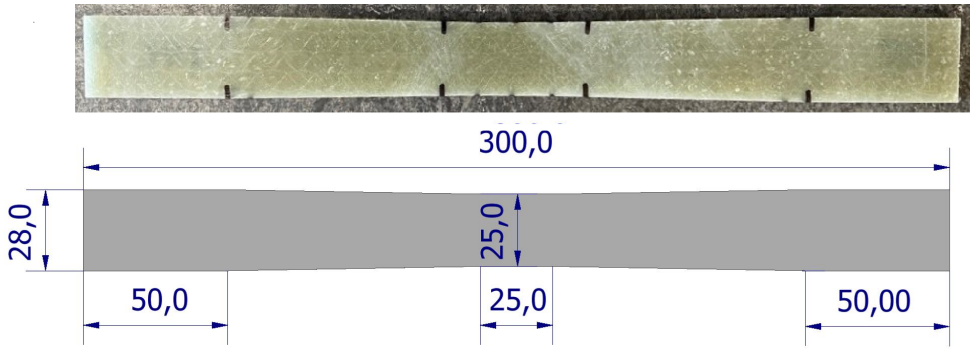


Figure 3.25: Tensile coupon with dimensions in mm

3.4.4. Results

This section will describe the results of the tensile tests. This can be divided into two parts. Firstly, the failed coupons are presented and discussed. Secondly, the tensile property retention is presented, by showing a stress-strain graph of the selected reference LV_f coupons and the normalized tensile property retention graphs against the number of FT cycles.

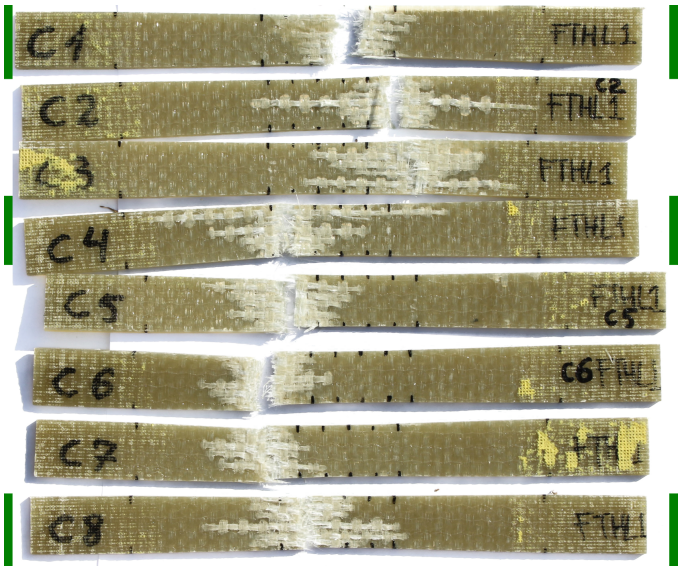
Failed coupons

All coupons aged for 20 FT cycles were tested first. During these tests, the suitability of the gripping pressure and length was determined. Table 3.1 shows the gripping pressure and length used for the first set of coupons. By testing these properties on the aged material, there was a higher certainty of sufficient valid results for the reference coupons. After these tests, gripping length and pressure were maintained at respectively 57 mm and 7.3 MPa. Only when a coupon slipped, the pressure was temporarily increased to 10 MPa.

Figure 3.26 shows all tested LV_f coupons, in green indicating the selected coupons. These figures show that out of these 56 tested coupons, only two coupons failed at the grips and 22 coupons failed outside of the extensometer range. Of the 32 remaining coupons, 31 coupons were selected as valid, of which only 12 coupons failed in the smallest middle section. This raises the question if this complex coupon geometry is necessary for these tests.

Table 3.1: Gripping pressure and length during testing of coupons aged 20 FT cycles. Underlined: failure close to grips. **Bold**: failure at grips. [1] After slipping, pressure increased to 10 MPa

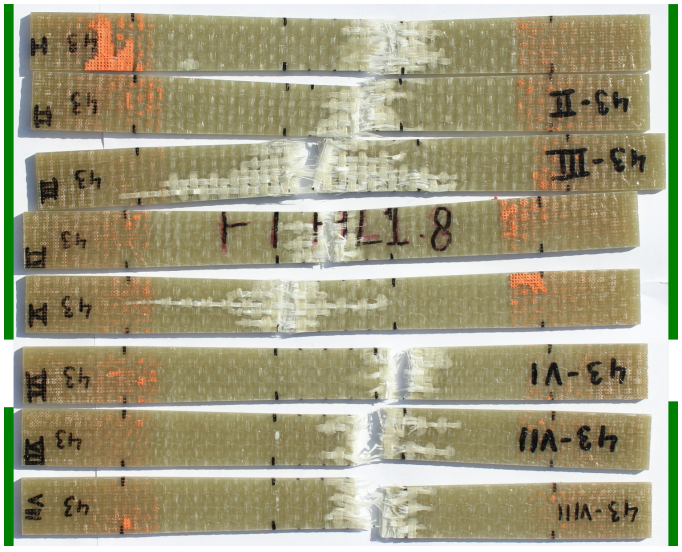
	LV_f		HV_f	
Coupon number	Grip pressure [MPa]	Grip length [mm]	Grip pressure [MPa]	Grip length [mm]
1	4	50	10	50
2	10	50	10	50
3	10	50	10	50
4	10	50	**7.3**	**50**
5	10	50	7.3	57
6	10	50	7.3	57
7	10	50	7.3	57
8	10	50	7.3	57



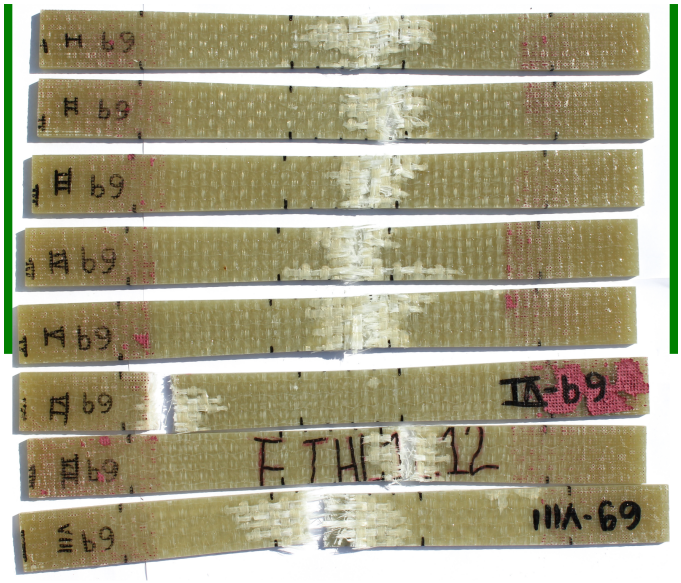
(a) Tested reference LV_f coupons



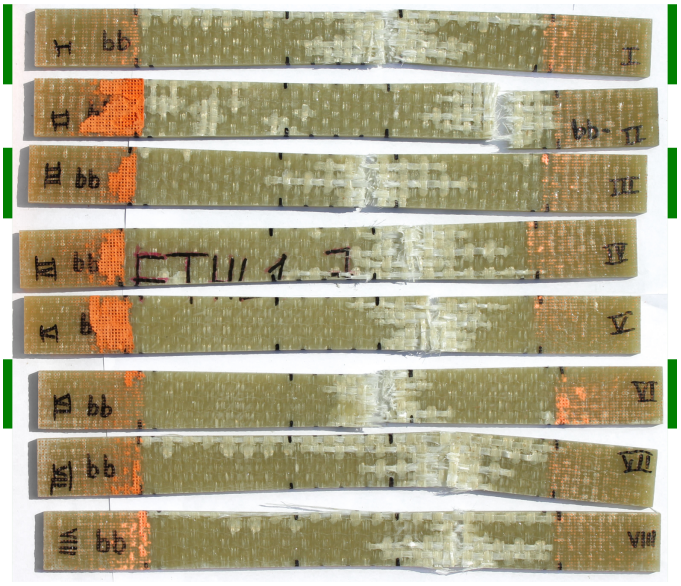
(b) Tested 20 FT cycles aged LV_f coupons



(c) Tested 43 FT cycles aged LV_f coupons



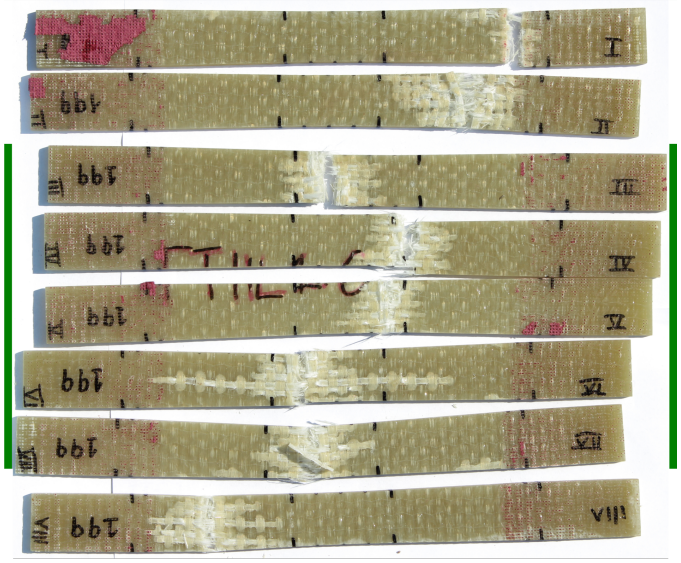
(d) Tested 69 FT cycles aged LV_f coupons



(e) Tested 99 FT cycles aged LV_f coupons



(f) Tested 153 FT cycles aged LV_f coupons



(g) Tested 199 FT cycles aged LV_f coupons

Figure 3.26: Pictures showing failed LV_f coupons. Selected coupons are indicated by a green ribbon.

For two coupons, one aged 20 FT cycles and one aged 69 FT cycles there was a delamination over the full length of the coupon. A picture of such a failure is shown in Figure 3.27, clearly showing the delamination between plies. After ageing for 99 FT cycles and above, 5 coupons showed delamination smaller than 50 mm. These results were taken into account when failed within the middle 50 mm of the coupon.

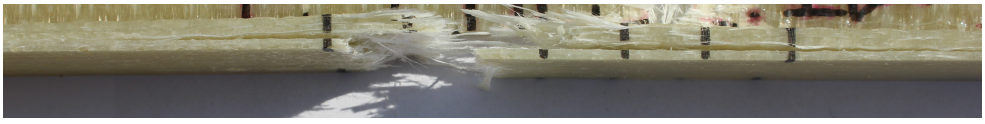
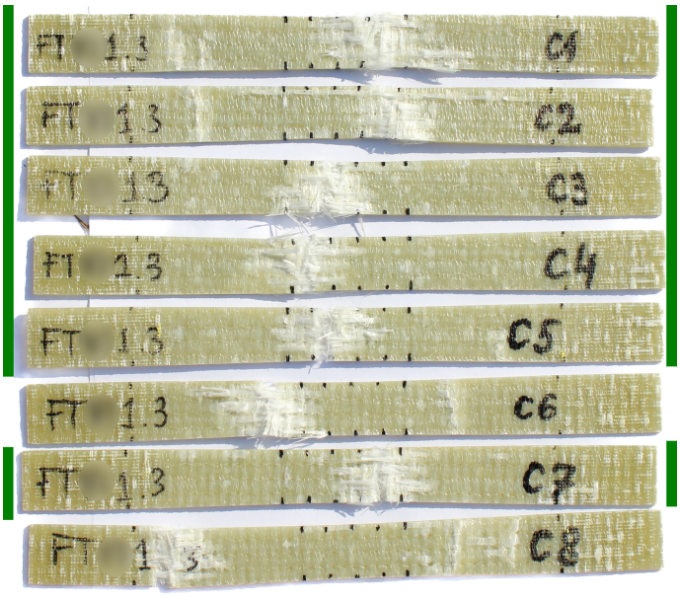


Figure 3.27: Picture of delamination between plies for coupon 8 of LV_f material, aged for 69 FT cycles

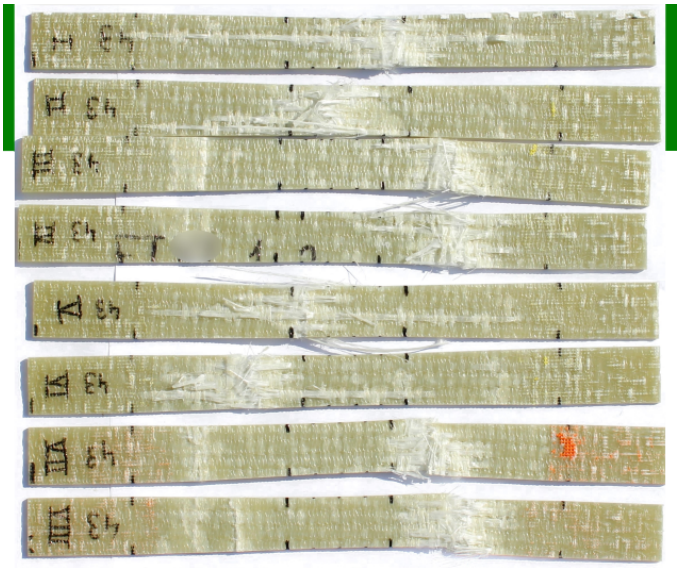
Figure 3.28 shows all tested coupons of HV_f material, in green showing the selected coupons. The figures show that from the 56 tested coupons, 7 failed at the grips and 16 failed outside of the extensometer range. From the 33 remaining coupons, 29 results were selected as valid, of which 16 coupons failed within the minimum middle section.



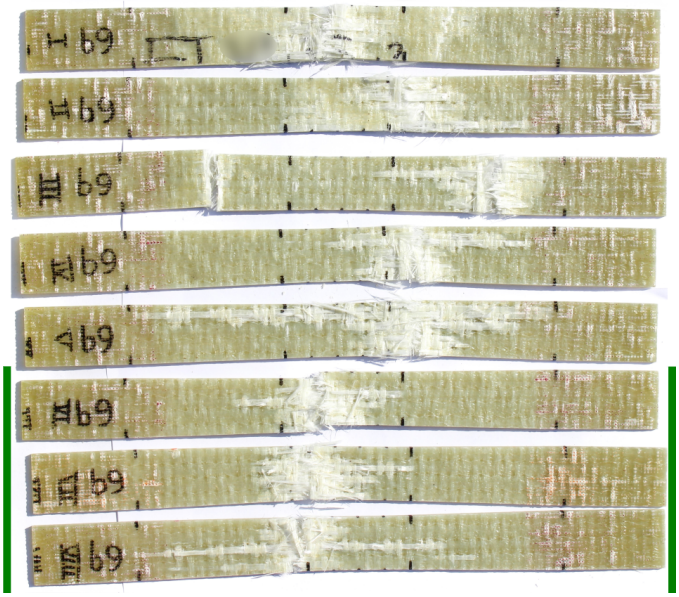
(a) Tested reference HV_f coupons



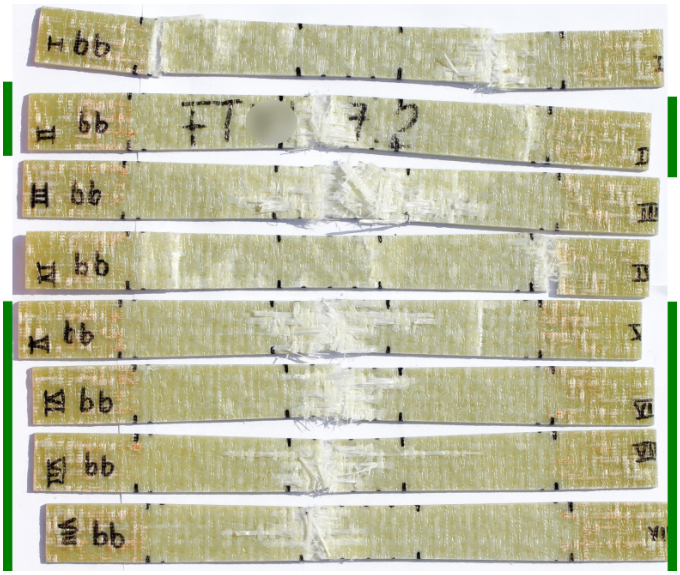
(b) Tested 20 FT cycles aged HV_f coupons



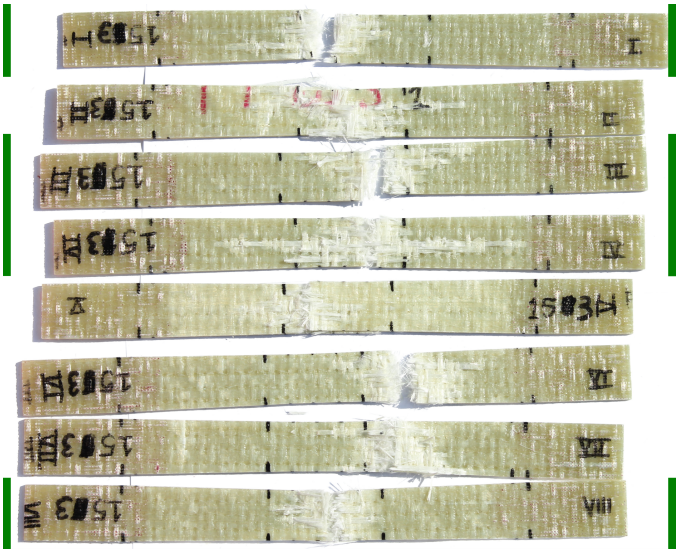
(c) Tested 43 FT cycles aged HV_f coupons



(d) Tested 69 FT cycles aged HV_f coupons



(e) Tested 99 FT cycles aged HV_f coupons



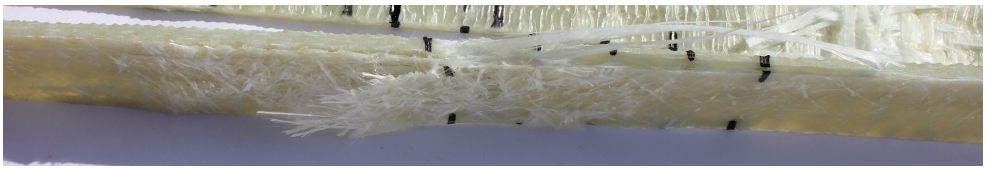
(f) Tested 153 FT cycles aged HV_f coupons



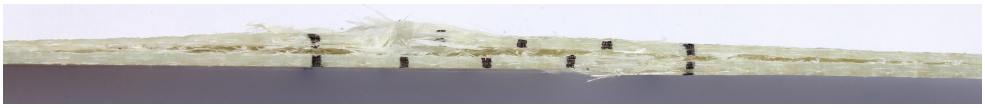
(g) Tested 199 FT cycles aged HV_f coupons

Figure 3.28: Pictures showing failed HV_f coupons.Selected coupons are indicated by a green ribbon.

Four coupons failed within the extensometer range and one outside showed significant delamination. Figure 3.29 shows two of these coupons with significant delamination along the ply. For HV_f four out of these five cases of delamination were for coupons aged 99 FT cycles or more.



(a) Picture of HV_f coupon 5 aged 43 FT cycles



(b) Picture of HV_f coupon 5 aged 153 FT cycles

Figure 3.29: Pictures showing HV_f coupons showing delamination

Tensile property retention results

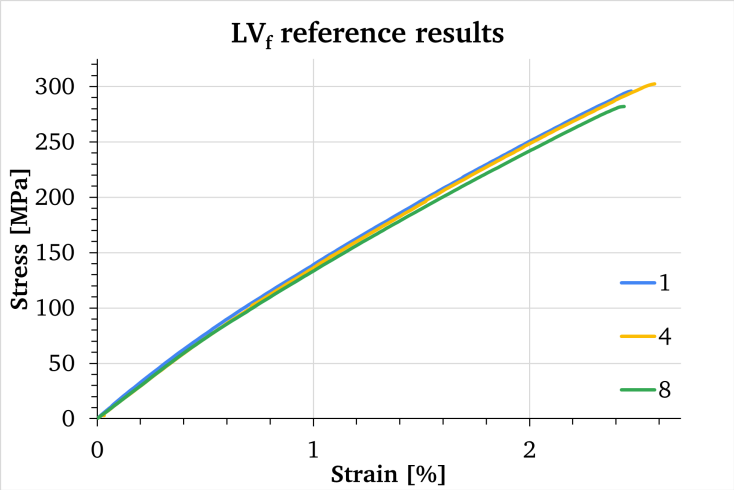
Figure 3.30 shows the stress-strain curves for reference LV_f material and the retention of tensile strength, strain and stiffness versus the number of FT cycles. The results are normalised based on fibre volume fraction and the displayed error bars represent one standard deviation.

The strict selection criteria resulted in less than three coupons being eligible for LV_f material aged 20 FT cycles and HV_f material aged 43 FT cycles. Two LV_f coupons aged for 43 FT cycles showed significantly lower tensile strength, one with a substantially lower failure strain and one with a considerably lower stiffness. These coupons were located at the bottom of the plate, which was always directed at the bottom of the internal water tank during ageing. Apart from these two coupons, there is no trend between the location on the aged plate and the failure mode, failure location or tensile property retention of the coupons.

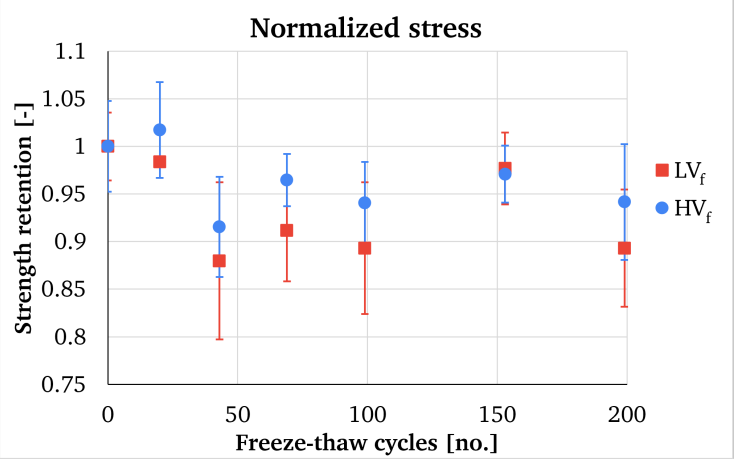
During the experiments, the time between taking material out of ageing and testing was minimised. Table 3.2 shows the days between taking the plates out of the ageing and testing them. This time is minimised to prevent the potential recovery of material properties when taken out of ageing as much as possible. Conditions during testing, such as temperature and humidity varied minimally.

Table 3.2: Waiting days in between stop of ageing and tensile test

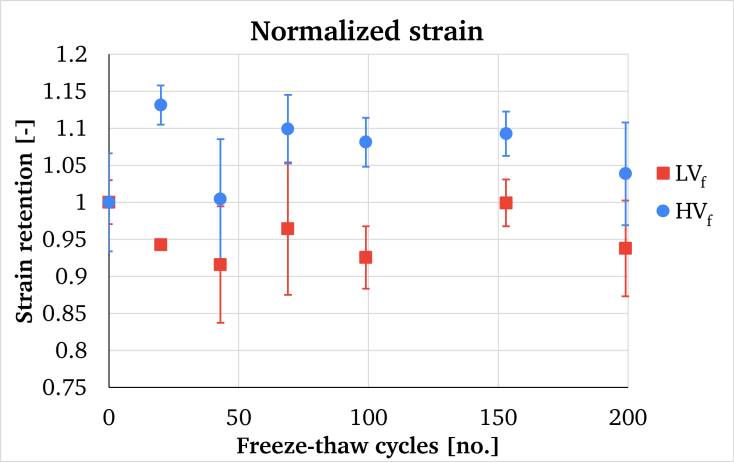
Number of FT cycles	20	43	69	99	153	199
Waiting days until tensile test	10	9	13	8	11	10



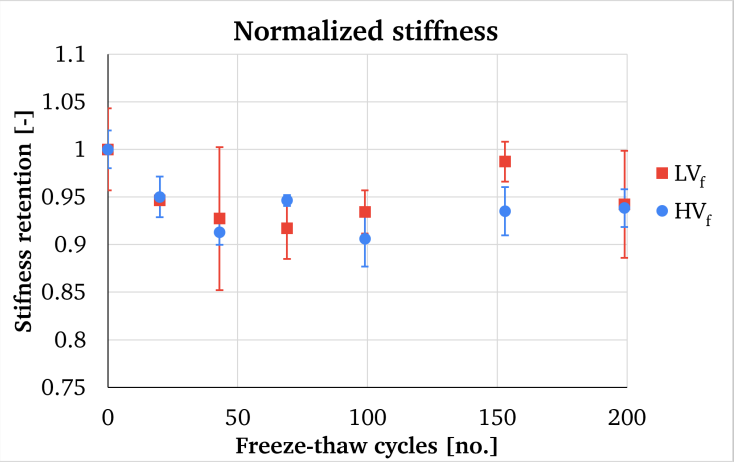
(a) Stress-strain graphs of valid LV_f material reference coupons 1, 4 and 8



(b) Normalized tensile strength retention



(c) Normalized failure strain retention



(d) Normalized E-modulus retention

Figure 3.30: Results conducted tensile tests

Figure 3.30 shows that all tests show a large standard deviation in both materials. As both materials are produced by different methods, production defects cannot cause this similar deviation. However, both materials have a non-symmetric layup. This may result in non-uniform internal stress distribution in the materials developed during post-curing, ageing and testing, resulting in less uniform results.

The figures indicate a reduction of tensile stress and stiffness for both materials. In tensile strength, the trend seems to be that HV_f material shows 5 percentage point less reduction in properties than LV_f material. This could be caused by FT ageing primarily affecting the resin, of which per volume more is present in LV_f material.

This effect of the difference in resin volume is also visible in the retention of strain, where LV_f material shows a reduction, and HV_f an increase in failure strain when exposed to FT cycles. However, it should be

noted that for HV_f material the coupons tested after 20, 53, 99, 153 and 199 FT cycles have an up to 5% higher resin volume fraction compared to the reference coupons and after 43 FT cycles. This higher amount of resin could make the material less stiff and brittle, resulting in a higher failure strain, but a lower stiffness.

Table 3.3 shows a summary of the retention of tensile properties for both materials after 199 FT cycles.

Table 3.3: Percentage retention $\pm$ standard deviation of tensile properties after 199 FT cycles

Property retention [%]			
	Strength	Strain	Modulus
LV_f	-10.7 $\pm$ 6.2	-6.2 $\pm$ 6.5	-5.8 $\pm$ 5.6
HV_f	-5.8 $\pm$ 6.1	3.8 $\pm$ 6.9	-6.2 $\pm$ 2.0

3.4.5. Discussion

Section 2.2.1 has shown that the expected reduction of tensile strength after exposure to FT cycles is 10%. However, this was on different types of composites, with vastly different fibre volume fractions. Section 3.2.5 has shown that external degradation of the material is visible and measurable, however, Section 3.3.6 does not show this to impact the uptake of moisture for the material. These contradictory results compared to the expected result in the question if the tensile properties are even affected by FT cycles, as internal degradation seems to be minimal.

This section has shown that there is degradation of the tensile properties. It has shown that the effects are more pronounced in LV_f material than in HV_f material. This is expected to be caused by the higher resin volume in LV_f, as this is the main component damaged by FT cycles. Table 3.3 shows that LV_f material shows an 11% reduction in tensile strength which was expected from the literature, compared to a 6% reduction for HV_f material. All reduction is still within suggested conversion factors of 0.85 in standards [41]. However, whether this conversion factor would be sufficient for combined environmental factors, is questionable.

The main difference between the materials is the increase in rupture strain for HV_f material when exposed to 199 FT cycles to almost 4%. This is expected to be caused by the aforementioned higher resin volume fraction for coupons tested after 20, 53, 99, 153 and 199 FT cycles. This could make the material less stiff and brittle, resulting in a higher failure strain, whilst showing a reduction in stiffness.

The results, however, show a large standard deviation for both materials and over the full ageing range. As this presents in both materials, whilst the production method differs, it is caused by more than possible manufacturing defects. The primary cause for this is expected to be the non-symmetric layup applied in the composites. This could lead to a non-uniform distribution of internal stresses developed during production, post-curing, ageing and testing, leading to less consistent results and failure modes when tested.

This high standard deviation could also partially be attributed to only using 1/8 of the maximum capacity of the rotel. Using such a small part of the capacity of the machine could lead to inaccuracies in force readings from the machine.

Due to this high standard deviation, it is not possible to conclude whether degradation has stabilised after 199 FT cycles. In environments with higher FT cycles, this should thus be investigated.

On top of that, it is not clear whether the change in ageing conditions after 47 FT cycles due to the stopping of circulation during the thawing stages as described in Section 3.1.3 has impacted the results. The high standard deviation of the results clouds the judgement of the minimum retention at 43 FT cycles and if it can be attributed to higher thawing stage water temperatures, or is within the experimental scatter.

Apart from these inconsistencies, this section has shown that FT cycles primarily negatively influence the tensile properties of LV_f and HV_f material. This means that, apart from the internal degradation not being immediately visible in saltwater uptake of the material, the matrix, and probably the fibre-matrix interface are impacted influencing the load transfer from matrix to fibres. This degradation has also resulted in coupons showing inter-laminar failures. This raises the question of whether especially inter-laminar shear is as unaffected by FT cycles as the literature would suggest. Especially in large-scale joints, with thicker composites, this is the main load-carrying mechanism, it is important to investigate this failure, to ensure the assumption FT cycles will not affect this property is a valid one.

3.4.6. Conclusion

This chapter has shown that next to surface degradation, there is proof of degradation of tensile properties when exposed to FT cycles. It shows the tensile modulus being affected similarly for both materials, but rupture strain and strength being affected less in HV_f materials. This is expected to be caused by the lower resin volume percentage in these materials, resulting in less of the component which is the most affected by FT cycles.

It should however be noted that all results show a high standard deviation. As this is visible in both Lv_f and HV_f material, it is expected to be caused by the non-symmetric layup of the composites, resulting in a non-uniform distribution of internal stresses developing during production, post-curing, ageing and testing, causing less consistent results and failure modes.

4

Thermal response

This chapter describes how the thermal response of Ms and Fs X90 joints is evaluated. This is done for LV_f material joints by exposing them to a warm morning and cold night. Section 4.1 will introduce the chapter and its relevance to the research, after which Section 4.2 will discuss the applied methodology. It will discuss the performed validation experiment and the methodology applied for modelling the heat transfer and the development of strains due to exposure to thermal loading. Section 4.3 discusses the used geometries and material properties, after which the results are presented in Section 4.4. Firstly, the results of the validation experiment and the adaptation of the heat transfer model are discussed. Secondly, these changes are applied on a Ms and Fs X90 FEA model, analysing heat transfer and the development of strains when exposed to the same warm morning as the validation experiment. Thirdly, this is repeated on a cold night. These results and their implications are then discussed and concluded in respectively Section 4.5 and Section 4.6.

4.1. Introduction

As discussed in Section 1.1.3, the effects of FT cycles can be divided into two parts, the effect of temperature and the effect of the presence of moisture, especially during sub-zero temperature exposure. In the previous chapter, the combination of these factors is experimentally evaluated on surface degradation, saltwater uptake and tensile property retention. However, the main step to take to be able to predict the effects is to develop numerical models. The first step to be taken on this subject is to be able to numerically estimate the thermal response of a wrapped composite joint. As up until now, no numerical methodology has been developed for the wrapped composite joint yet, the influence of temperature on the uneven expansion and contraction of the composite wrap and steel is unknown and unpredictable. Due to recent research determining the CTE of the composite [59], it is now possible to start this development.

To increase the feasibility of this research within the time frame, the scope is limited to assessing the effect of these changes in temperature while considering the composite as a whole, instead of as a combination of resin and fibre with a different CTE as well. To validate the thermal response, the temperature change of a mechanically tested LV_f Ms X90 joint with embedded TC is tracked while exposed to warm weather during a morning. Due to unavailability, this experiment is not repeated with a HV_f Ms X90 joint. It should however be noted, that the effects cannot simply be translated from one to another. Apart from the lower CTE due to the higher fibre volume fraction, the thermal conductivity will be higher, as it is higher for glass fibre than for vinyl ester resin [41]. This is expected to result in a faster conduction of heat when the fibre volume fraction is higher.

4.2. Methodology

4.2.1. Experimental



Figure 4.1: Setup of thermal validation experiment

To validate FEA results, a mechanically tested Ms X90 joint is put outside in the sun as shown in Figure 4.1. From 09:50 - 13:40 on a sunny day, a FLIR E96 thermal camera is used to evaluate the external temperature of the joint every 5 minutes. Using the software FLIR Thermal Studio temperatures are extracted from the thermal images at 7 locations. On top of that, 8 embedded TCs are tracked every minute. Figure 4.2 shows in blue two locations on the steel measured with a thermal camera, and in red on the wrap. The numbers indicate the TC placement, where TCs 7 to 9 are placed directly on the steel, and the other TCs are embedded in the wrap, on top of the first layer at a few mm distance from the steel.

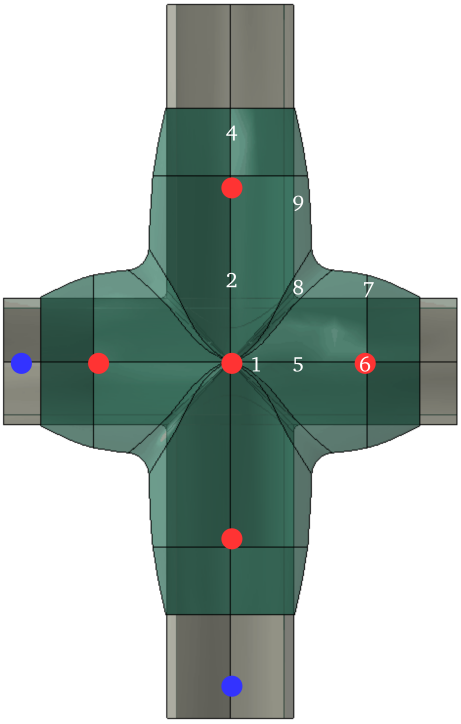


Figure 4.2: Locations of extracted temperatures of thermal images (blue dots on steel, red dots on composite wrap) and TC (numbered 1-2 and 4-9)

The weather conditions during this sunny morning are extracted from the Dutch PV Portal Database of KNMI, which contains data that is measured at the weather station of Rotterdam The Hague Airport, approximately 6 km from the experiment location [61]. The following data is extracted every 10 minutes:

- Time - in UTC +00
- Irradiance [W/m^2]
- Ambient temperature [°C]
- Wind speed [m/s]
- Cloud coverage [okta]

This extracted data is presented in Appendix C.

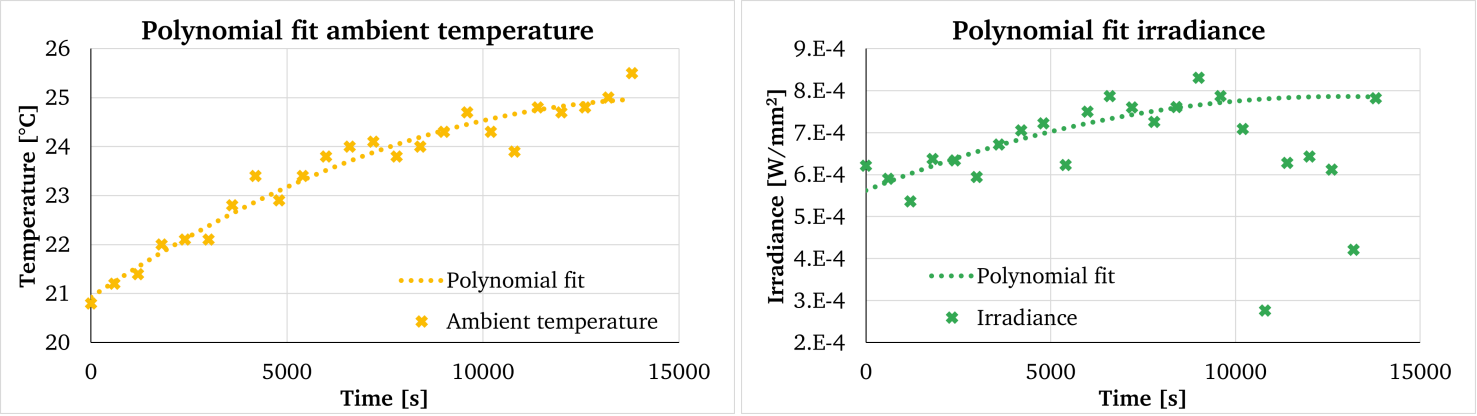
4.2.2. Numerical

Abaqus CAE is used to model the heat transfer and the development of strains due to temperature changes. First, this section discusses how the measured weather data of KNMI is taken into account and what assumptions of weather are made for the cold night in the models. Second, it describes how the heat transfer caused by these two types of weather is modelled via convection, conduction and radiation applied in the model. Third, and last, it is described how the developed strains caused by the changes in temperature of the material are extracted.

Weather data input

Warm morning

To adequately input the temperature and irradiance data in the model without introducing too many fluctuations due to measurement errors, or sudden changes, polynomial functions are used to describe the progression. Figure 4.3 shows the data from KNMI with markers, combined with the polynomial fit used in Abaqus to describe the irradiance and ambient temperature. The following equations are used:



(a) Ambient temperature with used polynomial fit

(b) Irradiance with used polynomial fit

Figure 4.3: Used simplifications for weather data

$$T = -1.780 \cdot 10^{-8} \cdot t^2 + 5.380 \cdot 10^{-4} \cdot t + 20.93 \tag{4.1}$$

$$E = -1.346 \cdot 10^{-12} \cdot t^2 + 3.467 \cdot 10^{-8} \cdot t + 5.625 \cdot 10^{-4} \tag{4.2}$$

Where

$E =$ irradiance [W/mm^2]

Next to that, the wind speed is assumed to be equal to the average. To define the begin temperature, the joint is divided into the general solid and the composite outer face. This is done to mimic initial temperature conditions more closely. No difference is made between steel bulk temperature and surface temperature, as this results in modelling errors in the first steps.

The temperature of the general solid and composite outer face is based on their average temperature based on respectively internal TC and thermal camera images. This results in the following initial temperatures for a warm morning:

- General solid - 24.38 °C
- Composite outer face - 30.56 °C

The steel outer face temperature is 27.9°C at the start of the experiment. Modelling it as 24.38 °C introduces a temperature roughly 3 °C below the average surface temperature.

Cold night

For the cold night a theoretical night is applied where the joint has a uniform starting temperature of -10

°C beginning of the night. During the night, it will cool down to -30 °C. Figure 4.4 shows the ambient temperature curve used. As it is modelled through the night, there will be no solar irradiance. However, the joint will still emit heat by radiation. Next to emitting radiation, heat is also transferred by conduction and convection. For simplification, it is assumed the wind speed is the same as the average wind speed during the validation experiment.

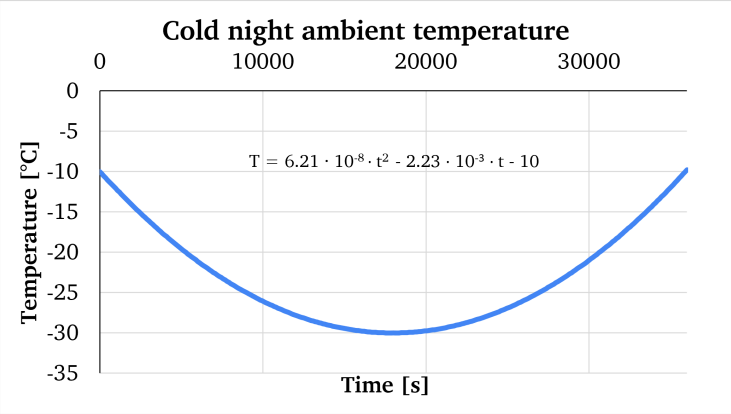


Figure 4.4: Ambient temperature with used polynomial fit for cold night

Heat transfer analysis

This section describes how the heat transfer analysis is conducted with Abaqus CAE. For the analysis, the composite is discretised to one solid, without separate definitions of matrix and fibre.

As time-varying weather data is used, a transient heat transfer analysis is performed with standard linear hex DC3D8 heat transfer mesh elements. To reduce computation time, mesh size is increased towards the composite wrap's exterior surface. Heat transfer is modelled by defining convection, conduction and radiation, outputting nodal temperatures over time. The different modes of heat transfer are briefly explained in the following sections but in more detail in Section 2.1.3.

Convection

To define convection, Abaqus defines an interaction of the surrounding with the object. It is governed by the following equation [62]:

$$q_{convection} = -h\left(\theta - \theta^0\right) \tag{4.3}$$

Where

q = heat flux across the surface [W/m^2]
h = heat transfer coefficient, or film coefficient [W/m^2°C]
θ = temperature of the surface [°C]
θ^0 = ambient temperature, or sink temperature [°C]

The heat transfer coefficient is determined using the formulas as presented in Section 2.1.3. The formulas presented are combined in a script, included in Appendix D. In this calculation method, a few assumptions are made. These assumptions are as follows:

- It is assumed the convective surface is one-half of the joint surface area, or in other words, the surface area visible in Figure 4.2. This surface area is also used to calculate the perimeter.
- It is assumed the flow over this surface area can be simplified as a flat plate.
- The heat transfer coefficient is assumed constant and calculated using average ambient temperature, average external joint temperature and average wind velocity. The heat transfer coefficient is thus assumed to be a certain value for all Ms joint analysis, and a certain other value for all Fs joint analysis. For the analysis of the cold night, the heat transfer coefficient is kept equal to the one calculated for the warm morning, as the difference between the air and the material in a less fictitious situation is unknown.

- All surfaces are assumed to be the upper surface of a hot plate. This assumption affects the results when convection is free or mixed.
- Convective fluid properties, in this case air, are assumed independent of temperature. Property values at 25 °C are used.

Conduction
Conduction is divided into two types in Abaqus:

- Conduction within one solid
- Conduction between solids

Conduction within one solid is automatically taken into account when the thermal conductivity and density of the material are defined and there is a temperature gradient within the material.

Between solids, there are two options present. When no interaction is defined, Abaqus assumes there is perfect conduction between the different objects that are in contact with each other. When conductance is defined as an interaction property, it is possible to define the conductance between the surfaces with the gap conductance k, which is dependent on the clearance between the surfaces, the contact pressure transmitted, the average temperature and the average mass flow rate [63]. In this case, as no loading apart from temperature is applied, the composite wrap and steel are in contact. It is assumed there is ideal conductance between the two, omitting the necessity of defining the interaction between the two solids.

Radiation
Radiation in Abaqus is governed by the following equation [62]:

$$q_{radiation} = \sigma \cdot \varepsilon \left[\left(\theta - \theta^Z\right)^4 - \left(\theta^0 - \theta^Z\right)^4 \right] \tag{4.4}$$

Where

ε = emissivity of the surface [$-$]
σ = Stefan-Boltzmann constant $5.6697 \cdot 10^{-8}$W/m^2°C^4
θ^Z = absolute zero temperature [°C]

Two types of radiation are taken into account:

1. Incoming solar irradiance
   A load representing the incoming electromagnetic waves of the sun.
   As the surface of the Ms X90 joint is white with black speckles, part of the solar radiation will be reflected. The absorptivity is used to determine the ratio of solar radiation that is absorbed.
2. Outgoing emission of heat
   An interaction of the heated joint with the environment by outgoing electromagnetic waves based on the emissivity of the object.

Thermal strain analysis

After the heat transfer analysis is completed, the nodal temperatures can be extracted and applied in a mechanical model by applying the results to a predefined temperature field. A separate model is generated for this, as Abaqus does not allow for a general static step after a heat transfer step. The interaction between steel and composite is defined as general contact, defining the surfaces which are in contact, with their normal, tangential and cohesive contact interaction properties. These properties, along with other material properties, are taken from prevalidated wrapped composite joint numerical models.

Together with the definition of CTE, the nodal temperature field will introduce stresses and strains in the composite and steel. A simplification is applied, by defining at t = 0, the joint is strain-free. Thermal strain build-up during production, testing or ambient conditions before the modelled time frame is thus not taken into account.

4.3. Materials

This section will discuss the used materials in this analysis. This will be done by first briefly discussing the differences between the Ms and Fs X90 geometry, and secondly by defining all relevant material properties for the heat transfer analysis.

4.3.1. Geometries

Two types of joint are taken into consideration; a Ms and Fs X90 joint. The Ms X90 joint has a steel diameter of 168.3 mm. This size joint is also used for the validation experiment. The joint used for the validation experiment is a joint that has been mechanically tested, this however will not impact the heat transfer significantly, as the damages to the material are not large enough for wind to move through parts of the joint and thus influence the temperature distribution significantly. The Fs joint has a steel diameter of 610 mm and is a representative scale for a jacket supporting a 14 MW turbine in an environment of 40 m water depth. The difference between the two scales in steel and composite is about a factor of 3.6.

The used geometry for the Ms joint is not an exact replica of the joint used in the validation experiment, but the design of the joint.

4.3.2. Material properties

To be able to model the joint, the following material properties should be known:

- Specific Heat
- Conductivity
- Emissivity
- Absorptivity
- Coefficient of Thermal Expansion
- Properties of air

To simplify the analysis, all material properties are assumed to be independent of temperature. This is primarily done due to the lack of availability of data on the change of material properties with temperature. On top of that, all material is assumed to be uniform.

Specific Heat

The specific heat of steel and composite are both taken from literature. For the wrap, a specific heat of 1650 J/kgK is used [64]. For the low alloy steel, the specific heat is 530 J/kgK [50]. In reality, the specific heat would increase for higher temperatures and decrease with lower temperatures. This means that in a colder environment, less energy is needed to result in a temperature change.

In the heat transfer analysis it is assumed the volume is constant. This means that all energy incoming to the system causes a raising of the temperature of the system, as the primary concern here is how the heat is transferred in the material.

Thermal conductivity

For the composite wrap a conductivity of 0.198 W/mK is used [64]. For low alloy steel a conductivity of 55 W/mK is used [50]. In reality, the thermal conductivity would decrease when the temperature is lower.

Emissivity

Based on [65] it is assumed that the white surface with black speckles has an emissivity of 0.90, which is close to a radiating black body.

Absorptivity

Based on [65] it is assumed that the white surface with black speckles has an absorptivity of 0.50. Next to that, the lower half of the joint is exposed to heat coming from the wooden pallet. The emissivity of the wooden pallet can be estimated as 0.85 [66]. The surface will thus result in an indirect absorptivity in the joint of $0.5 \cdot 0.85 = 0.425$.

Coefficient of thermal expansion

For the composite wrap a coefficient of thermal expansion in the longitudinal and transverse direction of $2.15 \cdot 10^{-5}$/°C is used and through the thickness of $7.82 \cdot 10^{-5}$/°C [59]. For steel, the coefficient of thermal expansion is assumed to be isotropic and $1.1 \cdot 10^{-5}$/°C [50].

Properties of air

To determine the heat transfer coefficient, various properties of air should be known. During analysis, the properties are assumed constant when temperature changes. Table 4.1 shows the properties at 25 °C.

Table 4.1: Properties of air at 25°C. [1] [67], [2] [68]

Property	Value
Thermal conductivity[1] [J/kg°C]	0.02551
Specific heat capacity[1] [W/m°C]	1007
Density[1] [kg/m^3]	1.184
Dynamic viscosity[1] (μ) [kg/ms]	$1.849 \cdot 10^{-5}$
Kinematic viscosity[1] (ν) [m^2/s]	$1.562 \cdot 10^{-5}$
Thermal volume expansion coefficient[2] (β) [°C^{-1}]	0.0038

4.4. Results

The results are presented and divided into three parts. First, the results of the Ms joint heat transfer analysis when exposed to the warm morning are presented next to the experimental results to validate and adapt the model to better fit the reality in Section 4.4.1. Second, the model with its adaptations is evaluated and compared to a Fs joint regarding temperature distribution and strain development along the steel-composite interface in Section 4.4.2. Third, these models are used to determine the temperature distribution and strain development when exposed to a cold night in Section 4.4.3.

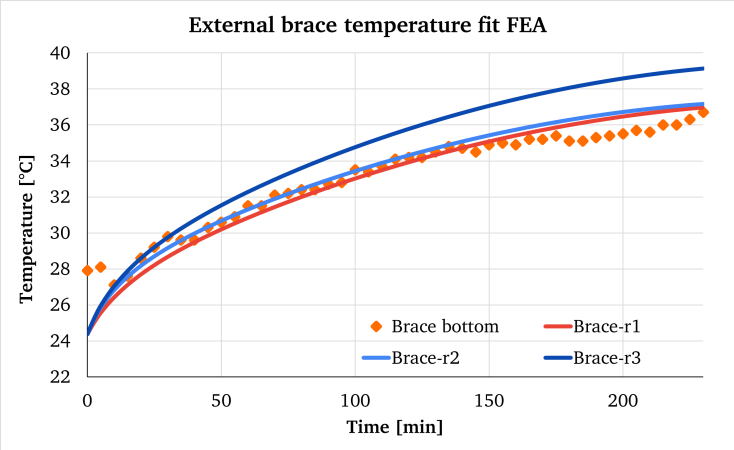
4.4.1. Validation experiment

Using the developed script presented in Appendix D, the heat transfer coefficient for a Ms X90 joint is calculated to be h =13.27 W/m^2°C. The type of flow present can be fully described by forced convection, which is turbulent, but where the laminar region cannot be neglected.

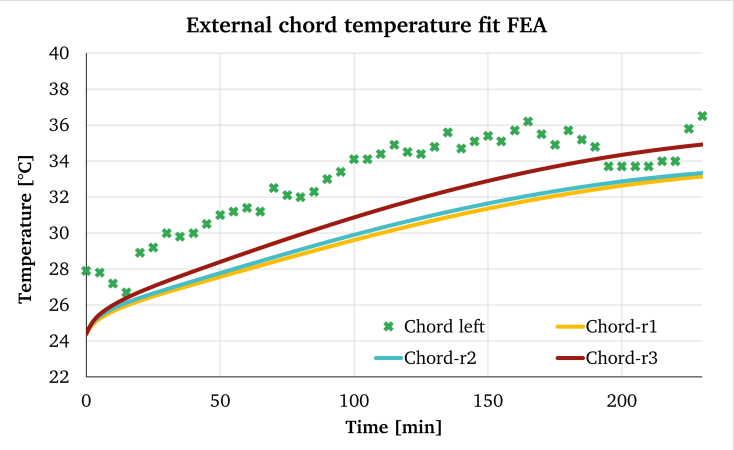
To determine the fit of the model and alter input, first, the steel material is considered. Figure 4.5 shows the comparison between FEA and TC, and FEA and thermal camera imaging. Three FEA runs are shown:

- r1 Initial run with all conditions as described in previous sections.
- r2 Change of steel specific heat to 410 J/kgK, which is the lower limit [50].
- r3 Whilst keeping the steel specific heat at 410 J/kg°C, changing heat transfer coefficient to h =10 W/m^2°C.

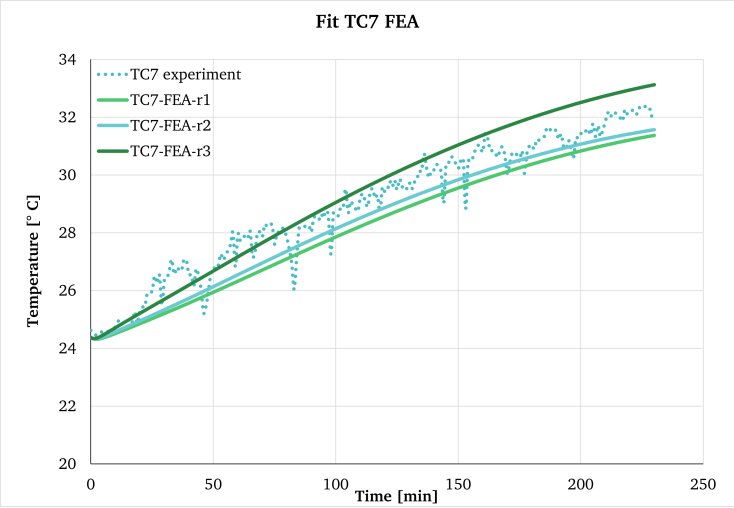
During the experiment, it was visible that in Delft there were clear skies, but the weather data from Rotterdam showed cloudy skies the whole morning, with a value of 8 okta for cloud coverage [61]. This may indicate the irradiance values are also an underestimation of the situation at the experiment location.



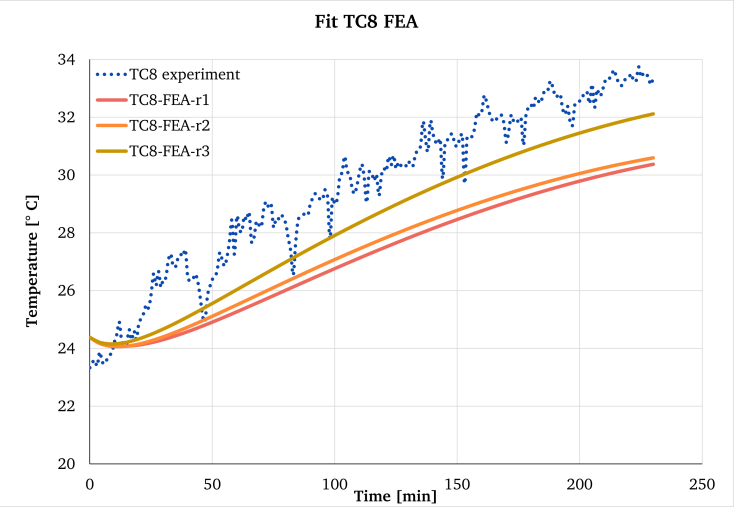
(a) Comparison steel brace temperature with FEA



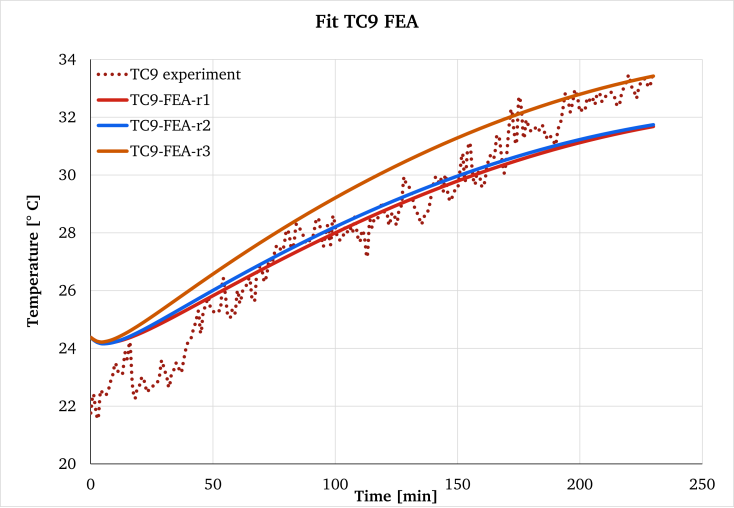
(b) Comparison steel chord temperature with FEA



(c) Comparison steel TC7 temperature with FEA



(d) Comparison steel TC8 temperature with FEA



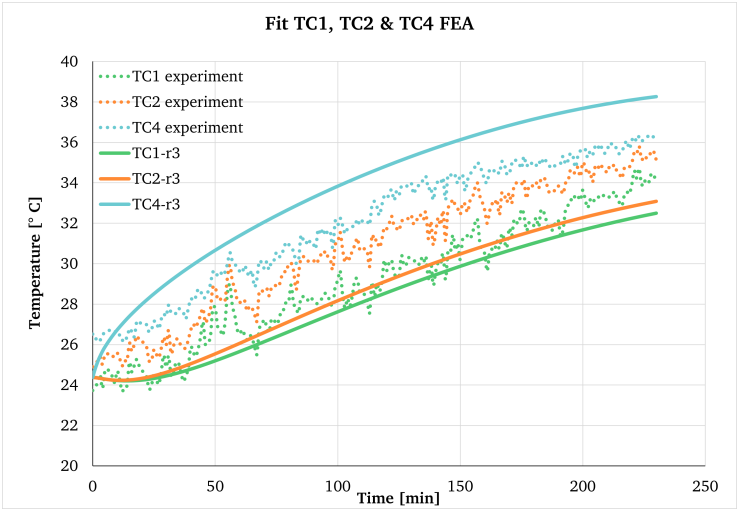
(e) Comparison steel TC9 temperature with FEA

Figure 4.5: Comparison steel temperature with FEA

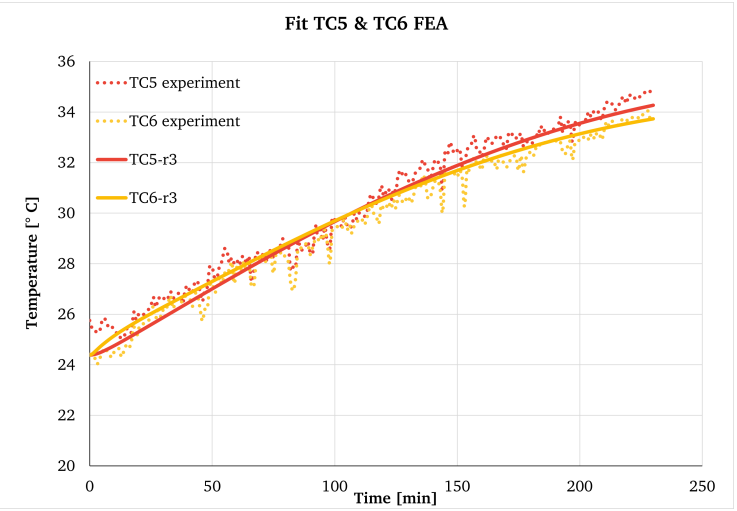
This brings to attention the following:

- Change of specific heat only has a minor impact on the heating rate of the material.
- Heat transfer coefficient has a large impact on the heating rate of the material internally and externally. The heat transfer coefficient is thus changed to $h = 10\text{W/m}^2\text{°C}$ for further Ms analysis.
- Temperature of the steel chord is not followed accurately by the model. This is probably caused by the fact that in the experiment more surface of the chord is exposed to direct solar irradiance than represented in the model. A similar reasoning is applicable to the overestimation of the temperature of the brace, then explained by a larger surface being exposed to direct solar irradiance in the model than in the experiment. However, the internal temperature is the main concern, as thermal strains on the interface of composite and steel are of interest. No changes are made to the model definition to change this discrepancy.
- All model runs show that when the defined begin temperature is higher than the actual temperature, in the first steps there is a slower heat transfer or even a decrease in temperature, visible for TC8 and TC9. When the defined begin temperature is too low, it results in a steep increase of heat transfer in the first steps, as is visible for the external brace and chord temperature. This is probably primarily caused by the lower specific heat and higher conductivity of steel compared to the composite wrap, where these effects will shown to be less in Figure 4.6.

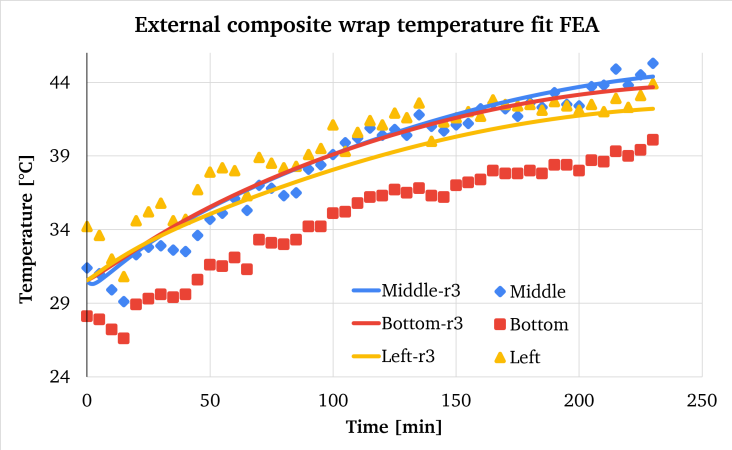
With these points in mind, the material properties of the composite are kept equal in further analysis, as changing the properties to better fit, would result in changing them drastically, and venturing outside of the realistic ranges. On top of that, insufficient literature on the thermal material properties of glass fibre-reinforced vinyl ester composites is available to make a good estimation of the range applicable. In Figure 4.6 the composite temperature graphs are presented for the external and internal temperature of the composite wrap.



(a) Comparison composite TC1, TC2 and TC4 temperature with FEA



(b) Comparison composite TC5 and TC6 temperature with FEA



(c) Comparison composite wrap temperature with FEA

Figure 4.6: Comparison composite wrap temperature with FEA

This shows there are a few regions where there are significant differences between FEA and composite temperature:

- The external temperature of the wrap on the bottom brace is overestimated by FEA. This can partially be explained by the external brace temperature being too high, as seen in Figure 4.5a. On top of that, this model does not take into account the exact position of the sun relative to the joint. Figure 4.1 shows that only the left part of the lower brace is directly in the sun, whereas the model assumes the whole top half. This can lead to an overestimation of the real temperature.
- TC2 temperature is underestimated by FEA. There is no direct reason to explain this difference.
- TC4 temperature is overestimated by FEA. This can directly be related to the brace temperature being overestimated as well, via conduction resulting in too high composite temperature.

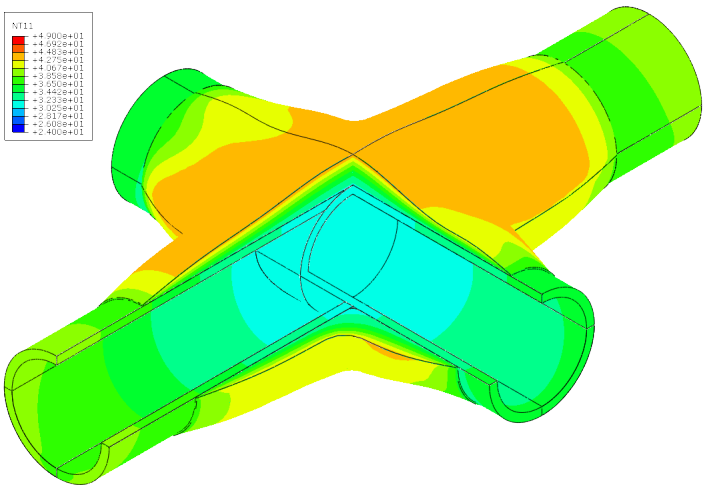
For a Fs joint, the specific heat of steel is kept at its lower limit of 410 J/kgK. As the geometry of the Fs and Ms is scaled but vastly different in size, it is not realistic to assume the same heat transfer coefficient. This value is for the Fs joint recalculated with the formulas presented in Appendix D.

4.4.2. Heat transfer and strain development during warm morning

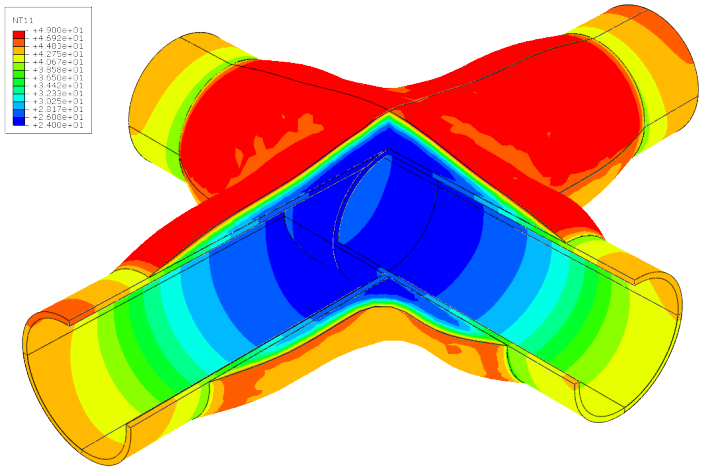
This section will analyse the difference in heat transfer between a Ms and Fs X90 joint when exposed to a warm morning and determine the developed strains due to these temperature changes.

Comparing temperature profile Ms X90 with Fs X90

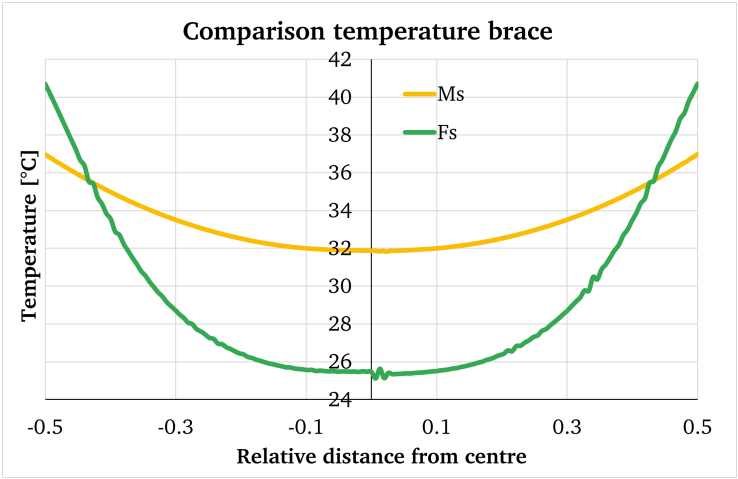
For modelling of the Fs X90 joint the heat transfer coefficient is calculated for the bigger geometry. The flow can be described as a forced convection flow, where free convection is negligible and the laminar region cannot be neglected. The heat transfer coefficient can be calculated to be $h = 6.508$ W/m^2°C.



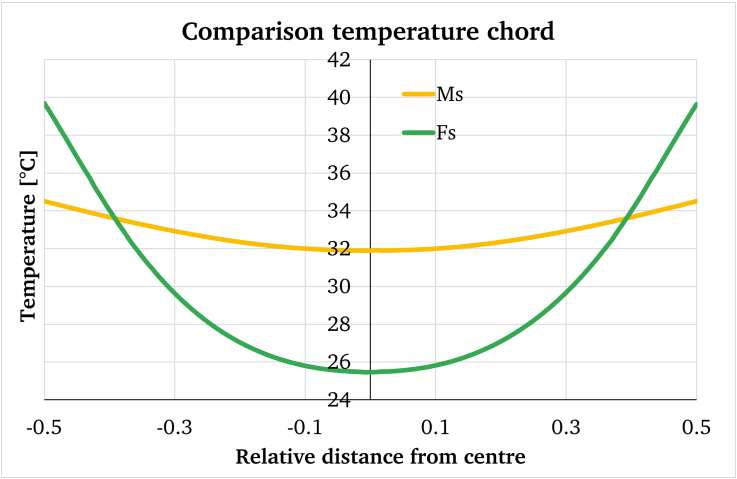
(a) Thermal profile of a Ms X90 joint after almost 4 hours outside



(b) Thermal profile of a Fs X90 joint after almost 4 hours outside



(c) Temperature over the relative length of the brace for Fs and Ms



(d) Temperature over the relative length of the chord for Fs and Ms

Figure 4.7: Thermal profile and temperature over chord and brace of Ms and Fs joint after 4 hours of exposure to sun and ambient temperatures

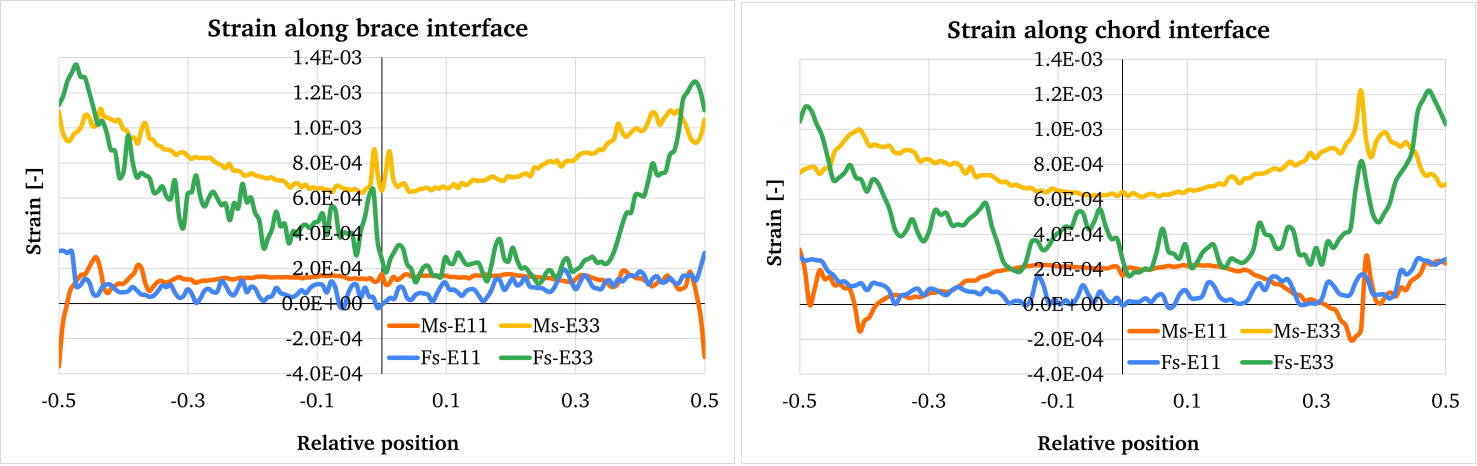
Figure 4.7 shows the thermal profiles and temperatures along the chord and brace for a Ms and Fs X90 joint after exposure to the same ambient temperature and solar radiation. It is visible that the Fs joint primarily warms op externally, whereas the Ms joint warms up more evenly throughout the profile of the wrap, resulting in higher temperatures on the steel-composite interface. For the Ms joint, there is a temperature difference of 13 °C within the whole joint. For the Fs joint, this is 24 °C. When comparing the maximum temperatures occurring along the steel-composite interface, this is respectively 40.7 °C for the Fs joint and 37.0 °C for the Ms joint. This shows the maximum developed temperature of a Fs joint is 10% higher than that of a Ms joint.

Comparing thermal strains Ms X90 with Fs X90

When the first mechanical model was run, the discovery was made that the method for defining general contact between the composite and steel was not suitable for the Fs, as it ran into numerical errors caused by the alterations that are made to nodes in the first steps to resolve the contact between the composite wrap and the steel brace and chord. To mitigate this problem, all parts in contact with each other were defined with a separate surface-to-surface contact definition, only allowing for adjustment to remove overclosure at the beginning steps. This allowed the Fs model to successfully run as well.

However, it should be mentioned that the change of interaction drastically changed the results for the Ms joint. This indicated that the methodology of defining contact when running this static analysis needs extra attention in further research.

Figure 4.8 shows the maximum strain developing in in-plane (11) and through-thickness (33) direction in the steel-composite interface after the almost 4-hour experiment. In all graphs, especially Fs, a large fluctuation is visible. After investigation, this fluctuation was proven to be dependent on the defined interaction between the steel and composite, not on the mesh size.



(a) Strains along brace for Fs and Ms

(b) Strains along chord for Fs and Ms

Figure 4.8: Developed numerically determined strains in in-plane (11) and through-thickness (33) direction for a Ms and Fs X90 joint at the end of the 4-hour warm morning along brace and chord steel-composite interface

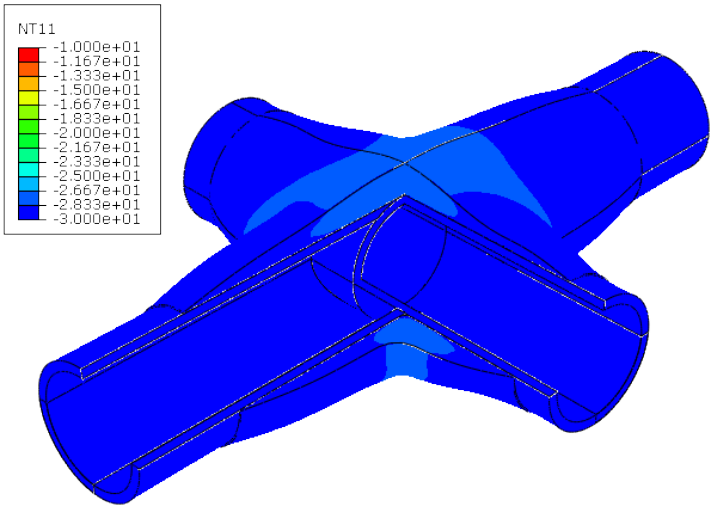
The maximum developed strains in the in-plane direction are $3.13 \cdot 10^{-4}$ at the middle of the chord for the Ms joint and $3.01 \cdot 10^{-4}$ at the edges of the brace for the Fs joint. For the through-thickness direction, the difference between Ms and Fs is larger, with a maximum strain of $12.2 \cdot 10^{-4}$ along the Ms chord, and $13.6 \cdot 10^{-4}$ along the Fs brace. This shows there are only small differences between Ms and Fs regarding the maximum developed strains. The difference between the maximum and minimum strain is higher for the Fs joint, which is to be expected considering the temperature of the Fs joint in the root remaining close to the begin temperature. However, the fluctuations in results do show the necessity of a further investigation of the definition of the contact between the surfaces and the movement of nodes in the first analysis steps.

4.4.3. Heat transfer and strain development during cold night

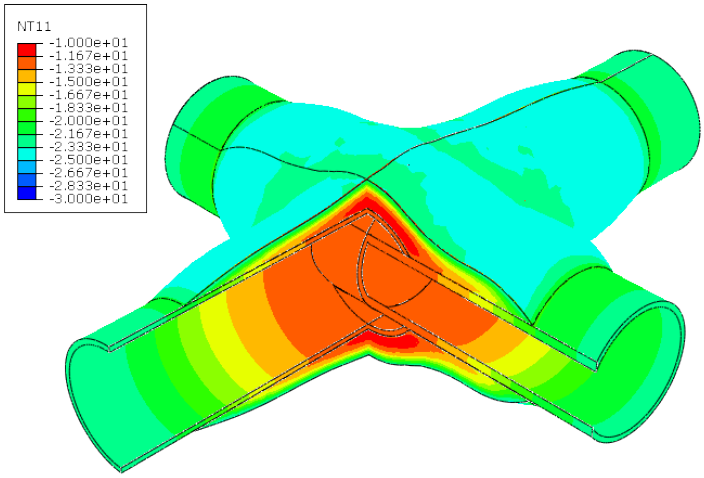
This section will analyse the difference in heat transfer between a Ms and Fs X90 joint when exposed to a hypothetical cold night and determine the developed strains due to these temperature changes.

Comparing temperature profiles Ms X90 with Fs X90

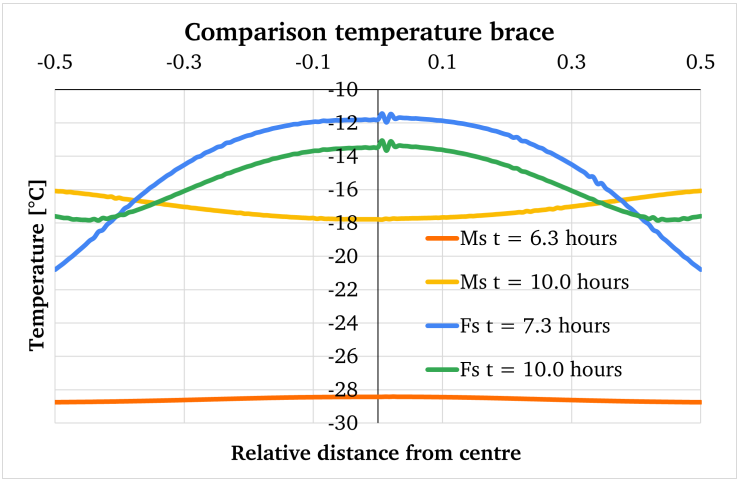
Figure 4.4 shows the minimum temperature in the night is reached after 5 hours. As the joint gradually cools down, the Ms joint reaches its minimum temperature after 6.3 hours, and the Fs joint after 7.3 hours.



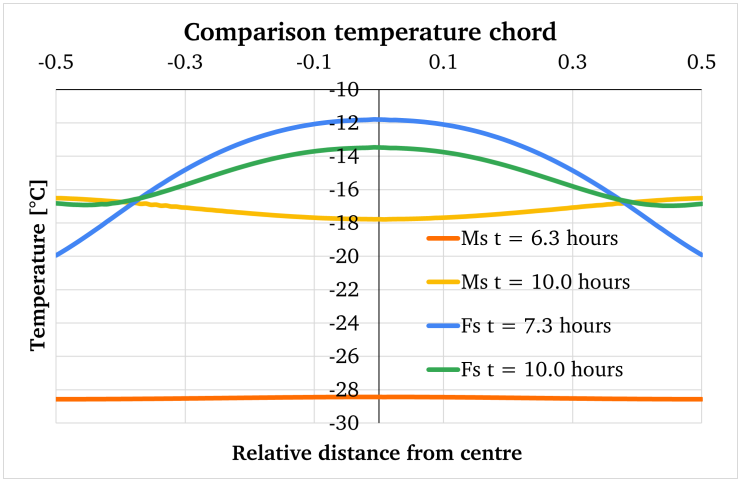
(a) Thermal profile of a Ms X90 joint after 6.3 hours of cold night exposure



(b) Thermal profile of a Fs X90 joint after 7.3 hours of cold night exposure



(c) Temperature over the relative length of the brace for Fs and Ms



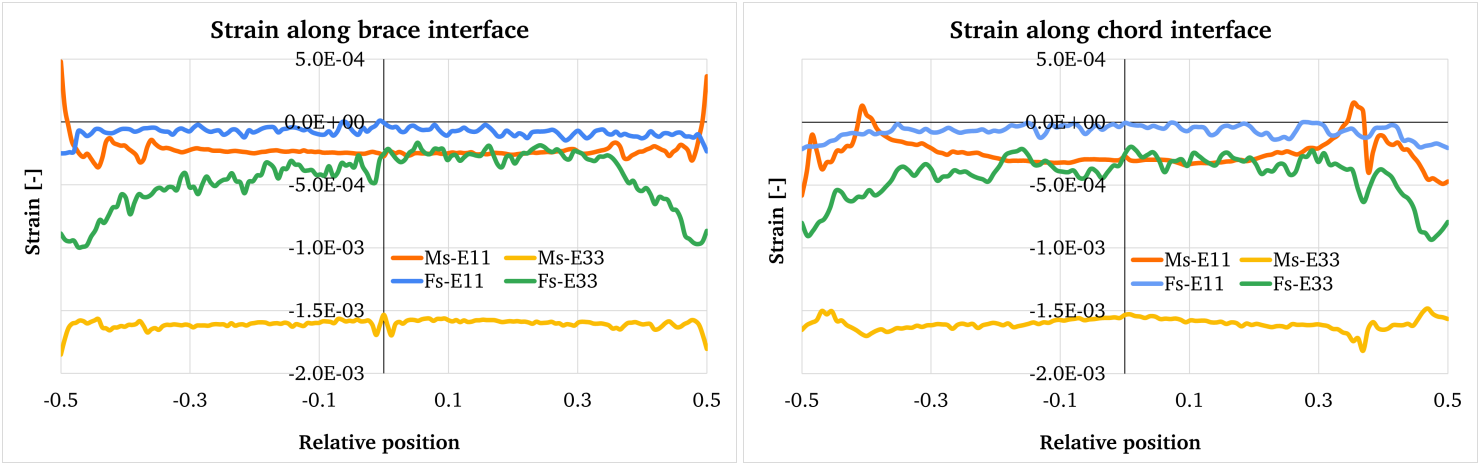
(d) Temperature over the relative length of the chord for Fs and Ms

Figure 4.9: Thermal profile and temperature over chord and brace of Ms and Fs joint at minimum reached temperature for the edges of the wrap, respectively 6.3 and 7.3 hours, of exposure to a cold night

Figure 4.9 shows the temperature over the relative length of the brace and chord at this minimum, and at the end of the 10-hour night. Next to this, the temperature profile of both joints is shown at the minimum. A similar temperature distribution is seen as with the warm morning, the Fs joint cools down slower and less uniformly. This results in a minimum temperature along the steel-composite interface of -20.8 °C for the Fs joint and -28.7 °C for the Ms joint. This means the minimum temperature for an Fs joint is almost 28% higher than for a Ms joint, which follows the magnitude of the temperature difference after a warm morning.

Comparing thermal strains Ms X90 with Fs X90

Figure 4.10 shows the strain developing in the steel-composite interface at the time of the minimum temperature occurring, 6.3 hours for a Ms joint and 7.3 hours for an Fs joint. Similar to the graphs for the warm morning, large fluctuations are visible due to the interaction between the steel and composite. It does however show a clearer difference between Fs and Ms joints when considering the through-thickness strains developed.



(a) Strains along brace for Fs and Ms

(b) Strains along chord for Fs and Ms

Figure 4.10: Developed numerically determined strain in in-plane (11) and through-thickness (33) direction when the joints reached their coldest point at the edges of the wrap along the brace and chord steel-composite interface

The minimum developed strains in the in-plane direction are $-5.84 \cdot 10^{-4}$ along the chord for a Ms joint, and $-2.50 \cdot 10^{-4}$ along the brace for a Fs joint. For the through-thickness direction, $-18.5 \cdot 10^{-4}$ along the brace of a Ms joint, and $-9.95 \cdot 10^{-4}$ along the brace of a Fs joint.

4.5. Discussion

This chapter evaluated the effect of temperature change on the strains developed at the steel-composite interface Ms and Fs X90 wrapped composite joints. Firstly, the numerical approach of determining the heat transfer is validated with an experiment on a Ms X90 joint. Secondly, the heat transfer for this Ms X90 joint and a Fs X90 joint is evaluated over the same warm morning, and developing strains along the steel-composite interface are determined. Thirdly this similar procedure is applied for Ms and Fs X90 joints when exposed to a hypothetical cold night.

This chapter has shown the first proposed methodology for determining the heat transfer in Ms and Fs wrapped composite joints is a suitable method. The fit between the numerical and experimental approaches was good, especially considering the simplifications in place, which were the following:

- Weather data used as input for the numerical model is not extracted at the location of the experiment, but at Rotterdam The Hague Airport. This is an open location with no surrounding buildings, resulting in wind speeds higher than in the heavily built area at the TU Delft Campus where the experiment was conducted. On top of that in Rotterdam the skies were clouded, represented by a cloud coverage of 8 okta, whereas in Delft there were almost clear skies at the moment of the experiment. This leads to a lower irradiance value than is expected to be the case in Delft. This may indicate that the numerical model is now overestimating the heat transfer rate, as there is a good fit with a lower irradiance then leads to an overestimation of the heating rate of the joint in this numerical model when considering a correct, higher solar irradiance.
- For begin temperature, a simplified temperature distribution was used, which resulted in the beginning temperatures not always aligning with the experiment, and resulting in a steeper gradient between material and ambient temperature in the numerical model than in the experiment, which can lead to an overestimation or underestimation of heat transfer rate in the model in the begin steps, which is also visible in the results.
- The full top half of the joint is assumed to be exposed to the sun, whereas in reality, it is under an angle and hitting another surface than now modelled. This results in an overestimation of the temperature of the bottom brace, and an underestimation of the chord temperature compared to the validation experiment.

- Properties of air, composite and steel are assumed to be independent of temperature. In reality, however, the specific heat and thermal conductivity would decrease as temperature decreases, probably resulting in a slower response to thermal effects than is now visible from the numerical analysis. The temperature change and developed strains would thus be lower than represented by these models when exposed to temperatures lower than 25 °C.
- For the calculation of the heat transfer coefficient, numerous simplifications were made:
  - The heat transfer coefficient is calculated with temperature-independent air properties.
  - Average ambient and external joint temperatures are used. If the difference between the two increases, this will result in a higher Grashof number. This will result in a flow leaning more towards free convection, which would lead to a higher heat transfer coefficient. This results in a faster exchange of heat between the object and the surroundings, from the warmer to the colder component, moving quicker towards an equilibrium between the two than will be the case with a lower heat transfer coefficient.
  - Average wind velocity is used. A lower wind velocity directly results in a lower heat transfer coefficient. Assuming the average will thus impact the accuracy of the coefficient.
  - The flow is assumed to be over a flat plate, which is a crude approximation of the shape of a wrapped composite joint. Flow around the object is expected to be more turbulent because of this shape, and greatly influences the heat transfer coefficient and thus results.
  - All these assumptions lead to the situation where all assumed flow can be described as forced convection, where free convection is negligible but the laminar region is not. When all these changes are applied, it could be the case that the type of flow can be characterised differently at a different timestep, drastically impacting the heat transfer coefficient.

But, as mentioned, all these assumptions still result in a heat transfer model which is close to the validation experiment. Investigation into thermal material property changes over temperature, applying these to the heat transfer coefficient and a further investigation into the determination of the heat transfer coefficient can greatly increase the accuracy of the model.

It should be noted that all these results represent a LV_f material. For HV_f, it is expected that the thermal conductivity of this material would be higher, based on the high thermal conductivity of glass fibre, compared to vinyl ester. This may result in a more uniform temperature distribution in a Fs HV_f joint, with higher and lower temperatures at the root of the joint, than is the case with LV_f. To accurately address these differences, experiments determining the thermal material properties, or execution of a similar validation experiment, is necessary.

After the nodal temperatures are extracted from the heat transfer models and are applied to a mechanical model, the longitudinal and through-thickness strains along the chord and brace steel-composite interface are evaluated. After exposure to a warm morning, it shows the longitudinal strains for Fs and Ms are the order of magnitude $3 \cdot 10^{-4}$, and the through-thickness strains $13 \cdot 10^{-4}$ near the edges of the wrap. During a cold night when the internal temperatures have reached their minimum, this difference between Ms and Fs joint is larger, showing a minimum longitudinal strain of $-6 \cdot 10^{-4}$ for the Ms joint, and $-2.5 \cdot 10^{-4}$ for the Fs joint. Next to that, a minimum through-thickness strain of $-18.5 \cdot 10^{-4}$ for the Ms joint, and $-9.95 \cdot 10^{-4}$ for the Fs joint has developed. These differences can be directly attributed to the Fs joint cooling down less, and less uniformly than the Ms joint. When there is no solar irradiance in play, all temperature changes are dependent on convection. Due to the high specific heat and low thermal conductivity of the composite, the heat transfer will be quicker when the composite is thinner, and a larger fraction of the material is closer to the steel, which conducts heat faster and can thus act as a cooling element for the composite from the inside out.

This results in smaller temperature changes in the root of the joint, which is the main load-distributing location. However, there are significant through-thickness strains and temperature changes in both scales along the edges of the wrap. It should be investigated if thermal cycles, not only FT cycles but all temperature cycles could negatively impact the steel-composite interface at this location, and if the potential detrimental effects at this location, can grow to the root of the joint.

On top of that, the composite is now modelled represented as one solid, with one CTE, whereas in reality, the material consists of fibres and resin with a different CTE, and the material at the interface does not

necessarily have a similar ratio between fibres and resin. With a more resin-rich first layer, the CTE at the interface would increase, increasing the difference in CTE between the steel and the composite at the interface, which will result in higher strains and stresses at the interface when exposed to temperature changes.

4.6. Conclusion

This chapter has shown the first thermal analysis of a Ms and Fs joint. It has shown that the temperature profile in a Ms scale LV_f joint will be more uniform than in a Fs joint. This is caused by the factor 3.6 larger scale, resulting in thicker material which heats up and cools down slower at the root of the joint. At the root of the joint, the interface is thus exposed to a smaller temperature range, which is less detrimental for the material.

Next to the thermal analysis, a mechanical analysis is performed to extract longitudinal and through-thickness strains along the steel-composite interface. This has shown a maximum occurring shrinkage and expansion strains of the magnitude of $\cdot 10^{-3}$ in the through-thickness direction at the edges of the wrap for a Fs joint. With the low amount of FT cycles in mind, this is not expected to cause significant environmental fatigue. However, the analysis of the warm morning is an indication that ambient temperature changes of 5 °C can already result in through-thickness strains of order of magnitude of 10^{-3}. Temperature changes over a full day, which are easily more than 5 °C, and will thus result in higher strains and accompanying stresses. It should be further investigated what the impact of these daily temperature cycles, above and below zero, is on the interface of the joint.

Mainly this research opens up further possibilities of modelling temperature effects on the wrapped composite joints for temperature tests and environmental studies.

5

Wrapping up

5.1. Conclusion

The goal of this research is to gain an initial insight into the effects of freeze-thaw cycles on the durability of the wrapped composite joint. This has been done by addressing a vast amount of different subjects. This research was centred around the following research question:

What is the impact of freeze-thaw cycles on the durability of the wrapped composite joint?

To answer this main research question, the following five sub-questions were defined to guide the research. The main answers to these questions will be presented, together with the strengths and limitations of the used methods and findings in this research. To close off, the main research question is answered.

1. *What method can be used for FT ageing of composite material used in the wrapped composite joint?*

   To answer this question, historical climate model data was used to evaluate maximum and minimum temperatures and yearly FT cycles over the North Sea, the goal application area for the wrapped composite joint. The minimum temperature was found to be -20 °C and the maximum temperature 23 °C. When considering FT cycles ranging from -10 °C to 0 °C, without accounting for diurnal cycles, it was found that in the northern parts of the North Sea a maximum of 6 FT cycles per year can be expected, which was roughly translated to 199 FT cycles in a service life of about 35 years.

   These findings are translated into an ageing methodology closely related to ASTM D7792, with exposure to -20°$C$for 3 hours, and exposure to +23°C for 3 hours, whilst submerged in 3.5 weight% saltwater. Ageing was performed automatically with a system developed for this research consisting of a climate chamber and a specially designed water supply and extraction system. The time from the beginning of water extraction to the climate chamber reaching -20°C is 30 minutes.

   The use of an automated ageing methodology opened up the possibilities for a more consistent and repeatable ageing methodology. However, the water body proved too big for the climate chamber to prevent cooling down by the surrounding elements, such as the stainless steel water tank, during the first thawing stages. This resulted in the cooling of the thawing water. Nonetheless, this did not seem to impact saltwater diffusivity.

   Next to that, the cooler of the climate chamber showed frost buildup throughout the ageing regime, which interrupted ageing 7 times during the 199 FT cycles. A manual solution was found by turning off the cooler during the thawing stages. These challenges proved that the method can introduce difficulties, however, after these first uses of the system, there is a clear view of its shortcomings and how these can be adapted in future research conducted with this system.

2. *What physical effects can be observed on the composite material as a consequence of the FT cycles?*

   This research investigated the visual change, height profile, surface roughness and wetting angle of FT-aged material to assess surface degradation.

   The necessity of a coating system of sufficient quality was made clear by fibre blooming occurring for HV_f material already after 29 FT cycles of exposure, and further progressing as ageing continued. This change was also visible in the surface roughness of HV_f material increasing more than 200% after 119 FT cycles, and a reduction of 16% of the wetting angle.

These effects were less visible for LV_f plates, showing no clear visual changes, only a 5% reduction of wetting angle and a 30% increase of surface roughness. This is expected to be caused by the LV_f plates having a thicker outer layer with only resin, which can act as a sacrificial layer during ageing. For HV_f material, the limited thickness of this layer results in earlier exposure of fibres to ageing, increasing the necessity of protection methods for ageing when using HV_f material compared to LV_f material in offshore conditions.

This research has thus shown that there is visible and measurable surface degradation as a result of FT cycles.

3. *What changes in saltwater uptake can be seen as a result of exposure to FT cycles compared to constant immersion?*

   Gravimetric measurements were conducted during FT ageing to asses whether the measured surface degradation translated into a faster uptake of moisture. On top of the experiments, FEA was used to model the continuous submersion of LV_f plates. HV_f and LV_f plates were produced with coated edges, to prevent diffusion from taking place in more than one direction. Experimental results show a slightly lower weight gain of plates during the thawing stage of FT cycles than under continuous submersion for an equivalent amount of time. The numerical analysis supports this finding for LV_f plates.

   As only 30 minutes elapse from emptying the water tank to ramping down the temperature of the climate chamber, it is not expected the material will lose weight during this period. However, as the material is not dried back after ageing, it is not clear if apart from weight gain, due to water uptake, there is also weight loss due to degradation. The results do not seem to indicate this but do not definitively answer this question.

   On top of that the comparison of results, both experimentally and numerically, is done with specimens of different geometry, open edges, and non-post-cured and post-cured, compared to the FT cycles aged post-cured material used in this research with closed edges.

   In general, the measuring methodology is prone to errors, as drying specimens before weighing with a paper towel does not result in a consistent dryness of the outer surfaces of the material at each measurement. Especially HV_f plates present difficulties when drying the surface, as they have high variability in surface height, resulting in water getting trapped and being difficult to remove before weighing. This visibly results in measurements with high deviations.

   However, the results do not raise the suspicion that FT cycles heavily impact the rate of diffusion. If it impacts the maximum possible moisture content of the material however is not clear with these experiments, as saturation is visibly not reached yet.

4. *What is the effect of FT cycles on the tensile properties of the composite material?*

   After 20, 43, 69, 99, 153 and 199 FT cycles quasi-static tensile tests were performed on HV_f and LV_f tensile coupons according to ISO 527 type 4 geometry. Test results are normalized to their reference and to their fibre volume fraction to determine whether the amount of resin present in the material impacts the magnitude of the impact of degradation.

   After 199 FT cycles a reduction of 10.7% and 5.8% of tensile strength for respectively LV_f and HV_f material is seen. The reduction of tensile strength for LV_f material is as expected from the literature, however, for HV_f it is lower. A reduction of 6.2% of the failure strain was seen in LV_f material and an increase of 3.8% in HV_f material. This difference is expected to be caused by the higher resin volume fraction of HV_f material tested after 20, 53, 99, 153 and 199 FT cycles, compared to the reference material. Finally, a reduction of 5.8% and 6.2% of E-modulus was seen for respectively LV_f and HV_f material.

   It can be concluded that FT cycles degrade composite tensile material properties, resulting in generally better material property retention for HV_f material than for LV_f material, except for the similar retention of tensile modulus.

   The results have however shown a necessity to investigate the integrity of the interface between the plies after exposure to FT cycles.

5. *What is the impact of temperature changes on the steel-composite interface of a Fs X90 joint?*

   In a first step to numerically predicting the temperature-induced effects in the wrapped composite joint, thermal models were developed, evaluating temperature changes and strain developments along the steel-composite interface.

   The developed heat transfer models for LV_f material showed a decent fit with Ms experimental validation data, despite significant simplifications. The same type of heat transfer definition is applied to a Fs joint, which is a suitable methodology, as thermal material properties are independent of scale when assumed the material is uniform.

   Using the extracted nodal temperatures, it is shown that especially along the edges of the wrap, the through-thickness strains in a Fs joint increase to a magnitude of 10^{-3} when exposed to a warm morning, or a similar magnitude in shrinkage for a cold night, and about half of that in the root of the joint. This suggests a significant strain development by only a small change of temperature, in the case of the warm morning. This temperature change, and larger, the joint will be exposed to daily. The effects of these fluctuations and the temperature changes the edges of the wrap are exposed to, should be investigated, to determine whether the damages developed by these exposures on the edges can move toward the root of the joint and damage the main load-carrying components of the joint.

The questions and answers above provide a framework to answer the main question in this research, "*What is the impact of freeze-thaw cycles on the durability of the wrapped composite joint?*". It has become clear that the exposure to FT cycles significantly degrades the surface of the material, increasing surface roughness and decreasing the wetting angle. The necessity for a sacrificial outer layer, or suitable coating is imperative to prevent the exposure of fibres of joints placed in the splash and tidal zone and further development of fibre blooming, which can eventually lead to delamination of the outer fibre layers.

This surface degradation, however, seemingly does not increase the saltwater uptake of the material, which is contradictory to expectations. Further research is necessary to be able to accurately answer this question, without the unknown possibility and magnitude of weight loss influencing the total weight change experimentally registered and thus clouding potential increase in saltwater uptake. This will help determine whether the onset of internal degradation caused by the presence of saltwater will be earlier when a material is exposed to FT cycles in the splash and tidal zone.

Even though external and internal degradation is not directly measurable by an increase in saltwater uptake, the reduction of tensile properties by approximately 10% or less does indicate there is internal degradation. This reduction within the full service lifetime of an offshore structure is not an unexpected magnitude. However, the showing of failure between plies in tensile tests after exposure to FT cycles, makes it necessary to investigate the through-thickness shear retention of the composite, as this is the main load-carrying mechanism for especially larger-scale joints, and would greatly impact joint durability if affected by FT cycles.

In a first step to numerically predicting the temperature-induced effects in the wrapped composite joint, thermal models were developed, evaluating temperature changes and strain developments along the steel-composite interface. The temperature of the root of Fs joints is expected to only slightly change when exposed to temperature cycles, which indicates the direct negative effects of these cycles at that location will be limited. However, the edges of the wrap show significant temperature changes and the development of through-thickness strains. As a result, the edges of the wrap, and the interface between composite and steel at this location will be impacted by temperature cycles, as well as other types of temperature cycles than FT cycles. Investigation into these effects is necessary to determine if the damages can be contained in the edges of the wrap, and not develop into the root of the joint as temperature changes and environmental influences continue.

Where some questions are answered, also more questions arise, and the need for additional research on this subject becomes clear, which is addressed in the next section, Section 5.2.

5.2. Recommendations

This research has formed a first indication of the impact of FT cycles on the wrapped composite joint. Further research is however necessary to answer the questions that have arisen through this research and to improve the quality of future research. These subjects are addressed per section, linked to the previously answered research sub-questions. To close off, general recommendations about handling this subject are made.

- Increasing robustness of FT ageing methodology
  - Primary difficulties with developing a system have shown high dependency on different parts of the equipment, the water pumps, the freezing element of the climate chamber, etc. If the material is saturated in saltwater before FT ageing commences, saltwater particles are already present in the material, and high humidity (>95% relative humidity) can be used during the thawing stages, simplifying the methodology. This can result in more uniform ageing conditions, and reduce variability in results. This method should however be tested to see if the climate chamber is capable of reducing the relative humidity sufficiently before freezing commences to prevent frost buildup on the cooler.
    On top of simplifying the ageing methodology, saturating the material before executing FT cycles is expected to result in more detrimental ageing. As it is unknown what the moisture content is of material in the splash and tidal zone, this methodology can ensure it is not underestimated.
  - Ageing performed with the setup as-is, should start with sufficient time spent on improving the system by:
    - Reducing cooling down of thawing water by using pumps that can run the full thawing cycle to keep the water temperature stable, or using a smaller water body that the climate chamber can still prevent from cooling down.
    - Building extra fail-safes when communication with the Arduino unexpectedly fails.
    - Adding a filtration system between the outgoing water and the pumps, to make sure they are not damaged by for example corrosion particles from the stainless steel tank, or other residue coming from the plates. This also ensures that the material is aged in 'clean' water.
  - Prevent frost build-up by controlling humidity in the climate chamber when outside of the technical reach by either
    - Including a tube of dry air to prevent frost buildup by lowering humidity with an extra system.
    - Turn off the freezing element automatically during the thawing stage. When the climate chamber has reached a stable temperature, and the water body is stable in temperature, this will not impact the ageing.
- Physical effects of FT ageing
  - More detailed microscopic research on the exterior of the material and the internal failure surfaces of tested specimens after FT cycles can increase understanding of the components of the material that are the most affected by ageing and aid in designing, developing and protecting composite material that will be exposed to FT cycles during service lifetime.
  - For HV_f material it is important to investigate possibilities of more resin-rich outer layers of the material, or suitable protection systems to prevent the exposure of fibres to the external environment.
- Effects of FT cycle degradation on the saltwater uptake
  - To ease measurement and decrease the deviation between measurements, smaller-sized specimens should be tracked during ageing. This eases the handling of the specimens, opens up the possibility of using higher accuracy scales and eases cleaning of the surface.
  - Alternative methods for drying plates with a high surface roughness before weighing should be investigated to reduce variability between measurements, especially for HV_f material.
  - To be able to conclude without question if saltwater uptake increases due to FT cycle exposure degradation, it is advised to dry already aged material and expose it to continuous submersion afterwards. Material of the same geometry and post-curing conditions without being exposed to

FT cycles should be submerged next to it, to be able to compare the two different datasets with each other.

- Testing of material properties
  - As the results have not shown a clear stabilisation of degradation, it is advised to increase the total amount of FT cycles, and the testing interval, to, for example, 50, 100, 200 and 300 FT cycles. Especially keeping in mind the increasing service lifetime of structures as technology advances, only taking into account the maximum the structure may encounter in offshore life on the North Sea, may not be sufficient.
  - A symmetric lay-up should be used for every test to remove potential effects of non-uniform internal stress development due to the non-symmetric lay-up. This may reduce the high standard deviation now visible in the results.
  - Tensile coupons showing significant inter-laminar failure show the necessity to test not only shear properties after exposure to FT ageing but also fracture toughness.
  - Literature has shown that the effects of FT degradation on fatigue life are unknown. Knowledge of these effects can only be gained experimentally and should be considered.
  - Test bi-material interface failure coupons after exposure to FT cycles by air, as moisture will not reach the interface during ageing. The temperature cycles will result in strains on the interface due to differences in the CTE of the materials. The effects of this on the interface are not predictable without experimental validation and are crucial to wrapped composite joint design. To develop tools for predicting these effects, it is advised to investigate possibilities of numerically validating the ageing and experiments until failure.
- Effect of temperature changes on joints
  - More in-depth research on this topic opens up different possibilities for accurately predicting strains and stresses not only during service life but also during temperature testing of material, increasing the reliability of developed models.
  - To increase the accuracy of these models, an investigation of the flow and heat transfer around the wrapped composite joint is necessary to create an accurate representation of the joint in service life conditions. This should be done by using a computational fluid dynamics approach to help determine the heat transfer coefficient with more accuracy.
  - It is advised to validate the thermal properties of both composite and steel at different temperatures by experimental tests and include this in the models. This must be done for both LV_f and HV_f material, as the latter will present with a higher thermal conductivity, which can greatly impact the response to thermal loading. This is expected to, for example, result in more temperature fluctuations at the root of the joint, which may negatively impact the environmental durability of HV_f joints compared to LV_f joints.
  - To gain a full understanding of the complex working of environmental influences together with joint geometry, it is advised to conduct tests with material that is tested under real conditions. By, for example, applying optical fibres and thermocouples in the material, it can be evaluated what thermal cycles and strains a joint endures, greatly increasing understanding, and the possibilities to model complex exposures.

In general, it is advised, especially when considering material with two different fibre volume fractions, to not lose sight of what implications changes in fibre volume fraction, application environment and envisioned service lifetime can present and critically asses whether conclusions of previous research can change.

References

[1] Joyce Lee Rebecca Williams Feng Zhao. *GEWC Global Offshore Wind Report 2022*. Tech. rep. Global Wind Energy Council, 2022.

[2] Rijksoverheid. *The Esbjerg Declaration on The North Sea as a Green Power Plant of Europe*. 2022. URL: https://www.rijksoverheid.nl/documenten/publicaties/2022/05/18/the-esbjerg-declaration-on-the-north-sea-as-a-green-power-plant-of-europe.

[3] B.C. O'Kelly and M. Arshad. *20 - Offshore wind turbine foundations – analysis and design*. Ed. by Chong Ng and Li Ran. Woodhead Publishing, 2016, pp. 589–610. DOI: 10.1016/B978-0-08-100779-2.00020-9. URL: https://www.sciencedirect.com/science/article/pii/B9780081007792000209.

[4] The Wind Power. *Arcadis Ost 1 (Germany)*. 2024. URL: https://www.thewindpower.net/windfarm_en_16726_arcadis-ost-1.php.

[5] DEME. *DEME's next generation vessel 'Orion' succesfully installs first monopile at Arcadis Ost*. June 2022. URL: https://www.deme-group.com/news/demes-next-generation-vessel-orion-successfully-installs-first-monopile-arcadis-ost.

[6] Paul Dvorak. *New materials and construction method promise 100-year life for offshore turbine jacket foundation*. 2024. URL: https://www.windpowerengineering.com/new-materials-construction-method-promise-100-year-life-offshore-turbine-jacket-foundation/.

[7] Easy Composites. *Glass Fibre Reinforcements*. 2024. URL: https://www.easycomposites.co.uk/glass-fibre-reinforcements.

[8] Tree Composites B.V. *Introducing the TC-joint*. 2024. URL: https://www.treecomposites.com/over/.

[9] P. He and M. Pavlovic. "Feasability of wrapped FRP circular hollow section joints". In: *Proceedings of the 17th International Symposium on Tubular Structures* (2020). DOI: 10.3850/978-981-11-0745-0043-cd.

[10] Ruben Ucaggi. *Offshore Wind Turbine Jacket Foundation*. URL: https://grabcad.com/library/offshore-wind-turbine-jacket-foundation-2.

[11] American Bureau of Shipping. *Guidance notes on cathodic protection of offshore structures*. Tech. rep. 2018. URL: https://ww2.eagle.org/content/dam/eagle/rules-and-guides/current/offshore/306-cathodicprotection-offshore-structures/cathodic-protection-offshore-gn-dec18.pdf.

[12] GROW. *Wrapped Composite Joints for Next generation offshore wind support structures - Phase 2 (WrapNode-II)*. 2023. URL: https://grow-offshorewind.nl/project/wrapnode-2.

[13] Jakub Smoleń, Karolina Bechcińska, Weronika Smok, Piotr Olesik, and Krzysztof Stępień. "Assessment of the effectiveness of selected coatings for protection against UV radiation in glass fiber reinforced composites (GFRP)". In: *Composites Theory And Practice* 24 (Apr. 2024), pp. 65–71. DOI: 10.62753/ctp.2024.09.1.1.

[14] Kate Mokobia, Eribe M. Jonathan, Glory Oyiborhoro, Muniratu Maliki, and Ikhazuagbe Hilary Ifijen. "Environmental Degradation of Polymer-Based Composite Materials: Challenges and Mitigation Strategies". In: *TMS 2024 153rd Annual Meeting & Exhibition Supplemental Proceedings* (2024), pp. 1218–1236.

[15] Milad Bazli, Armin Jafari, Hamed Ashrafi, Xiao-Ling Zhao, Yu Bai, and R.K. Singh Raman. "Effects of UV radiation, moisture and elevated temperature on mechanical properties of GFRP pultruded profiles". In: *Construction and Building Materials* 231 (2020), p. 117137. DOI: 10.1016/j.conbuildmat.2019.117137. URL: https://www.sciencedirect.com/science/article/pii/S0950061819325851.

[16] Marcio Arouche and Marko Pavlović. "Effect of offshore environmental conditions on the mechanical behavior of glass fiber reinforced polymers (GFRPs)". In: Aug. 2023. DOI: 10.5281/zenodo.8104754.

[17] Marcio Moreira Arouche, Sigurdur Egilsson, Weikang Feng, and Marko Pavlovic. “Effect Of Temperature On The Mode II Fatigue Delamination Of A Glass Fiber Reinforced Polymer (Gfrp)”. English. In: *Proceedings of the 21st European Conference on Composite Materials*. Ed. by Christophe Binetury and Frédéric Jacquemin. Vol. 3. 21st European Conference on Composite Materials, ECCM21 ; Conference date: 02-07-2024 Through 05-07-2024. The European Society for Composite Materials (ESCM) and the Ecole Centrale de Nantes., 2024, pp. 289–294. URL: https://eccm21.org/.

[18] P. Karatsi. *Durability of composite to steel bi-material joints*. 2023.

[19] ASTMD7792. *Standard Practice for Freeze/Thaw Conditioning of Pultruded Fiber Reinforced Polymer (FRP) Composites Used in Structural Designs*. Tech. rep. ASTM International, 2015.

[20] ASTMC666. *Standard Test Method for Resistance of Concrete to Rapid Freezing and Thawing*. Tech. rep. ASTM International, 2015.

[21] ASTMD6944-15. *Standard Practice for Determining the Resistance of Cured Coatings to Thermal Cycling*. Tech. rep. ASTM International, 2020.

[22] S.A. Grammatikos, R.G. Jones, M. Evernden, and J.R. Correia. “Thermal cycling effects on the durability of a pultruded GFRP material for off-shore civil engineering structures”. In: *Composite Structures* 153 (2016), pp. 297–310. DOI: http://dx.doi.org/10.1016/j.compstruct.2016.05.085.

[23] J. Rivera and V.M. Karbhari. “Cold-temperature and simultaneous aqueous environment related degradation of carbon/vinylester composites”. In: *Composites Part B: Engineering* 33.1 (2002), pp. 17–24. DOI: 10.1016/S1359-8368(01)00058-0. URL: https://www.sciencedirect.com/science/article/pii/S1359836801000580.

[24] Abu T. Shahid, Mateus Hofmann, Mário Garrido, João R. Correia, and Inês C. Rosa. “Freeze–Thaw Durability of Basalt Fibre Reinforced Bio-Based Unsaturated Polyester Composite”. In: *Materials* 16.15 (2023). DOI: 10.3390/ma16155411. URL: https://www.mdpi.com/1996-1944/16/15/5411.

[25] V. M. Karbhari, J. Rivera, and J. Zhan. “Low-Temperature Hygrothermal Degradation of Ambient Cured E-Glass/Vinylester Composites”. In: *Journal of Applied Polymer Science* 86 (2002), pp. 2255–2260.

[26] A. Paul et al. *Thermodynamics, Diffusion and the Kirkendall Effect in Solids*. Springer International Publishing Switzerland, 2014. DOI: 10.1007/978-3-319-07461-0_3.

[27] Chi-Hung Shen and George S. Springer. “Moisture Absorption and Desorption of Composite Materials”. In: *Journal of Composite Materials* 10.1 (1976), pp. 2–20. DOI: 10.1177/002199837601000101.

[28] Abderrazak Chilali, Mustapha Assarar, Wajdi Zouari, Hocine Kebir, and Rezak Ayad. “Effect of geometric dimensions and fibre orientation on 3D moisture diffusion in flax fibre reinforced thermoplastic and thermosetting composites”. In: *Composites Part A: Applied Science and Manufacturing* 95 (2017), pp. 75–86. DOI: 10.1016/j.compositesa.2016.12.020. URL: https://www.sciencedirect.com/science/article/pii/S1359835X16304481.

[29] Carol L. Schutte. “Environmental durability of glass-fiber composites”. In: *Materials Science and Engineering: R: Reports* 13.7 (1994), pp. 265–323. DOI: 10.1016/0927-796X(94)90002-7. URL: https://www.sciencedirect.com/science/article/pii/0927796X94900027.

[30] Weiping He, Xu Li, Piao Li, Shirui Fang, and Anxin Ding. “Experimental Investigation on Hygroscopic Aging of Glass Fiber Reinforced Vinylester Resin Composites”. In: *Polymers* 14 (Sept. 2022), p. 3828. DOI: 10.3390/polym14183828.

[31] J.C. Arnold, S.M. Alston, and F. Korkees. “An assessment of methods to determine the directional moisture diffusion coefficients of composite materials”. In: *Composites Part A: Applied Science and Manufacturing* 55 (2013), pp. 120–128. DOI: 10.1016/j.compositesa.2013.08.012. URL: https://www.sciencedirect.com/science/article/pii/S1359835X13002364.

[32] Xu Jiang, Henk Kolstein, and Frans S.K. Bijlaard. “Moisture diffusion in glass–fiber-reinforced polymer composite bridge under hot/wet environment”. In: *Composites Part B: Engineering* 45.1 (2013), pp. 407–416. DOI: 10.1016/j.compositesb.2012.04.067. URL: https://www.sciencedirect.com/science/article/pii/S135983681200306X.

[33] Yuehua Yuan and T. Randall Lee. “Contact Angle and Wetting Properties”. In: *Surface Science Techniques*. Ed. by Gianangelo Bracco and Bodil Holst. Berlin, Heidelberg: Springer Berlin Heidelberg, 2013, pp. 3–34. DOI: 10.1007/978-3-642-34243-1_1.

[34] Robert N. Wenzel. “RESISTANCE OF SOLID SURFACES TO WETTING BY WATER”. In: *Industrial and Engineering Chemistry* 28.8 (1936), pp. 988–994. DOI: 10.1021/ie50320a024.

[35] Marouan Rejeb, Ahmed Koubaa, Fayez Elleuch, François Godard, Sébastien Migneault, Mohamed Khlif, and Hatem Mrad. “Effects of Coating on the Dimensional Stability of Wood-Polymer Composites”. In: *Coatings* 11.6 (2021). DOI: 10.3390/coatings11060711.

[36] Yi Lu, Ning Tang, Ruyue Lian, Jianping Qi, and Wei Wu. “Understanding the relationship between wettability and dissolution of solid dispersion”. In: *International Journal of Pharmaceutics* 465.1 (2014), pp. 25–31. DOI: https://doi.org/10.1016/j.ijpharm.2014.02.004. URL: https://www.sciencedirect.com/science/article/pii/S0378517314000866.

[37] M. Thirumaleshwar. *Fundamentals of heat and mass transfer*. Pearson, 2009.

[38] Donatello Annaratone. *Engineering Heat Transfer*. Springer-Verlag Berlin Heidelberg, 2010. DOI: 0.1007/978-3-642-03932-4.

[39] Gokhan Demircan, Mustafa Ozen, Murat Kisa, Abuzer Acikgoz, and Yusuf Işıker. “The effect of nano-gelcoat on freeze-thaw resistance of glass fiber-reinforced polymer composite for marine applications”. In: *Ocean Engineering* 269 (2023), p. 113589. DOI: 10.1016/j.oceaneng.2022.113589. URL: https://www.sciencedirect.com/science/article/pii/S0029801822028724.

[40] T. Juska, P. Dutta, L. Carlson, and J. Weitsman. “Gap Analysis for Durability of Fiber Reinforced Polymer Composites in Civil Infrastructure”. In: The Civil Engineering Research Foundation, 2001. Chap. 5.

[41] European committee for standardization. *TS 19101: 2021 Design of fibre-polymer composite structures*. Tech. rep. TB, 2023.

[42] Hui Li, Qi Lin, and Hui Zhang. “Freeze–thaw resistance of unidirectional-fiber-reinforced epoxy composites”. In: *Journal of Applied Polymer Science* 123 (Mar. 2012). DOI: 10.1002/app.34870.

[43] Tarikul Hasan, João R. Correia, Mário Garrido, Susana Cabral-Fonseca, Francisco Soares, Marco Jorge, and José Sena-Cruz. “Effects of freeze-thaw cycles on the mechanical and thermomechanical properties of GFRP laminates produced by vacuum infusion”. In: *11th International Conference on FRP Composites in Civil Engineering*. 2023.

[44] Jia-Wei Shi, Wen-Hai Cao, Lei Chen, and Ang-Lin Li. “Durability of wet lay-up BFRP single-lap joints subjected to freeze–thaw cycling”. In: *Construction and Building Materials* 238 (2020), p. 117664. DOI: 10.1016/j.conbuildmat.2019.117664. URL: https://www.sciencedirect.com/science/article/pii/S0950061819331174.

[45] Yu-Yang Pang, Gang Wu, Hai-Tao Wang, Zhi-Long Su, and Xiao-Yuan He. “Experimental study on the bond behavior of the CFRP-steel interface under the freeze–thaw cycles”. In: *Journal of Composite Materials* 54.1 (2020), pp. 13–29. DOI: 10.1177/0021998319851191.

[46] Jia-Wei Shi, Hong Zhu, Gang Wu, and Zhi-Shen Wu. “Tensile behavior of FRP and hybrid FRP sheets in freeze–thaw cycling environments”. In: *Composites Part B: Engineering* 60 (2014), pp. 239–247. DOI: 10.1016/j.compositesb.2013.11.026. URL: https://www.sciencedirect.com/science/article/pii/S1359836813007002.

[47] Mohsen Heshmati, Reza Haghani, and Mohammad Al-Emrani. “Durability of CFRP/steel joints under cyclic wet-dry and freeze-thaw conditions”. In: *Composites Part B: Engineering* 126 (2017), pp. 211–226. DOI: 10.1016/j.compositesb.2017.06.011. URL: https://www.sciencedirect.com/science/article/pii/S1359836817302238.

[48] Ankit Agarwal, Stephen Foster, Ehab Hamed, and Zora Vrcelj. “Testing of steel-CFRP adhesive joints under freeze-thaw cycling”. In: *From Materials to Structures: Advancement through Innovation* (2012). DOI: 10.1201/b15320-143.

[49] S. Tam and Shamim Sheikh. “Behavior of fibre reinforced polymer (FRP) and FRP bond under freeze thaw cycles and sustained load”. In: *Fourth Int. Conf. Compos. Civ. Eng. (CICE 2008), Zurich, Switz.* (Jan. 2008), pp. 22–24.

[50] Mike Ashby. *Material property data for engineering materials*. Tech. rep. Ansys, 2021. URL: https://www.ansys.com/academic/educators/education-resources/booklet-material-property-data-for-engineering-materials.

[51] EN 12371. *Natural stone test methods - Determination of frost resistance*. Tech. rep. European Committee for Standardization, 2010.

[52] DNVGL-ST-0437. *Loads and site conditions for wind turbines*. Tech. rep. Det Norske Veritas, 2016.

[53] Lijuan Li. *CAS FGOALS-g3 model output prepared for CMIP6 CMIP historical*. Version 20190826 (r1i1p1f1), 20190827 (r3i1p1f1), 20191030 (r4i1p1f1), 20200412 (r5i1p1f1). 2019. DOI: 10.22033/ESGF/CMIP6.3356. URL: https://doi.org/10.22033/ESGF/CMIP6.1783.

[54] Pascal Bourgault, David Huard, Trevor James Smith, Travis Logan, Abel Aoun, Juliette Lavoie, Éric Dupuis, Gabriel Rondeau-Genesse, Raquel Alegre, Clair Barnes, Alexis Beaupré Laperrière, Sébastien Biner, David Caron, Carsten Ehbrecht, Jeremy Fyke, Tom Keel, Marie-Pier Labonté, Ludwig Lierhammer, Jwen-Fai Low, Jamie Quinn, Philippe Roy, Dougie Squire, Ag Stephens, Maliko Tanguy, and Christopher Whelan. “xclim: xarray-based climate data analytics”. In: *Journal of Open Source Software* 8.85 (2023), p. 5415. DOI: 10.21105/joss.05415.

[55] Keyence. *Arithmetical Mean Height (Ra, Pa, Wa) | Surface Roughness Parameters*. 2024. URL: https://www.keyence.com/ss/products/microscope/roughness/line/parameters.jsp.

[56] A.F. Stalder, T. Melchior, M. Müller, D. Sage, T. Blu, and M. Unser. “Low-Bond Axisymmetric Drop Shape Analysis for Surface Tension and Contact Angle Measurements of Sessile Drops”. In: *Colloids and Surfaces A: Physicochemical and Engineering Aspects* 364.1-3 (2010), pp. 72–81. URL: http://bigwww.epfl.ch/publications/stalder1001.html.

[57] ASTMD5229. *Standard Test Method for Moisture Absorption Properties and Equilibrium Conditioning of Polymer Matrix Composite Materials*. Tech. rep. ASTM International, 2020.

[58] MIT. *Mass diffusion analysis*. 2024. URL: https://abaqus-docs.mit.edu/2017/English/SIMACAEANLRefMap/simaanl-c-massdiffusion.htm.

[59] Janneke Kortsmit. *Wrapped Composite Joint Additional Graduation Work. Study into linear coefficient of thermal expansion and modelling of diffusion behaviour in composites*. 2024. URL: https://resolver.tudelft.nl/uuid:e3d14ebf-05f8-4de6-82a4-84369cb528fc.

[60] ISO527-4. *Determination of tensile properties - Part 4: Test conditions for isotropic and orthotropic fibre-reinforced plastic composites*. Tech. rep. European Committee for Standardization, 2023.

[61] TU Delft. *Meteorological data portal*. URL: https://pvportal-3.ewi.tudelft.nl/PVP3.1/Meteo/DataPortal.php.

[62] MIT. *Thermal loads*. URL: https://abaqus-docs.mit.edu/2017/English/SIMACAEPRCRefMap/simaprc-c-thermal.htm#simaprc-c-thermal-t-ModelingThermalRadiation-sma-topic1.

[63] MIT. *Thermal contact properties*. 2024. URL: https://abaqus-docs.mit.edu/2017/English/SIMACAEITNRefMap/simaitn-c-thermalinteraction.htm.

[64] N.V. Raju, Indra Reddy, M. Kumar, and Koona Ramji. “Study on thermo physical properties of hemp, jute and glass fiber reinforced polyester composites”. In: *Materials Today: Proceedings* 5 (Jan. 2018), pp. 5918–5924. DOI: 10.1016/j.matpr.2017.12.191.

[65] John H. Henninger. *Solar Absorptance and Thermal Emittance of Some Common Spacecraft Thermal-Control Coatings*. Tech. rep. NASA, 1984.

[66] Eva Barreira, Ricardo M. S. F. Almeida, and Maria L. Simões. “Emissivity of Building Materials for Infrared Measurements”. In: *Sensors* 21.6 (2021). DOI: 10.3390/s21061961. URL: https://www.mdpi.com/1424-8220/21/6/1961.

[67] Engineers Edge. *Viscosity of Air, Dynamic and Kinematic*. Aug. 2024. URL: https://www.engineersedge.com/physics/viscosity_of_air_dynamic_and_kinematic_14483.htm.

[68] The Engineering Toolbox. *Air - Density, Specific Weight and Thermal Expansion Coefficient vs. Temperature and Pressure*. Aug. 2024. URL: https://www.engineeringtoolbox.com/air-density-specific-weight-d_600.html.

[69] World Climate Research Program. *CMIP Overview*. Accessed 17-04-2024. URL: https://wcrp-cmip.org/cmip-overview/.

[70] V. Eyring, S. Bony, G.A. Meehl, C. A. Senior, B. Stevens, R.J. Stouffer, and K.E. Taylor. "Overview of the Coupled Model Intercomparison Project Phase 6 (CMIP6) experimental design and organization." In: *Geoscientific Model Development* 9.5 (2016), pp. 1937–1958. DOI: 10.5194/gmd-9-1937-2016.

[71] Lijuan Li, Yongqiang Yu, Yanli Tang, Pengfei Lin, Jinbo Xie, Mirong Song, Li Dong, Tianjun Zhou, Li Liu, Lu Wang, Ye Pu, Xiaolong Chen, Lin Chen, Zhenghui Xie, Hongbo Liu, Lixia Zhang, Xin Huang, Tao Feng, Weipeng Zheng, Kun Xia, Hailong Liu, Jiping Liu, Yan Wang, Longhuan Wang, Binghao Jia, Feng Xie, Bin Wang, Shuwen Zhao, Zipeng Yu, Bowen Zhao, and Jilin Wei. "The Flexible Global Ocean-Atmosphere-Land System Model Grid-Point Version 3 (FGOALS-g3): Description and Evaluation". In: *Journal of Advances in Modeling Earth Systems* 12.9 (2020). DOI: 10.1029/2019ms002012.

A

Climate Modelling

This chapter describes the process followed to determine the temperature range and amount of FT cycles the material can be subjected to during service life at the North Sea. First a short introduction is given on climate data in general and the used climate data in this research. Secondly, the results of the analysis are shown, and thirdly, the script used to extract the data is provided.

A.1. Introduction CMIP6 and CAS FGOALS-g3

The Coupled Model Intercomparison Project (CMIP) is a result of climate researchers around the world modelling global climate. From 1995 onwards global climate of the past, present and future is modelled, compared, improved and shared, increasing understanding of the complex interactions between different parts of Earth's climate system. The current 6^{th} phase of the CMIP consists of over 14 PB of climate data [69].

For this research, the question of how future climate changes will not be taken into account, as this vastly increases complexity venturing outside of the scope of this research. When using CMIP6 data for historical climate simulations, there is a distinction between seven types of simulations, which all have their method for handling natural forcings, such as solar radiation and volcanic stratospheric aerosols, and anthropogenic (caused by human activity) forcings such as greenhouse gases. These differences in input will of course result in differences in the output. However, as the historical data will only be a simplified road map for this research, it is assumed that *historical* experiments are sufficient. These simulations are CO-2 concentration driven, based on prescribed global annual mean time-varying CO2 and greenhouse gas concentrations [70]. All data on which these historical simulations are based are prescribed until 2014, meaning that regarding the CMIP6, from 2015 onwards is the 'future'. For this research, only historical simulations of one institution and source, Chinese Academy of Sciences' (CAS) FGOALS-g3, are used [53]. Research comparing results of different historical datasets is left to the reader, and considered outside of the scope of this research.

FGOALS-g3 represents one of three subversions of the third version of the Flexible Global Ocean-Atmosphere -Land System (FGOALS) model. All of these models couple atmospheric, oceanic, sea ice and land components to model the climate as a whole. [71] shows the global averaged surface temperature anomalies compared with measured temperatures, indicating a good agreement between both. When considering sea surface temperatures, [71] shows modelled sea surface temperature at the North Sea is around 3 °C too cold, when comparing with observed data, shown in Figure A.1.

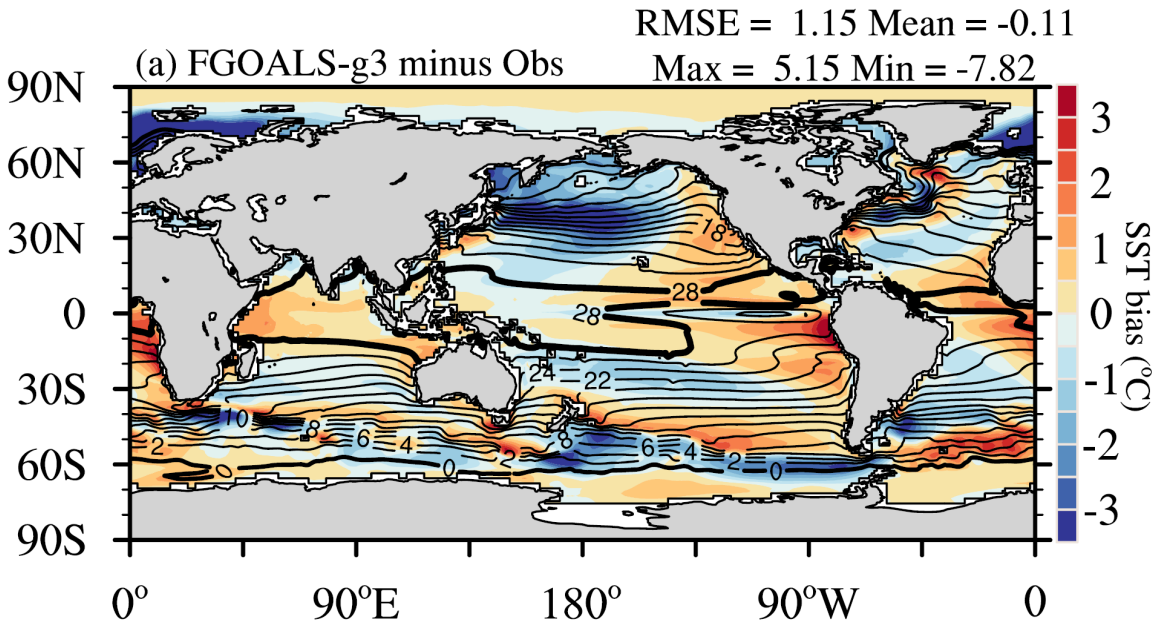


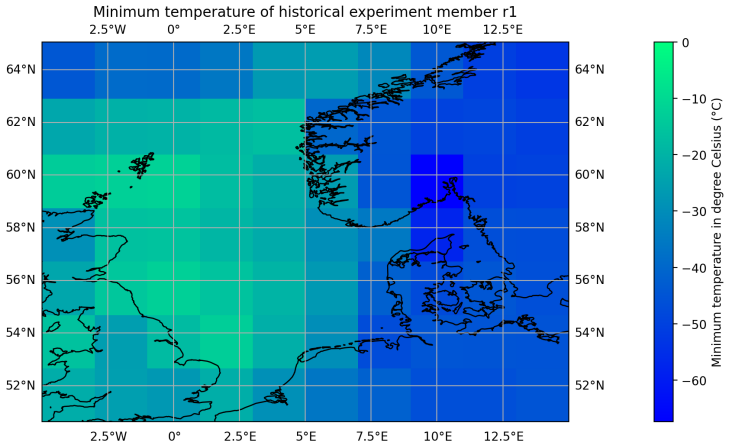
Figure A.1: Bias sea surface temperature FGOALS-g3 [71]

A.2. Extracted data and results

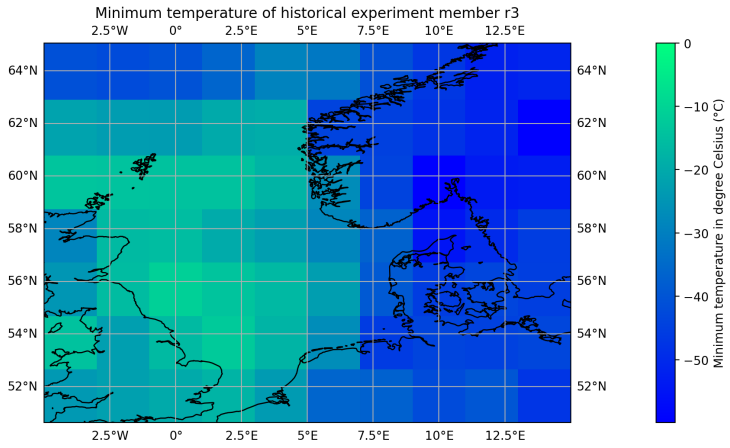
For determination of the maximum and minimum temperature and the number of FT cycles, the minimum and maximum daily near-surface temperatures are used, respectively tasmin and tasmax. These values represent the temperature of the air at 2 m height. This is done for all available daily *historical* ensemble members containing tasmax and tasmin:

- r1i1p1f1
- r3i1p1f1
- r4i1p1f1
- r5i1p1f1

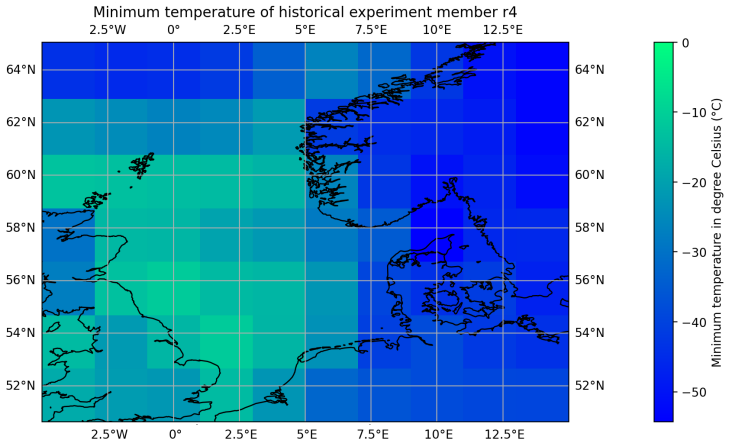
Differences between these ensemble member realisations (r) are the initial conditions used, which will cause small differences in results. Below are the results for these ensembles for tasmin (Figure A.2), tasmax (Figure A.3) and mean (Figure A.4) and maximum amount of freeze-thaw cycles using xclim [54] is shown.



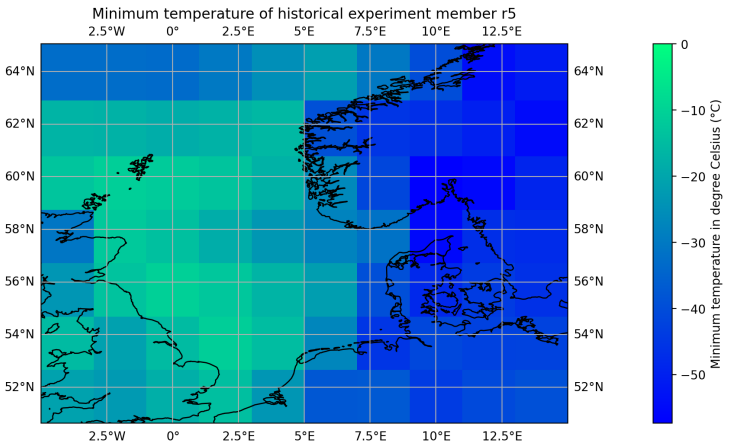
(a) Minimum daily near-surface temperature realisation 1 [53]



(b) Minimum daily near-surface temperature realisation 3 [53]

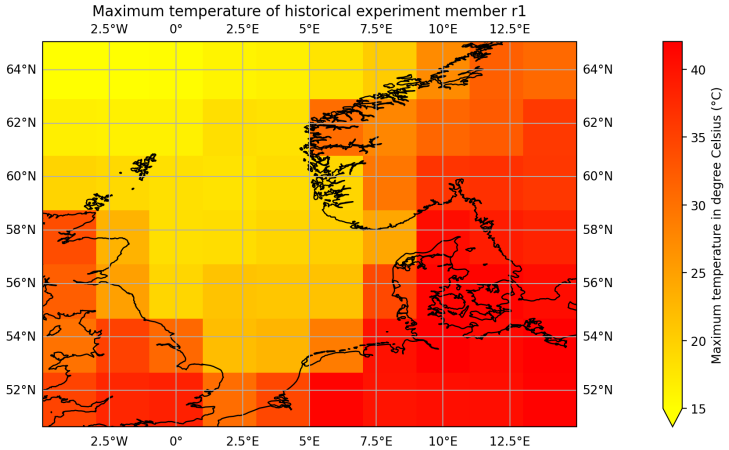


(c) Minimum daily near-surface temperature realisation 4 [53]

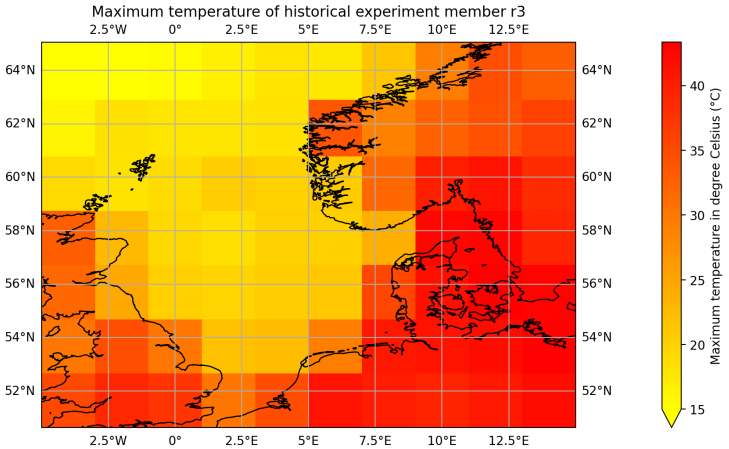


(d) Minimum daily near-surface temperature realisation 5 [53]

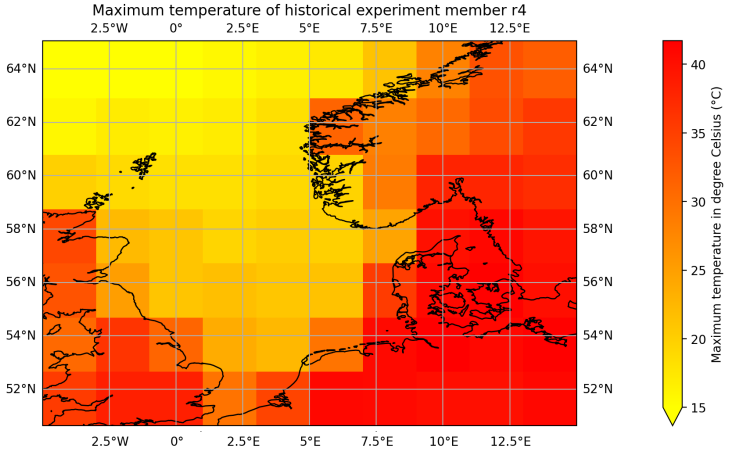
Figure A.2: Minimum daily near-surface temperature [53]



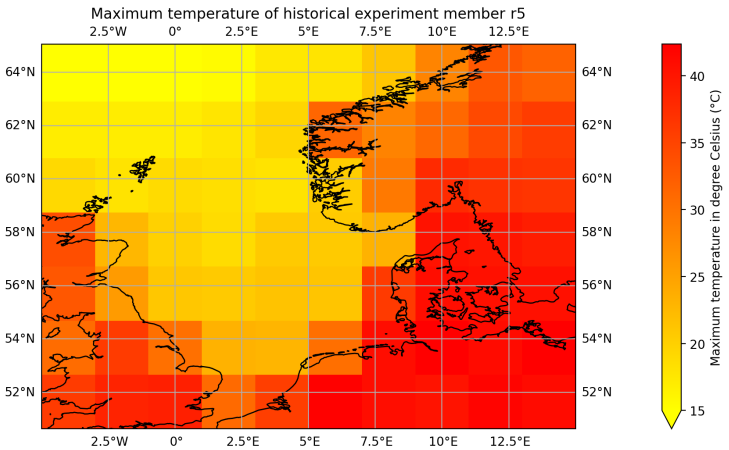
(a) Maximum daily near-surface temperature realisation 1 [53]



(b) Maximum daily near-surface temperature realisation 3 [53]

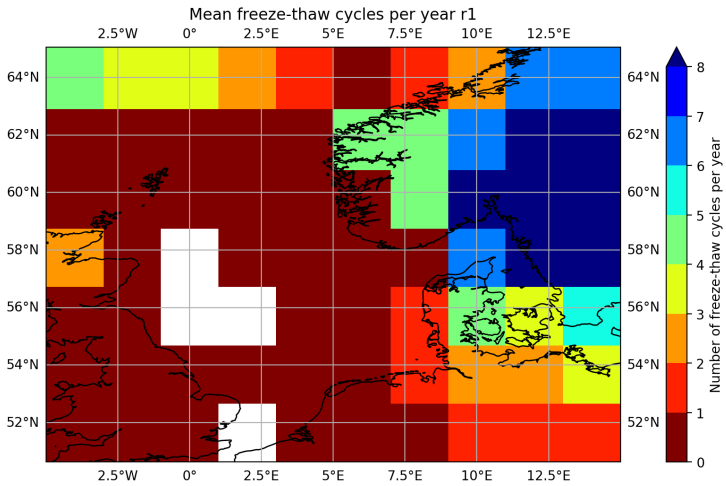


(c) Maximum daily near-surface temperature realisation 4 [53]

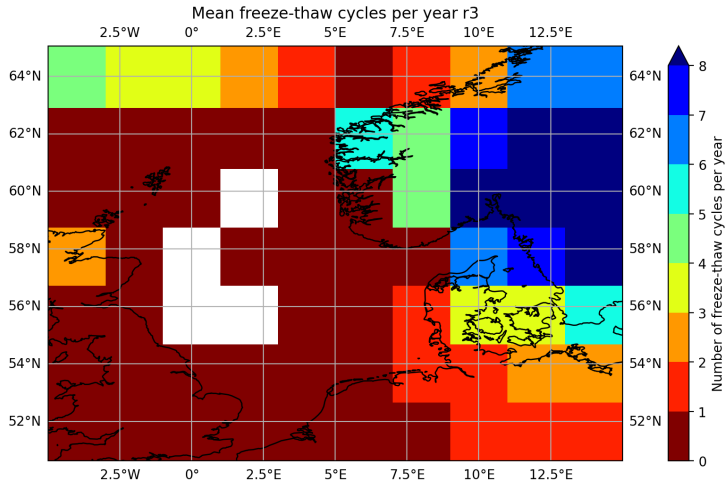


(d) Maximum daily near-surface temperature realisation 5 [53]

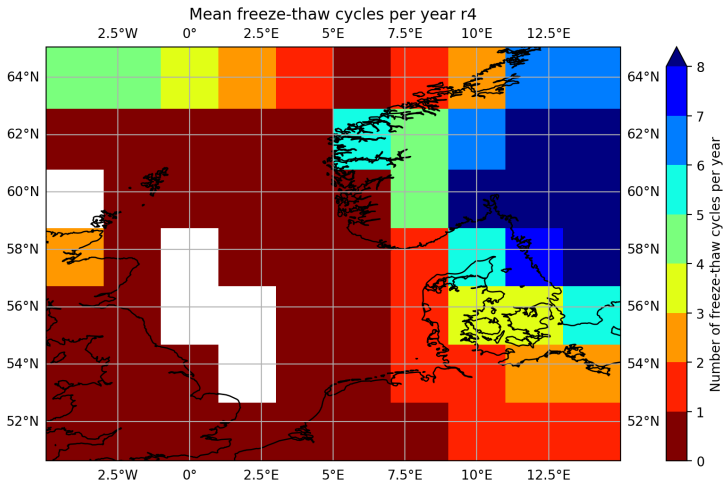
Figure A.3: Maximum daily near-surface temperature [53]



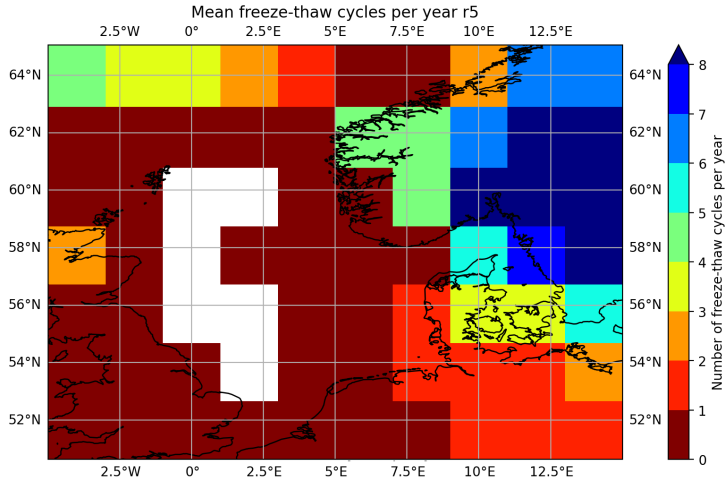
(a) Mean yearly amount of FT cycles realisation 1 [53]



(b) Mean yearly amount of FT cycles realisation 3 [53]

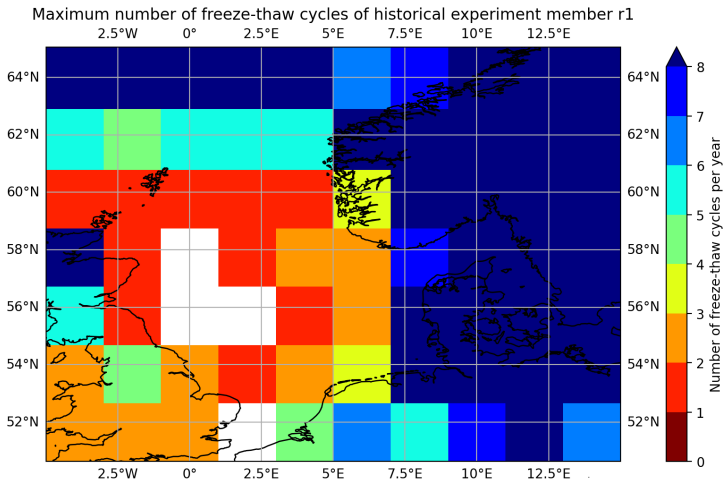


(c) Mean yearly amount of FT cycles realisation 4 [53]

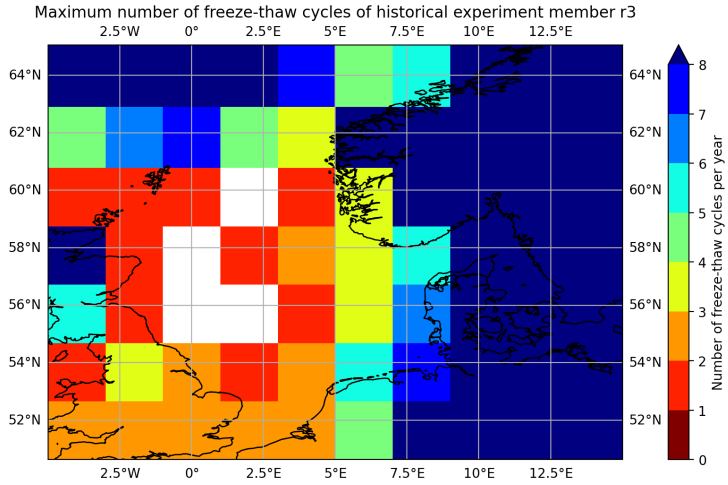


(d) Mean yearly amount of FT cycles realisation 5 [53]

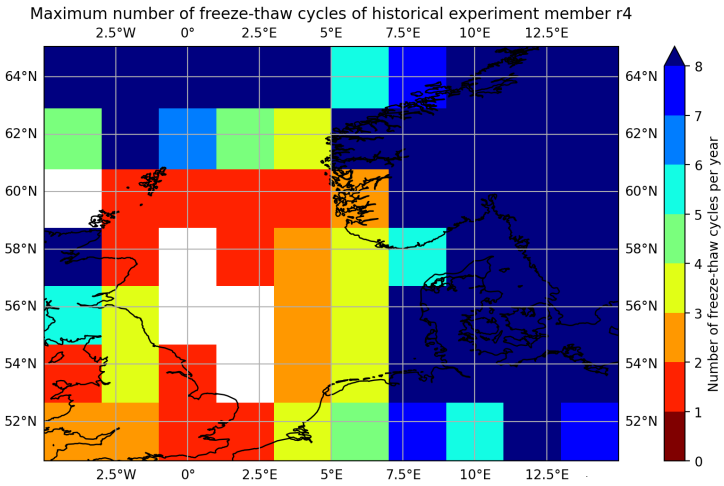
Figure A.4: Mean yearly amount of FT cycles [53]



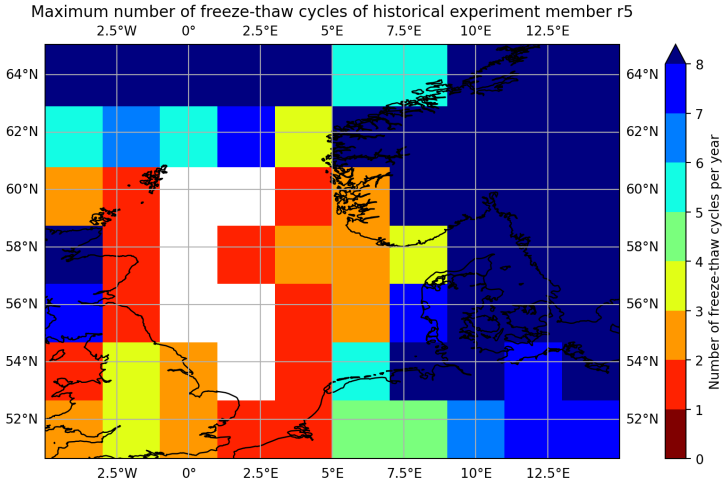
(a) Maximum yearly amount of FT cycles realisation 1 [53]



(b) Maximum yearly amount of FT cycles realisation 3 [53]



(c) Maximum yearly amount of FT cycles realisation 4 [53]



(d) Maximum yearly amount of FT cycles realisation 5 [53]

Figure A.5: Maximum yearly amount of FT cycles [53]

A.3. Jupyter Notebook climate data manipulation

To access the data Google Colab is used. Via Google Colab it is possible to connect to Google Cloud Storage, where an abundance of CMIP6 data is openly accessible to manipulate. Here the data repository Pangeo is used.

By using Google Colab, hardware limitations by running large climate models locally are prevented, opening up a range of possibilities to analyze large climate datasets. Python codes are run through a Jupyter Notebook environment linked to Google Drive. The code used in this research is included below.

```
!pip install pandas==2.0.3
!pip install --upgrade xarray zarr gcsfs cftime nc-time-axis requests
!pip install --upgrade intake-esm

!pip install --upgrade intake-esm

!apt-get install libproj-dev proj-data proj-bin
!apt-get install libgeos-dev
!pip install cython
!pip install cartopy
!pip uninstall -y shapely # Otherwise cartopy won't work
!pip install shapely --no-binary shapely
!pip install xclim

from matplotlib import pyplot as plt
import numpy as np
import pandas as pd
import xarray as xr
import zarr
import fsspec
import gcsfs
import intake
import cartopy.crs as ccrs
from tqdm import tqdm
import xclim

%matplotlib inline
%config InlineBackend.figure_format = 'retina'
```

```
plt.rcParams['figure.figsize'] = 12, 6

cat_url = "https://storage.googleapis.com/cmip6/pangeo-cmip6.json"
col = intake.open_esm_datastore(cat_url) # run twice after eachother to work,

experiment = 'historical' # look at historical forcing experiments
varmin = 'tasmin'               # look at minimum and maximum near surface air temperature (tas)
varmax = 'tasmax'
table = 'day'            # look at daily data

col_subsettot = col.search(experiment_id = experiment,
                           table_id = table,
                           institution_id = 'CAS',
                            source_id = 'FGOALS-g3')

# get names of indexes for which the variable_id is not tasmin or tasmax
index_names = col_subsettot.df[ ~(col_subsettot.df['variable_id'] == 'tasmin') &
↪   ~(col_subsettot.df['variable_id'] == 'tasmax')  ].index

# drop these row indexes from dataFrame
col_subsettot.df.drop(index_names, inplace = True)

ds_dict = col_subsettot.to_dataset_dict(zarr_kwargs={'consolidated': True, 'decode_times':
↪   True},storage_options={'token': 'anon'}) # load the data

filtered_ds_dict = {}

for key, dataset in ds_dict.items(): # iterate through the dictionary to fill with all datasets with more
↪   than 1 variable
    if len(dataset.data_vars) > 1:
        filtered_ds_dict[key] = dataset

for keys in filtered_ds_dict.keys():
  for coord in filtered_ds_dict[keys].coords:
    if coord not in ['lat','lon','time']:
      filtered_ds_dict[keys] = filtered_ds_dict[keys].drop(coord) # drop all coordinates that are not
      ↪   latitude, longitude or time

for keys in filtered_ds_dict.keys():
  # converting degrees east to degrees east and west
  lon_atrib = filtered_ds_dict[keys].coords['lon'].attrs
  filtered_ds_dict[keys].coords['lon'] = (filtered_ds_dict[keys].coords['lon'] + 180) % 360 - 180
  filtered_ds_dict[keys] = filtered_ds_dict[keys].sortby(filtered_ds_dict[keys].lon)
  filtered_ds_dict[keys].coords['lon'].attrs =lon_atrib

  # slicing only Europe
  filtered_ds_dict[keys] = filtered_ds_dict[keys].sel(lon=slice(-5,15), lat=slice(50,65))

  # setting units to celsius
  tasmin_atrib = filtered_ds_dict[keys].tasmin.attrs
  filtered_ds_dict[keys]["tasmin"] = filtered_ds_dict[keys].tasmin - 273.15
  filtered_ds_dict[keys].tasmin.attrs = tasmin_atrib
  filtered_ds_dict[keys].tasmin.attrs["units"] = "degC"

  tasmax_atrib = filtered_ds_dict[keys].tasmax.attrs
  filtered_ds_dict[keys]["tasmax"] = filtered_ds_dict[keys].tasmax - 273.15
```

```
  filtered_ds_dict[keys].tasmax.attrs = tasmax_atrib
  filtered_ds_dict[keys].tasmax.attrs["units"] = "degC"

ft_ds = {}
with xclim.set_options(data_validation='log'): # calculate freeze-thaw cycles per year for all datasets
  for key, dataset in filtered_ds_dict.items():
    ftcycles = xclim.indicators.atmos.daily_freezethaw_cycles(tasmin = filtered_ds_dict[key].tasmin,
    ↪  tasmax = filtered_ds_dict[key].tasmax,
                                                              thresh_tasmin = '-10 degC.', thresh_tasmax = "0
                                                              ↪  degC.")
    ft_ds[key] = ftcycles

ft_ds_mean = {}
for keys, dataset in ft_ds.items():
  ft_mean = ft_ds[keys].mean(dim="time")
  ft_mean = ft_mean.where(ft_mean != 0.) # values equal to zero are replaced by nan to enhance
  ↪  visibility whilst plotting
  ft_ds_mean[keys] = ft_mean # calculate the mean

num_members = len(ft_ds_mean['CMIP.CAS.FGOALS-g3.historical.day.gn'].member_id)
fig, ax = plt.subplots(nrows=num_members, ncols=1, figsize=(10, num_members * 5),
↪  subplot_kw={'projection': ccrs.PlateCarree()})

title_list = ["Mean freeze-thaw cycles per year r1",
              "Mean freeze-thaw cycles per year r3",
              "Mean freeze-thaw cycles per year r4",
              "Mean freeze-thaw cycles per year r5"]
# make sure ax is itterable regardless of size
if num_members == 1:
    ax = [ax]

for key, data_array in ft_ds_mean.items():
    for i, member in enumerate(data_array.member_id.values):
        member_data = data_array.sel(member_id=member)
        member_data.plot(ax=ax[i], transform=ccrs.PlateCarree(), vmin=0, vmax=8, levels=9,
        ↪  cmap=plt.get_cmap('jet_r'),cbar_kwargs={"label": "Number of freeze-thaw cycles per
        ↪  year"})
        ax[i].coastlines()
        ax[i].gridlines(draw_labels=True)
        ax[i].set_title(f"{title_list[i % len(title_list)]}")

plt.tight_layout()
plt.show()

ft_ds_max = {}
for keys, dataset in ft_ds.items():
  ft_max = ft_ds[keys].max(dim="time") # calculate the max yearly freeze-thaw cycles
  ft_max = ft_max.where(ft_max != 0.)
  ft_ds_max[keys] = ft_max

num_members_max = len(ft_ds_max['CMIP.CAS.FGOALS-g3.historical.day.gn'].member_id)
fig, ax = plt.subplots(nrows=num_members_max, ncols=1, figsize=(10, num_members_max * 5),
↪  subplot_kw={'projection': ccrs.PlateCarree()})

title_list = ["Maximum number of freeze-thaw cycles of historical experiment member r1",
              "Maximum number of freeze-thaw cycles of historical experiment member r3",
```

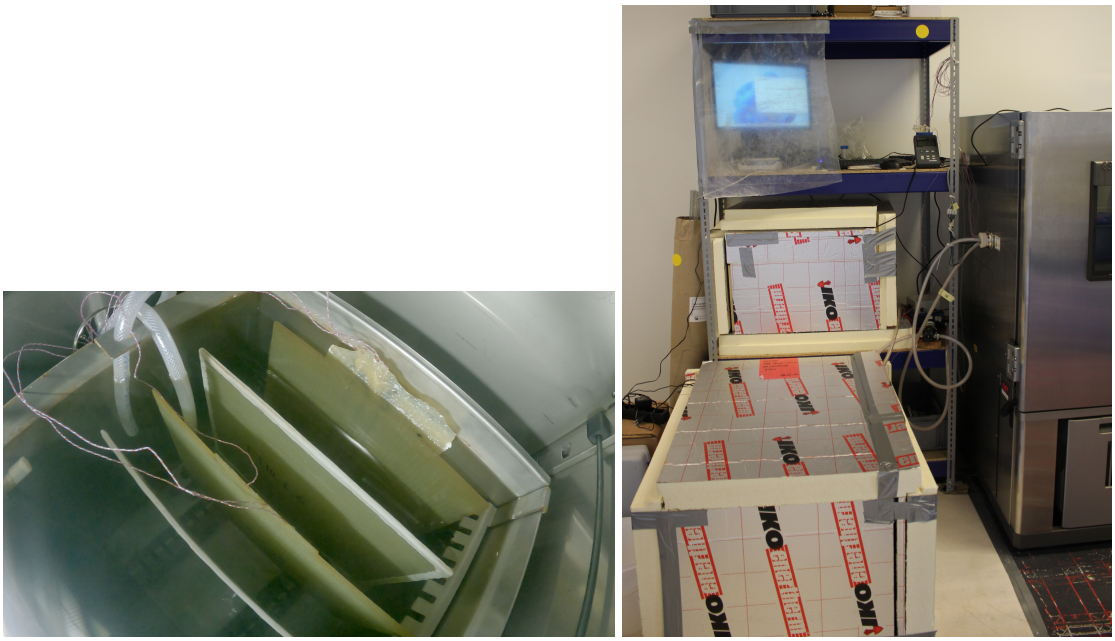
```
130             "Maximum number of freeze-thaw cycles of historical experiment member r4",
131             "Maximum number of freeze-thaw cycles of historical experiment member r5"]
132
133 if num_members_max == 1:
134     ax = [ax]
135
136 for key, data_array in ft_ds_max.items():
137     for i, member in enumerate(data_array.member_id.values):
138         member_data = data_array.sel(member_id=member)
139         member_data.plot(ax=ax[i], transform=ccrs.PlateCarree(), vmin=0, vmax=8, levels=9,
        ↪  cmap=plt.get_cmap('jet_r'), cbar_kwargs={"label": "Number of freeze-thaw cycles per
        ↪  year"})
140         ax[i].coastlines()
141         ax[i].gridlines(draw_labels=True)
142         ax[i].set_title(f"{title_list[i % len(title_list)]}")
143
144 plt.tight_layout()
145 plt.show()
146
147 ds_max = {}
148 ds_min = {}
149 # determine the maximum and minimum temperatures
150 for keys, dataset in filtered_ds_dict.items():
151   ds_max = filtered_ds_dict[keys].tasmax.max(dim="time")
152   ds_min = filtered_ds_dict[keys].tasmin.min(dim="time")
153   ds_max[keys] = ds_max
154   ds_min[keys] = ds_min
155
156 num_members = len(ds_max.member_id)
157 fig, axes = plt.subplots(nrows=num_members, ncols=1, figsize=(20, num_members * 5),
    ↪  subplot_kw={'projection': ccrs.PlateCarree()})
158
159 title_list = ["Maximum temperature of historical experiment member r1",
160             "Maximum temperature of historical experiment member r3",
161             "Maximum temperature of historical experiment member r4",
162             "Maximum temperature of historical experiment member r5"]
163
164 if num_members == 1:
165     axes = [axes]
166
167 for i, member in enumerate(ds_max.member_id.values):
168     member_data = ds_max.sel(member_id=member).squeeze()  # remove single-dimensional entries
        ↪  from the shape
169     im = member_data.plot(ax=axes[i], transform=ccrs.PlateCarree(),
        ↪  cmap=plt.get_cmap('autumn_r'), vmin=15,cbar_kwargs={"label": f"Maximum temperature in
        ↪  degree Celsius ({chr(176)}C)"})
170     axes[i].coastlines()
171     axes[i].gridlines(draw_labels=True)
172     axes[i].set_title(f"{title_list[i % len(title_list)]}")
173
174 fig.subplots_adjust(hspace=10)
175
176 plt.tight_layout()
177 plt.show()
178
179 num_members = len(ds_min.member_id)
```

```
180 fig, axes = plt.subplots(nrows=num_members, ncols=1, figsize=(20, num_members * 5),
    ↪  subplot_kw={'projection': ccrs.PlateCarree()})
181
182 title_list = ["Minimum temperature of historical experiment member r1",
183               "Minimum temperature of historical experiment member r3",
184               "Minimum temperature of historical experiment member r4",
185               "Minimum temperature of historical experiment member r5"]
186
187 if num_members == 1:
188     axes = [axes]
189
190 for i, member in enumerate(ds_min.member_id.values):
191     member_data = ds_min.sel(member_id=member).squeeze()
192     im = member_data.plot(ax=axes[i], transform=ccrs.PlateCarree(),
        ↪  cmap=plt.get_cmap('winter'),vmax = 0, cbar_kwargs={"label": f"Minimum temperature in
        ↪  degree Celsius ({chr(176)}C)"})
193     axes[i].coastlines()
194     axes[i].gridlines(draw_labels=True)
195     axes[i].set_title(f"{title_list[i % len(title_list)]}")
196
197 plt.tight_layout()
198 plt.show()
```

B

Freeze-thaw ageing setup

This appendix further describes the used FT ageing setup. Pictures of the setup can be seen in Figure B.1. First, the equipment used is further explained in Section B.1. Then the used script for the Arduino is presented in Section B.2, and the used script for the full setup in Section B.3.



(a) Internal water tank during thawing cycle with 2 thermocouple plates and 2 last aged plates

(b) External setup with PC, isolated external water tanks, and connection with climate chamber

Figure B.1: Images of ageing setup

B.1. Experimental equipment used

The setup involves two main parts. The first part is an Espec PL-2KPH climate chamber, which is used to accurately regulate the temperature of the specimens during ageing. The second part is the water tank with its components. Two relays form an electrical switch, capable of turning the connected water pumps on and off. The Arduino Nano is connected with the relay and two float switches to translate and control the workings of the water pumps as shown in Section B.2.

The complete system is controlled by a mini-PC via the program Mp3. The script ran by this program controls the climate chamber as well as the pumps. The full script used can be found in Section B.3.

Figure B.3 shows the used system of components. Figure B.2 shows the box in which the relay and Arduino are placed. The PC controls the full system and sends commands to the Arduino, which sets a switch high or low, to control the position of the relay. There is no independent decision-making or code embedded in the Arduino, as can be read in Section B.2. The Arduino controls the pumps based on the input from the PC, and the Arduino translates the floater position for the PC to read.

The heater positioned in the external water tank is an independent heater, which cannot be connected to the PC.

In this figure, no distinction is made between 230 V and 12 V power supply. In reality, the water pumps are 12 V pumps, that are connected to the power source via the relay and a circuit breaker. On top of this, the external water tank is grounded, to prevent high stray voltage in the tank from existing. To ensure stable temperature measurements of the thermocouple in the water of the external water tank, the thermocouple is placed in a closed tube with demineralised water, as the saltwater will cause small voltage peaks which result in unstable thermocouple readings. On top of that, no high-voltage components are present in the internal water tank, to enhance the safety of the system.

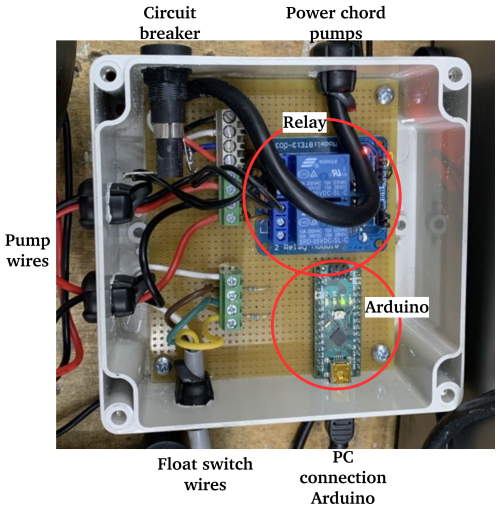


Figure B.2: Picture of Arduino, relay and connections

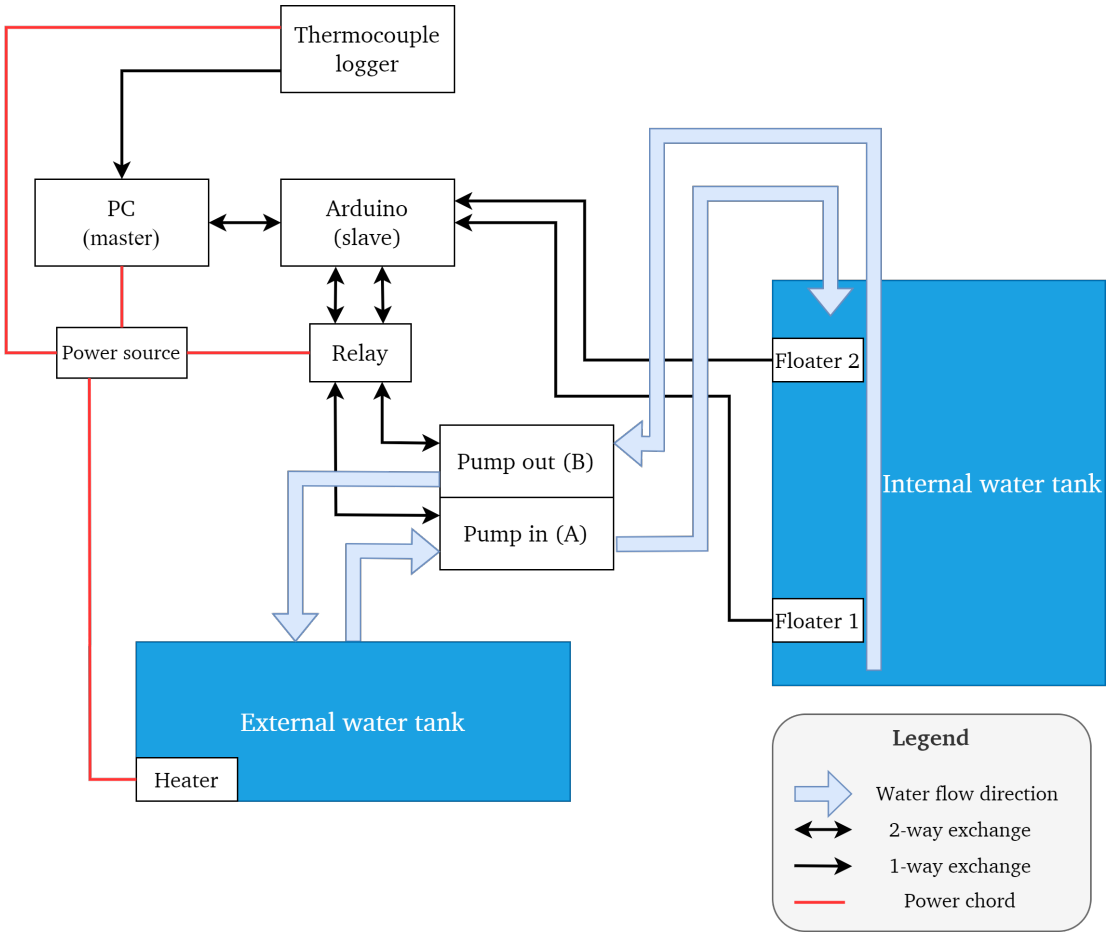


Figure B.3: Flow block diagram of setup

B.2. Arduino script

```
#include <Arduino.h>

const int OUT1 = 5;   // link pins on the Arduino to a name
const int OUT2 = 6;
const int OUT3 = 7;
const int OUT4 = 8;


const int INPUT1 = 9;
const int INPUT2 = 10;
const int INPUT3 = 11;
const int INPUT4 = 12;

#define version "Vriesdooi 1.0\n"

// put function declarations here:
int myFunction(int, int);   //make sure that functions return an integer

void setup()    //define variables and pin modes. Function runs after each powerup or reset of board
{
  pinMode(OUT1, OUTPUT);    //set the pins for pumps to output -- low impedence state, to make
   ↪  sure it has enough current to run the relay
  pinMode(OUT2, OUTPUT);
  pinMode(OUT3, OUTPUT);
  pinMode(OUT4, OUTPUT);

 digitalWrite(OUT1,HIGH);   //set voltage to 5V
 digitalWrite(OUT2,HIGH);
 digitalWrite(OUT3,HIGH);
 digitalWrite(OUT4,HIGH);

  pinMode(INPUT1, INPUT_PULLUP);    //causes float switches to read high when horizontal and
   ↪  low when open
  pinMode(INPUT2, INPUT_PULLUP);
  pinMode(INPUT3, INPUT_PULLUP);
  pinMode(INPUT4, INPUT_PULLUP);

  Serial.begin(9600);     // set the baud rate
  delay(100);             // pauses for 100 milliseconds
  Serial.print(version);  // prints the version name
}


char buf[255];    // create buffer with 255 characters to store data in temporarily
String str;

void loop()   //the loop constantly run by the program
{

while(Serial.available())
   {
     char inChar = (char)Serial.read();    //read the characters that are send to the arduino
     switch(inChar)                        //run the characters through the switch - case statement
     {
```

```
53        case 'a': {digitalWrite(OUT1,LOW);break;}     //change status of the pin to deactivate the relay,
          ↪ and thus deactivate the pump linked to pin 5
54        case 'A': {digitalWrite(OUT1,HIGH);break;}    //change status of the pin to activate the relay,
          ↪ thus activate the pump linked to pin 5
55        case 'b': {digitalWrite(OUT2,LOW);break;}
56        case 'B': {digitalWrite(OUT2,HIGH);break;}
57        case 'c': {digitalWrite(OUT3,LOW);break;}
58        case 'C': {digitalWrite(OUT3,HIGH);break;}
59        case 'd': {digitalWrite(OUT4,LOW);break;}
60        case 'D': {digitalWrite(OUT4,HIGH);break;}
61        case '?':                                     //when ? thrown print the version and the different
          ↪ commands
62        {
63          Serial.print(version);
64          Serial.print("commands:\na = out1 laag\nA = out1 hoog\nb = out2 laag\nB = out2 hoog\nc =
            ↪ out3 laag\nC = out3 hoog\nd = out4 laag\nD = out5 hoog\n");
65          break;
66        };

67

68      }
69    }       //print the switch float status
70    Serial.print(!digitalRead(INPUT1));
71    Serial.print(',');
72    Serial.print(!digitalRead(INPUT2));
73    Serial.print(',');
74    Serial.print(!digitalRead(INPUT3));
75    Serial.print(',');
76    Serial.print(!digitalRead(INPUT4));
77    Serial.print('\n');
78    delay(500);
79  }
```

B.3. Full setup script

```
1
2   -- Script written by Fred Schilperoort and Janneke Kortsmit
3   -- Coded in Lua for use in combination with Mp3
4
5   require "iuplua"
6
7   local this = debug.getinfo(1).short_src
8   b = 1
9   while b
10          do
11          this = string.sub(this,b+1)
12          b = string.find (this,"\\")
13          end
14
15          local np=DlgGetParent("Page00","Iup00")
16
17  ComClose(0)                         -- Arduino, number represents a local handle
18  ComOpen(0,9,9600)                   -- ComOpen(Handle, Comport, Baudrate (, bits) (,handshake)
19  ComDelimiter(0,10)                  -- ComDelimiter(Handle, Delimiter) ascii no. of delimiter, now \n,
    ↪ so LF
20
21  ComClose(1)                         -- climate chamber
```

```
22 ComOpen(1,11,9600)
23 ComDelimiter(1,10)
24
25 local heartbeatcnt1 = 0
26 local heartbeatcnt2 = 0
27
28 local floater1=0                -- bottom floater
29 local floater2=0                -- top floater
30 local pump1 = 1
31 local pump2 = 1
32 local Count = 0
33 local timeoutcnt = 0
34 local newdata = 0
35 local lastsend = 0
36 local templogstatus = 1
37
38 local heartbeat = 0
39 local heartbeat1 = iup.label{ title='*'}
40 local heartbeat2 = iup.label{ title='*'}
41
42 local Temp_command = nil
43 local target_temp = 0
44 local Act_Temp = 24
45 local Set_Temp = -20
46 local Max_Temp = 105
47 local Min_Temp = -30
48 local newdata =0
49 local AcceptResume = 0
50 local PausePressed = 0
51
52 -- setting up the graphical Iup00 window
53 Label01=iup.label{title="Time to float1:",size="150x"}                -- s untill bottom floater activated
54 Text01=iup.text{value="300",size="40x"}
55
56 Label02=iup.label{title="Max fill Time:",size="150x"}                -- s from bottom float to top float
57 Text02=iup.text{value="920",size="40x"}
58
59 Label03=iup.label{title="Follow-up time filling tank:",size="150x"}                -- s extra pump time
   ↪ after top float
60 Text03=iup.text{value="50",size="40x"}
61
62 Label04=iup.label{title="Time high temperature:",size="150x"}
63 Text04=iup.text{value="10800",size="40x"}
64
65 Label05=iup.label{title="Max empty time:",size="150x"}
66 Text05=iup.text{value="1300",size="40x"}
67
68 Label06=iup.label{title="Follow-up time emptying tank:",size="150x"}
69 Text06=iup.text{value="85",size="40x"}
70
71 Label07=iup.label{title="Time low temperature:",size="150x"}
72 Text07=iup.text{value="10800",size="40x"}
73
74 Label08=iup.label{title="Temperature low:",size="150x"}
75 Text08=iup.text{value="-20",size="40x"}
76
```

```
77  Label09=iup.label{title="Temperature high:",size="150x"}
78  Text09=iup.text{value="23",size="40x"}
79
80  Label10=iup.label{title="Number of cycles:",size="150x"}
81  Text10=iup.text{value="210",size="40x"}
82
83  Label11=iup.label{title="Circulating time: ", size="150x"}
84  Text11=iup.text{value="840", size="40x"}
85
86  Label12=iup.label{title="Circulating wait time:  ", size="150x"}
87  Text12=iup.text{value="1800", size="40x"}
88
89  Chan0Label= iup.label{title="Act_Temp:",size="70x"}
90  Chan1Label= iup.label{title="Set_Temp:",size="70x"}
91  Chan2Label= iup.label{title="Max_Temp:",size="70x"}
92  Chan3Label= iup.label{title="Min_Temp:",size="70x"}
93  Floater1Label= iup.label{title="Floater1:",size="50x"}
94  Floater2Label= iup.label{title="Floater2:",size="50x"}
95  Pump1Label= iup.label{title="Pump1:",size="50x"}
96  Pump2Label= iup.label{title="Pump2:",size="50x"}
97  CurrentTime = iup.label{title = "", size = "150x"}
98
99  CounterLabel= iup.label{title="Counter:    ",size="40x"}
100 Counter=iup.label{title="0",size="20x"}
101 StatusLabel= iup.label{title="Status:",size="40x"}
102 Status=iup.label{value="",size="200x"}
103 TimetogoLabel = iup.label{title="Time to go:    ", size = "60x"}
104 Timetogo = iup.label{title = "",size="150x"}
105 TemptogoLabel = iup.label{title = "Temp to go:    ", size = "60x"}
106 Temptogo = iup.label{title = "", size = "150x"}
107 EndStepLabel = iup.label{title = "Endtime step:    ", size = "100x"}
108 EndStep = iup.label{title = "", size = "150x"}
109
110 StartButton=iup.button{title="Start",size="50x"}
111 StopButton=iup.button{title="Stop",size="50x"}
112 PauseButton=iup.button{title="Pause",size="50x"}
113 ResumeButton=iup.button{title="Resume",size="50x"}
114 PauseTempButton=iup.button{title="Pause temperature logging", size = "150x"}
115 ResumeTempButton=iup.button{title="Resume temperature logging", size ="150x"}
116
117 hbox00=iup.hbox{CurrentTime}
118 hbox01=iup.hbox{Chan0Label,Chan1Label,Chan2Label,Chan3Label}
119 hbox02=iup.hbox{Floater1Label, Floater2Label}
120 hbox03=iup.hbox{Pump1Label, Pump2Label}
121 hbox04=iup.hbox{heartbeat1, heartbeat2}
122 hbox05=iup.hbox{Label01,Text01}
123 hbox06=iup.hbox{Label02,Text02}
124 hbox07=iup.hbox{Label03,Text03}
125 hbox08=iup.hbox{Label04,Text04}
126 hbox09=iup.hbox{Label05,Text05}
127 hbox10=iup.hbox{Label06,Text06}
128 hbox11=iup.hbox{Label07,Text07}
129 hbox12=iup.hbox{Label08,Text08}
130 hbox13=iup.hbox{Label09,Text09}
131 hbox14=iup.hbox{Label10,Text10}
132 hbox15=iup.hbox{Label11,Text11}
```

```
133 hbox16=iup.hbox{Label12,Text12}
134 hbox17=iup.hbox{StartButton,PauseButton, ResumeButton, StopButton}
135 hbox18=iup.hbox{CounterLabel,Counter}
136 hbox19=iup.hbox{StatusLabel,Status}
137 hbox20=iup.hbox{TimetogoLabel, Timetogo, TemptogoLabel, Temptogo}
138 hbox21=iup.hbox{EndStepLabel, EndStep}
139 hbox22=iup.hbox{PauseTempButton, ResumeTempButton}
140 vbox01=iup.vbox{hbox00,hbox01,hbox02,hbox03,hbox04,hbox05,hbox06,hbox07,hbox08,hbox09,hbox10,hbox11,hbox12,h
141
142
143 local dlg = iup.dialog{vbox01 ,title="Status and control",control="YES",size="FULLxFULL"}
144 iup.SetAttribute(dlg, "NATIVEPARENT", np)
145 dlg:showxy( iup.CENTER, iup.CENTER)
146
147 function StartButton:action()
148         print("start")
149         print(os.date("%X "),"Start")
150         NState=10                       -- sets which part of the loop to look at
151         return iup.DEFAULT
152 end
153
154 function StopButton:action()
155         print("Stop")
156         print(os.date("%X "),"Stop")
157         NState=15                       -- sets which part of the loop to look at
158         return iup.DEFAULT
159 end
160
161 function PauseButton:action()
162     print(os.date("%X"), "Pause pressed")
163         PauseButton.title = "Pressed"
164     PausePressed = 1
165     return iup.DEFAULT
166 end
167
168 function ResumeButton:action()
169     if AcceptResume == 1 then
170                 print(os.date("%X"), "Resume cycle")
171                 PausePressed = 0
172                 PauseButton.title = "Pause"
173                 Status.title = "Start freezing: Set temperature low"
174                 NState = 10             -- next loop
175         end
176     return iup.DEFAULT
177 end
178
179 function PauseTempButton:action()
180         print("temperature logging paused")
181         templogstatus = 0
182         return iup.DEFAULT
183 end
184
185 function ResumeTempButton:action()
186         print("temperature logging resumed")
187         templogstatus = 1
188         ComClose(2)                     -- thermocouple logger
```

```
189         ComOpen(2,6,38400,8,4)
190         return iup.DEFAULT
191 end
192
193 function StartPump1()
194         if pump1 == 0 then                  -- if pump is off
195                 ComPuts(0,"a")                -- command defined in Arduino
196                 pump1 = 1                       -- pump on
197                 print(os.date("%X "),"pump 1 on")
198                 Pump1Label.title = string.format("Pump1: %d",pump1)
199                 ChanPutVal(15,pump1)
200         end
201 end
202
203 function StartPump2()
204         if pump2 == 0 then
205                 ComPuts(0,"b")
206                 pump2 = 1
207                 print(os.date("%X "),"pump 2 on")
208                 Pump2Label.title = string.format("Pump2: %d",pump2)
209                 ChanPutVal(16,pump2)
210         end
211
212 end
213
214 function StopPump1()
215         if pump1 == 1 then
216                 ComPuts(0,"A")
217                 pump1 = 0
218                 print(os.date("%X "),"pump 1 off")
219                 Pump1Label.title = string.format("Pump1: %d",pump1)
220                 ChanPutVal(15,pump1)
221         end
222
223 end
224
225 function StopPump2()
226         if pump2 == 1 then
227                 ComPuts(0,"B")
228                 pump2 = 0
229                 print(os.date("%X "),"pump 2 off")
230                 Pump2Label.title = string.format("Pump2: %d",pump2)
231                 ChanPutVal(16,pump2)
232         end
233
234 end
235
236 floater1_last=2
237 floater2_last=2
238
239 function GetSwitchInput()
240         EStr,ECnt=ComGets(0)
241         if ECnt > 0 then
242                 heartbeatcnt1 = heartbeatcnt1+1
243                 if heartbeatcnt1 == 1 then heartbeat1.title = '/' end
244                 if heartbeatcnt1 == 2 then heartbeat1.title = '-' end
```

```
245             if heartbeatcnt1 == 3 then heartbeat1.title = '\\' heartbeatcnt1=0 end
246             data = {}
247             Start=0
248             Tok=nil
249             index = 1
250             Tok,Start=Tokenize(EStr,",",Start) -- tokenize string input from Arduino
251             while (Start >0)
252             do
253                     dataval=tonumber(Tok)
254                     data[index]=dataval
255             --        print(data)
256                     Tok,Start=Tokenize(EStr,",",Start)
257                     index = index+1
258             end
259             if(index >= 4) then
260                     floater1 = tonumber(data[1])
261                     floater2 = tonumber(data[2])
262                     if(floater1 ~=floater1_last) then
263                             floater1_last = floater1
264                             print(os.date("%X "),"Floater1 = ",floater1)
265                             Floater1Label.title = string.format("Floater1: %d",floater1)
266                             ChanPutVal(14,floater1)
267                     end
268                     if(floater2 ~=floater2_last)then
269                             floater2_last = floater2
270                             print(os.date("%X "),"Floater2 = ",floater2)
271                             Floater2Label.title = string.format("Floater2: %d",floater2)
272                             ChanPutVal(13,floater2)
273                     end
274             end
275     end
276 end
277
278
279
280 function SendCommand()                  -- send temperature command if empty, otherwise just ask
    ↪  for the temperature
281
282     if(Temp_command ~= nil)then
283             t = os.time()
284             target_temp = Temp_command
285             command = string.format("1,TEMP,S%.1f",Temp_command)
286             ComPuts(1,command)
287             Wait(0.5)
288             ComPuts(1, "1,MODE,CONSTANT")
289             Temp_command = nil
290     else
291             t = os.time()
292             if(t - lastsend) >5 then            --check if this is acceptable when heating and cooling,
                ↪  and see if maybe to make variable
293                     lastsend = t
294                     ComPuts(1,"1,TEMP?")
295             end
296     end
297 end
298
```

```
299 function GetTemperatureInput()
300     SendCommand()
301     EStr,ECnt=ComGets(1)                    --get response and count length of incoming
302     if ECnt>0 and ECnt ~= 16 and ECnt ~= 19 and ECnt ~= 17
        ↪ then                                  --if data is returned, take it apart. Response to setting
        ↪ temp and setting command are exluded (length 19 and 22)
303         heartbeatcnt2 = heartbeatcnt2+1
304         if heartbeatcnt2 == 1 then heartbeat2.title = '/' end
305         if heartbeatcnt2 == 2 then heartbeat2.title = '-' end
306         if heartbeatcnt2 == 3 then heartbeat2.title = '\\' heartbeatcnt2=0 end
307         data = {}
308         Start=0
309         Tok=nil
310         index = 1
311         Tok,Start=Tokenize(EStr,",",Start)
312         while (Start >0)
313         do
314             dataval=tonumber(Tok)
315             data[index]=dataval
316             Tok,Start=Tokenize(EStr,",",Start)
317             index = index+1
318         end
319         if(index >= 4) then
320             Act_Temp = tonumber(data[1])
321             Chan0Label.title = string.format("Act_Temp: %.1f",tonumber(data[1]))
322             ChanPutVal(0,tonumber(data[1]))
323             Set_Temp = tonumber(data[2])
324             Chan1Label.title = string.format("Set_Temp: %.1f",tonumber(data[2]))
325             ChanPutVal(1,tonumber(data[2]))
326             Max_Temp = tonumber(data[3])
327             Chan2Label.title = string.format("Max_Temp: %.1f",tonumber(data[3]))
328             ChanPutVal(2,tonumber(data[3]))
329             Min_Temp = tonumber(data[4])
330             Chan3Label.title = string.format("Min_Temp: %.1f",tonumber(data[4]))
331             ChanPutVal(3,tonumber(data[4]))
332             newdata = 1
333         end
334     end
335 end
336
337 function GetResult() -- get results from TC logger
338     s = {}
339     start = os.time()
340     timeout = 0
341     s[1]= -1
342     while(s[1] ==-1)                                -- wait for first character
343         do
344         s[1] = ComGetc(2)
345         if os.time()-start >= 1 then            -- reset the comport if the response of the logger
            ↪ takes longer than 1 second
346             timeoutcnt = timeoutcnt +1
347             return
348         end
349         yield()
350         end
```

```
351         for i=2,37 do                                   -- read data from the logger, 2nd to 37th input (for init, max/min value, increment)
352             s[i] = ComGetc(2)
353             end
354         if ((s[16] == 120) and (s[37] == 4)) then       -- Test for valid data, with two known non-changing values
355             timeoutcnt =0
356             local c = 4                                 -- c can be any. Now offsetted to leave room for climate chamber channels to be first in the list
357             for i=0,15,2 do
358                 lo = s[17+i]
359                 hi = s[18+i]
360
361                 val = hi*256
362                 val  = val + lo
363
364                 if val > 32768 then
365                     val = 65536 - val
366                     val = val * -1
367
368                     end
369                 val = val /10
370                 ChanPutVal(c,val)               -- writing to the channel
371                 c = c+1
372             end
373             heartbeat = heartbeat +1
374             if(heartbeat >9) then heartbeat =0 end
375             ChanPutVal(c,heartbeat)
376         end
377 end
378
379 function SendCommandTC()        -- send command to TC logger (Serial output copied from Omega app serial trace), check the com number
380         ComPutc(2,0x01)                 -- first number represents the local comport identified in the script here 0. Second is the encoded hexidecimal data sent to the logger in order to get a response back from it
381          ComPutc(2,0x16)
382         ComPutc(2,0x7b)
383         ComPutc(2,0x28)
384         ComPutc(2,0x48)
385         ComPutc(2,0x4c)
386         ComPutc(2,0x45)
387         ComPutc(2,0x48)
388         ComPutc(2,0x54)
389         ComPutc(2,0x43)
390         ComPutc(2,0x33)
391         ComPutc(2,0x34)
392         ComPutc(2,0x32)
393         ComPutc(2,0x34)
394         ComPutc(2,0x67)
395         ComPutc(2,0x78)
396         ComPutc(2,0x29)
397         ComPutc(2,0x7d)
398         ComPutc(2,0x7e)
399         ComPutc(2,0x04)
400         ComFlush(2)
```

```
401 end
402
403 NState=0
404 local StartTime=0
405 local Command_active =0;
406
407 print("Script: ",this," running")
408
409 ComClose(2)                              -- thermocouple logger
410 ComOpen(2,6,38400,8,4)
411
412 StopPump1()
413 StopPump2()
414
415 -- cycle starts with freezing
416
417 while AllowRunning(this) == 1
418 do
419
420     GetSwitchInput()
421     GetTemperatureInput()
422
423     if templogstatus == 1 then          -- gives the option if necessary to unplug the thermocouple
        ↪  device and keep the code running
424
425         SendCommandTC()
426         GetResult()
427
428         if (timeoutcnt > 4) then
429             print(os.date("%c"), "reset com port TC logger")
430             ComClose(2)
431             ComOpen(2,6,38400,8,4)
432             timeoutcnt=0
433         end
434     elseif templogstatus == 0 then
435         print(os.date("%X"), "temperature logging paused")
436         local TC_count = 4
437         for i = 0,15,2 do
438             ChanPutVal(TC_count,0.0)
439             TC_count = TC_count + 1
440         end
441     end
442
443     CurrentTime.title = os.date("%d/%m/%y  %H:%M:%S")
444
445   if NState == 0 then                   -- waiting for start button
446     Status.title = "Waiting for start"
447     Timetogo.title = ""
448         StopPump1()                                  --whilst start has not been pressed, pumps
          ↪  will not run
449         StopPump2()
450         NState=1
451
452   elseif NState == 10 then              -- start button is pressed, temperature is set to low
453     StartTime = os.clock()
454     Status.title = "Start freezing: Set temperature low"
```

```
455         Temp_command = tonumber(Text08.value)       --the low temperature setting
456                 NState = 20
457
458     elseif NState == 15 then                -- if something goes wrong
459         StopPump1()
460         StopPump2()
461         NState = 0
462
463     elseif NState == 20 then                -- wait for reaching low temperature
464                 difference = Act_Temp - target_temp
465         Temptogo.title = string.format("%.1f", difference)
466         if (math.abs(difference) <= 0.2) then
467             StartTime = os.clock()
468             Temptogo.title = ""
469             Status.title = "Keep freezing: Wait for time low"
470             NState = 30
471         end
472
473     elseif NState == 30 then                            -- wait for the set time on low temperature
474         T = os.clock() - StartTime
475         Teller = tonumber(Text07.value)     -- the low temp time setting
476                 EndDate = os.time() + Teller - T
477                 EndStep.title = os.date("%d/%m/%y  %H:%M:%S", EndDate)
478         Timetogo.title = string.format("%.1f", Teller - T)
479         if Teller - T <= 0 then
480             Status.title = "Start dry thawing: Set temperature high"
481                     EndStep.title = ""
482             Temp_command = tonumber(Text09.value)       --the high temperature setting
483             Timetogo.title = ""
484             NState = 40
485         end
486
487     elseif NState == 40 then        -- wait for reaching high temperature
488         difference = Act_Temp - target_temp
489         Temptogo.title = string.format("%.1f", difference)
490                 StartTime = os.clock()
491         if (math.abs(difference) <= 0.2) then
492                     Temptogo.title = ""
493             Status.title = "Fill water tank: Filling to Floater 1"
494                     StartTime = os.clock()
495             NState = 50
496         end
497
498     elseif NState == 50 then        -- wait for the set time on high temperature and turn on pump to
        ↪  reach floater 1
499         if floater1 == 0 then       -- if water passed the bottom floater (so the floater is in high position,
            ↪  so no signal coming through)
500             StartTime = os.clock()
501             Status.title = "Fill water tank: Filling to Floater 2"
502             Timetogo.title = ""
503             NState = 60
504         else                        -- if water has not passed bottom floater
505                     StartPump1()
506             T = os.clock() - StartTime
507             Teller = tonumber(Text01.value)         -- time to reach floater 1
508             Timetogo.title = string.format("%.1f", Teller - T)
```

```
509                 EndDate = os.time() + Teller - T
510                 EndStep.title = os.date("%d/%m/%y  %H:%M:%S", EndDate)
511             if Teller - T <= 0 then                 -- if floater 1 is not reached within time, stop the pumps
512                 Timetogo.title = "timeout pump 1, floater 1"
513                         EndStep.title = "Error"
514                 print(os.date("%X"), "timeout pump 1, floater 1")
515                 NState = 15
516             end                         -- NState remains 50 untill the floater is reached
517         end
518
519     elseif NState == 60 then            -- wait for floater 2 to be reached
520         if floater2 == 1 then           -- if water passed the top floater (so the floater is horizontal, so
            ↪  signal coming through)
521             StartTime = os.clock()
522             Timetogo.title = ""
523             Status.title = "Fill water tank: Follow-up filling time"
524             NState = 70
525         else
526             StartPump1()
527             T = os.clock() - StartTime
528             Teller = tonumber(Text02.value)         -- time to reach floater 2
529             Timetogo.title = string.format("%.1f", Teller - T)
530                     EndDate = os.time() + Teller - T
531                     EndStep.title = os.date("%d/%m/%y  %H:%M:%S", EndDate)
532             if Teller - T <= 0 then
533                 Timetogo.title = "timeout pump 1, floater 2"
534                 print(os.date("%X"), "timeout pump 1, floater 2")
535                         EndStep.title = "Error"
536                 NState = 15
537             end
538         end
539
540     elseif NState == 70 then            -- follow-up time after floater 2
541         T = os.clock() - StartTime
542         Teller = tonumber(Text03.value)         --the follow-up time setting
543         Timetogo.title = string.format("%.1f", Teller - T)
544                 EndDate = os.time() + Teller - T
545                 EndStep.title = os.date("%d/%m/%y  %H:%M:%S", EndDate)
546         if Teller - T <= 0 then
547             StopPump1()
548                     Status.title = "Wait untill circulation"
549                     StartThaw = os.clock()                          -- the time the plates are fully
                        ↪  submerged
550                     EndCirculation = os.clock()
551                     NState = 80
552         end
553
554         elseif NState == 80 then
555         CoolingTime = tonumber(Text12.value)        -- the wait time between circulation moments
556                 TotTeller = tonumber(Text04.value)
557                 CirculateTime = tonumber(Text11.value)
558                 Tot = os.clock() - StartThaw
559                 EndDate = os.time() + TotTeller - Tot
560                 EndStep.title = os.date("%d/%m/%y  %H:%M:%S", EndDate)
561                 if TotTeller - Tot - CoolingTime - CirculateTime <= 0 then              -- check if there is
                    ↪  still time to do a circulation cycle without clashing with emptying of tank
```

```
562                 StopPump2()
563                 StopPump1()
564                 StartTime = os.clock()
565                 Status.title = "Waiting for emptying"
566                 NState = 100                        -- to next step
567             else                                    -- if sufficient time for cycling
568                 T = os.clock() - EndCirculation
569                 Timetogo.title = string.format("%.1f", CoolingTime - T)
570                 if CoolingTime - T <= 0 then        -- if the end of the last circulation is bigger
                    ↪  than the circulation wait, go to the start circulation
571                     Status.title = "Start criculating"
572                     StartCirculate = os.clock()
573                     NState = 90
574                 end
575             end
576
577         elseif NState == 90 then                    -- start circulating if within limits
578             StartPump1()
579             StartPump2()
580         Tpump = os.clock() - StartCirculate
581         Teller = tonumber(Text11.value)             -- circulating time
582             Timetogo.title = string.format("%.1f", Teller - Tpump)      -- change this to correctly show
                ↪  time of circulating step
583         if Teller - Tpump <= 0 then
584             StopPump2()
585                 StopPump1()
586             Status.title = "Max circulating time reached, wait for next circulation"
587             StartTime = os.clock()
588                 EndCirculation = os.clock()
589             NState = 80
590         end
591
592         elseif NState == 100 then
593             TotTeller = tonumber(Text04.value)
594             Tot = os.clock() - StartThaw
595             EndDate = os.time() + TotTeller - Tot
596             EndStep.title = os.date("%d/%m/%y  %H:%M:%S", EndDate)
597             Timetogo.title = string.format("%.1f", TotTeller - Tot)
598             if TotTeller - Tot <= 0 then
599                 StartPump2()
600                 StartTime = os.clock()
601                 Status.title = "Empty water tank: wait for floater 1"
602                 NState = 110
603             end
604
605         elseif NState == 110 then
606             T = os.clock() - StartTime
607         Teller = tonumber(Text05.value)         -- empty time setting
608         Timetogo.title = string.format("%.1f", Teller - T)
609             EndDate = os.time() + Teller - T
610             EndStep.title = os.date("%d/%m/%y  %H:%M:%S", EndDate)
611         if Teller - T <= 0 then
612             Timetogo.title = "Error, max empty time reached"
613             print(os.date("% X"), "Error, max empty time reached")
614             NState = 15
615         end
```

```
616         if floater1 == 1 then       -- if bottom floater is in horizontal position
617             StartTime = os.clock()
618             Status.title = "Empty water tank: Follow up time"
619             NState = 120
620         end
621
622     elseif NState == 120 then       -- follow up time after bottom floater
623         T = os.clock() - StartTime
624         Teller = tonumber(Text06.value)     -- the follow-up time setting
625         Timetogo.title = string.format("%.1f", Teller - T)
626                 EndDate = os.time() + Teller - T
627                 EndStep.title = os.date("%d/%m/%y  %H:%M:%S", EndDate)
628         if Teller - T <= 0 then
629             StopPump2()
630             Timetogo.title = ""
631             Count = Count + 1
632             Counter.title = Count
633                         EndStep.title = ""
634                         ChanPutVal(17, Count)
635             if Count < tonumber(Text10.value) then
636                             if PausePressed == 1 then
637                                     Status.title ="Pause pressed, wait untill resume"
638                                     AcceptResume = 1
639                                     NState = 1
640                             elseif PausePressed == 0 then
641                                     Status.title = "Start freezing: Set temperature low"
642                                     NState = 10             -- next loop
643                             end
644             else
645                 Status.title = "End loops"
646                 NState = 140
647             end
648         end
649
650         elseif NState == 140 then
651                 Status.title = "End loops, conserve samples freezing"
652                 Temp_command = tonumber(Text08.value)
653                 NState = 150
654         end
655
656     yield()
657 end
658
659 StopPump1()
660 StopPump2()
661 iup.Destroy(dlg)
662 print(this," end")
663 ComClose(0)
664 ComClose(1)
665 ComClose(2)
```

C

KNMI data

Table C.1: KNMI weather data for 18/07/2024 [61]

Time	Time [s]	Irradiance [W/m^2]	$T_{ambient}$ [°C]	Wind [m/s]	Cloud coverage [okta]
18/07/2024 09:50	0	621	20.8	1.71	8
18/07/2024 10:00	600	590	21.2	1.98	8
18/07/2024 10:10	1200	536	21.4	1.19	8
18/07/2024 10:20	1800	637	22.0	1.73	8
18/07/2024 10:30	2400	634	22.1	1.52	8
18/07/2024 10:40	3000	594	22.1	0.94	8
18/07/2024 10:50	3600	672	22.8	1.05	8
18/07/2024 11:00	4200	705	23.4	1.15	8
18/07/2024 11:10	4800	722	22.9	1.09	8
18/07/2024 11:20	5400	623	23.4	0.96	8
18/07/2024 11:30	6000	750	23.8	1.01	8
18/07/2024 11:40	6600	787	24.0	1.09	8
18/07/2024 11:50	7200	760	24.1	1.48	8
18/07/2024 12:00	7800	726	23.8	1.13	8
18/07/2024 12:10	8400	761	24.0	1.25	8
18/07/2024 12:20	9000	831	24.3	1.19	8
18/07/2024 12:30	9600	787	24.7	1.95	8
18/07/2024 12:40	10200	709	24.3	1.56	6
18/07/2024 12:50	10800	276	23.9	1.93	7
18/07/2024 13:00	11400	628	24.8	1.48	7
18/07/2024 13:10	12000	643	24.7	1.73	8
18/07/2024 13:20	12600	612	24.8	1.71	6
18/07/2024 13:30	13200	421	25.0	1.58	6
18/07/2024 13:40	13800	782	25.5	2.10	6

D

Script calculating heat transfer coefficient

```
# Convective surface properties
A = area  # Convective surface area in m^2
P = perimeter  # Convective surface perimeter in m
Lc = A/P  # In m
Ts = 35.335  # Convective surface temperature

# Convective fluid properties, here air
Ta = 23.492  # Air temperature
U = 1.4379  # Velocity of air flow in m/s
k = 0.02551  # Thermal conductivity of air in J/kg K at 25 degree C
cp = 1007  # Specific heat capacity of air in W/mK at 25 degree C
rho = 1.184  # Density of air in kg/m^3 at 25 degree C
mu = 1.849*(10**(-5))  # Dynamic viscosity of air in  kg/m s at 25 degree C
nu = 1.562*(10**(-5))  # Kinematic viscosity of air in m^2/s at 25 degree C
beta = 0.00338  # Thermal volume expansion coefficient of air for 25 degree C
g = 9.81  # Gravitational acceleration

# Calculations of dimensionless numbers to determine type of flow
Re = U*Lc*rho/mu  # Reynolds number for type of flow
Re_crit = 5*10**5  # Critical Reynolds number

Gr = g*beta*abs(Ts-Ta)*Lc**3/(nu**2)  # Grashof number
Pr = mu*cp/k  # Prandtl number
x = Re_crit*nu/U  # Critical length over which flow is laminar

Ra = Gr*Pr  # Rayleigh number to determine type of free convection flow
Nu = 0

# Determining type of convection
if Gr / (Re**2) < 0.1:  # Forced convection, free negligible
    print("Re =", Re, " Forced convection, free convection negligible")
    if x / Lc < 1:
        print("Laminar region can be neglected")
        if 0.6 < Pr < 60 and Re > Re_crit:
            Nu = 0.036 * Re**(4/5) * Pr**(1/3)
        else:
            print("Pr or Re out of bounds, Pr =", Pr, " Re =", Re)
    else:
        print("Laminar region cannot be neglected")
        if Pr > 0.6 and Re < Re_crit:  # Only laminar flow
            Nu = 0.664 * Re**(1/2) * Pr**(1/3)
        elif 0.6 < Pr < 60 and Re > Re_crit:  # Laminar and turbulent flow
```

```
            Nu = (0.036 * Re**(4/5) - 836) * Pr**(1/3)
        else:
            print("Pr or Re out of bounds, Pr =", Pr, " Re =", Re)

elif Gr / (Re**2) > 10:  # Free convection, negligible forced convection
    print("Re =", Re, " Free convection, forced convection negligible")
    if 10**4 < Ra < 10**7:
        Nu = 0.54 * Ra**(1/4)
    elif 10**7 < Ra < 10**11:
        Nu = 0.15 * Ra**(1/3)
    else:
        print("Ra out of bounds, Ra =", Ra)

else:  # Mixed convection
    print("Re =", Re, " Mixed convection")
    if 10**4 < Ra < 10**7:
        Nu_free = 0.54 * Ra**(1/4)
    elif 10**7 < Ra < 10**11:
        Nu_free = 0.15 * Ra**(1/3)
    else:
        print("Ra out of bounds, Ra =", Ra)

    if x / Lc < 1:
        print("Laminar region can be neglected")
        if 0.6 < Pr < 60 and Re > Re_crit:
            Nu_forced = 0.036 * Re ** (4 / 5) * Pr ** (1 / 3)
        else:
            print("Pr or Re out of bounds, Pr =", Pr, " Re =", Re)
    else:
        print("Laminar region cannot be neglected")
        if Pr > 0.6 and Re < Re_crit:  # Only laminar flow
            Nu_forced = 0.664 * Re ** (1 / 2) * Pr ** (1 / 3)
        elif 0.6 < Pr < 60 and Re > Re_crit:  # Laminar and turbulent flow
            Nu_forced = (0.036 * Re ** (4 / 5) - 836) * Pr ** (1 / 3)
        else:
            print("Pr or Re out of bounds, Pr =", Pr, " Re =", Re)

    # Combine the Nusselt numbers for mixed convection
    Nu = (Nu_forced**3 + Nu_free**3)**(1/3)

# Calculate the convective heat transfer coefficient
h = Nu * k / Lc  # h in W/m^2K
print("h =", h, "W/m^2K")
```